Deciphering the Roles of 2 Intercalated Cell Proteins in Acid-Base and Ion Homeostasis: SLC26A7 and Claudin-4

By

AKM Shahid Ullah

A thesis submitted in partial fulfilment of the requirements for the degree of

Doctor of Philosophy

Department of Physiology

University of Alberta

ABSTRACT

Few of the many crucial physiological functions are maintaining acid/base balance and electrolyte homeostasis. The last segment of the nephron, collecting duct, fine tunes these functions by secreting acids and reabsorbing bicarbonate through the specialized type-A intercalated cells (Type-A IC). These cells harbour acid secreting protein H^+ATPase at the apical membrane and chloride-bicarbonate exchanger proteins, kidney anion exchanger 1 (kAE1) and SLC26A7 at the basolateral membrane. Mutations in either H^+ATPase or kAE1 can cause distal renal tubular acidosis (dRTA), principally characterized by defective urine acidification. In the collecting duct, there are also the principal cells and the type-B intercalated cells which regulate the electrolyte homeostasis with the proteins localized in their apical and basolateral membranes. Tight junction (TJ) proteins occupy the gap between the cells on the apical side, facilitating paracellular ion transfer between lumen and interstitium.

We characterized SLC26A7 protein's expression and function in relation to kAE1 and dRTA mutant kAE1 R901X in normal growth condition and hyperosmotic growth medium mimicking medullary habitat of the protein. We confirmed that SLC26A7 protein acts as a chloride/bicarbonate exchanger in Madin Darby Canine Kidney (MDCK) cells. We also found that the protein is mostly intracellular in both polarized and non-polarized cells, and demonstrate a lower chloride/bicarbonate exchange activity than that of kAE1 protein. Co-expressing SLC26A7 and kAE1 proteins did not demonstrate additive chloride/bicarbonate exchange function compared to when they are expressed alone. Our experiments also showed that osmolarity does not affect the chloride bicarbonate activity in the cells expressing SLC26A7. Furthermore, we mimicked acidotic condition by decreasing pH of the growth medium and found reduced abundance of SLC26A7

protein. All these experiments suggest that SLC26A7 functions as a chloride/bicarbonate exchanger in MDCK cells independent of osmolarity and its cellular abundance is dependent on extracellular osmolarity and pH conditions.

Our second set of study was on the tight junction protein claudin-4 (cldn-4), which acts as a chloride pore and sodium barrier in the collecting duct. Total knock out (KO) cldn-4 mice demonstrate lethal hydronephrosis, hypocalcemia and elevated fractional excretion of calcium and chloride ions. Principal cell (PC) specific cldn-4 KO show increased fractional excretion of chloride and sodium. We established IC specific cldn-4 KO mouse to obtain an overall picture of the role of cldn-4 in the collecting duct. At the steady state, IC cldn-4 KO mice do not demonstrate any gross physiological defect and are able to maintain normal acid-base and calcium homeostasis. To investigate if the mice are able to reabsorb sodium and chloride as efficiently as the WT, they were fed a NaCl depleted diet. In this condition, the mice displayed increased fractional excretion of sodium. At the basal state and salt depleted diet condition, the mice display increased expression of IC markers pendrin, kAE1 and sodium dependent chloride bicarbonate exchanger (NDCBE) without a change in the abundance of H^+ATPase. When given 0.28M NH_4Cl water, the mice are able to maintain pH homeostasis to the same degree as the WT mice. To investigate if the IC cldn-4 has any contribution to calcium homeostasis, the mice were fed a low calcium diet but displayed no perturbation in calcium homeostasis. Together all these investigations indicate that in the distal nephron, IC cldn-4 is not involved in pH and calcium homeostasis but is required for sodium reabsorption.

PREFACE

All the results and outcomes of this dissertation are the original work of AKM Shahid Ullah, unless otherwise mentioned.

Chapter 1

Sections *1.3.1.1.1.1, 1.3.1.1.1.2, 1.3.3 and 1.3.4 of Chapter 1 are parts of the review published previously in :*

Lashhab R, Ullah AKM Shahid, Cordat E. Renal collecting duct physiology and pathophysiology. *Biochem Cell Biol*. 2019;97(3):234-242. doi:10.1139/bcb-2018-0192.

Chapter 2

Chapter 2 is published but has been slightly modified in this thesis.

Ullah AKM Shahid, Rumley AC, Peleh V, Fernandes D, Almomani EY, Berrini M, Lashhab R, Touret N, Alexander RT, Herrmann JM, Cordat E. SLC26A7 protein is a chloride/bicarbonate exchanger and its abundance is osmolarity- and pH-dependent in renal epithelial cells. *Biochem Biophys Acta Biomembr.* 2020 Jun 1;1862(6):183238. doi: 10.1016/j.bbamem.2020.183238. Epub 2020 Feb 28. PMID: 32119864.

AKM Shahid Ullah participated in designing the experiments and performed the experiments, analyzed results, contributed manuscript preparation, prepared figures and participated in manuscript editing. Alina Rumley, Valentina Peleh, Daphne Fernandes, Ensaf Almomani, Mattia Berrini and Rawad Lashhab participated in conduction experiments. Dr. Nicolas Touret participated in data analysis. Drs. Johannes Herrmann and Todd Alexander participated in manuscript editing. Dr. Emmanuelle Cordat conceptualized the project, supervised, and coordinated the research and prepared the manuscript.

Valentina Peleh and Dr. Johannes Herrmann are affiliated to the Department of Cell Biology, University of Kaiserslautern, Kaiserslautern, Germany.

AKM Shahid Ullah, Alina Carly Rumley, Daphne Fernandes, Ensaf Almomani, Mattia Berrini, Rawad Lashhab, Dr. Nicolas Touret, Dr. R. Todd Alexander and Dr. Emmanuelle Cordat are affiliated to the University of Alberta, Edmonton, Alberta, Canada.

Chapter 3

Chapter 3 is prepared to submit for publication as follows

Ullah AKM Shahid, Arutyunov D, Alexander RT, Cordat, E. Loss of intercalated cell claudin-4 causes urinary sodium waste. (2022).

AKM Shahid Ullah participated in designing the experiments and performed the experiments, analyzed results, contributed to manuscript preparation, prepared figures and participated in manuscript editing. Dr. Denis Arutyunov participated in conducting experiments, and manuscript editing. Dr. Todd Alexander participated in manuscript editing. Dr. Emmanuelle Cordat conceptualized the project, supervised, and coordinated the research and prepared the manuscript.

AKM Shahid Ullah, Dr. Denis Arutyunov, Dr. R. Todd Alexander and Dr. Emmanuelle Cordat are affiliated to the University of Alberta, Edmonton, Alberta, Canada.

ACKNOWLEDGEMENT

First and foremost, I am indebted to the Almighty ALLAH, to whom all honor is due.

I would like to express my gratitude to Dr. James Young and Dr. Todd Alexander, members of my supervisory committee, for their continued support, helpful recommendations, and warm smiles during my stay in the department. It would be difficult for me to continue in Edmonton and complete my study without the Department of Physiology's constant aid from the beginning to the conclusion. My heartfelt gratitude goes to Sharon Orescan, Kim Sawada, Donna Simpson, Dancy Bogdanovic, and many more whom I never met but helped me several times. I want to thank the Faculty of Graduate Studies and Research for admitting me to the University of Alberta, as well as the other official assistance that helped make my time here a success.

The Health Sciences Laboratory Animal Services has been a huge help to us by taking excellent care of our experimental animals. We would be unable to carry out this research without their assistance. Special thanks to Nicole Vestby, Kimberly Seward, and all of the technicians that set up breeding, gathered genotyping samples, and kept the colonies running throughout normal and pandemic conditions. I also want to thank the staff at Biochemistry Stores, Glenis Wiebe and Delilah Gerein, for their ongoing and unwavering support in supplying us with the greatest stuff available in the simplest method possible.

I want to express my gratitude to the members of Dr. Alexander's lab for their assistance and cooperation. Wanling Pan, Debbie O'Neil, Dr. Megan Beggs, Shane Weibe, Justin Lee, Tate McDonald, Matthew Saurette, Rebecca Tan, and Dr. Allen Plain were always kind and helpful when it came to sharing equipment, reagents, expertise and experience, and lab meetings. Dr. Alexander, above all these people, was always the go-to person for any difficulties relating to

pretty much everything. With his expertise, knowledge, and experience, he constantly aided and directed.

Any amount of gratitude will not suffice to express my gratitude to my lab-mate Drs. Rawad Lashhab and Denis Arutyunov. They helped me learn new tools and procedures, some of which I had never seen or heard of before joining the lab, with their knowledge, experience, and passion. I am also grateful to all the technicians who helped us throughout the process, beginning with Mattia Berrini, Carly Rumley, Daphne Fernandes, and Kristina MacNaughton. I have had a great time learning and sharing knowledge and ideas with them, doing experiments, lamenting mistakes, and celebrating achievements. Members of the lab, Dr. Ensaf Almomani, Midhat Rizvi, Forough Chelangarimiyandoab, Grace Essuman, and undergraduate students Azka Ahmed, Jared Bouchard, and Priyanka Mungara all aided me with my experiments and procedures at various times. They have my gratitude.

I would also want to thank all of the IRTG program's German visitors, Dr. Velentina Peleh, Dr. Hawra Bzeih, and Dr. Sarder Hasib, from the Universities of Kaiserslautern and Saarbrucken. We shared our information, experiences, and cultures, all of which greatly enhanced my life. I would want to recall my time as a visiting student at Dr. Veit Flockerzi's lab in Germany. Dr. Flockerzi went above and beyond to make my move and stay as painless, enjoyable, and productive as possible. Special thanks to Dr. Kai Busch and Dr. Ahsan Raza, my contemporary graduate students from the Flockerzi lab, for keeping me company, teaching me new techniques, and not to mention the coffee breaks.

I would like to express my heartfelt gratitude to the funding sources, International Research Training Group-NSERC, Faculty of Medicine and Dentistry-U of A, Department of Physiology,

Kidney Foundation of Canada, and Canadian Institutes of Health Research for providing me with scholarships during my PhD.

My supervisor, Dr. Emmanuelle Cordat, is someone I cannot thank enough and cannot convey my thanks in words. Dr. Cordat welcomed me as a PhD student in the lab when I had almost given up hope of obtaining a PhD post to fulfil a long-held ambition. From the beginning to the finish of this thesis, she was there with me, steering my way with precious inspiration, solid thought, passion, encouragement, and all-enduring all-time support as well as critical critique. This thesis would be impossible without her reassuring smile and frequent pointing to the obvious. Not only did I study science from her, but I also learned how to be a good human being. Standing here at the end, all I can say is "MERCI BEAUCOUP, EMMANUELLE."

My heartfelt gratitude goes out to all of my friends and well-wishers who have always sheltered me with their love and provided me a shoulder whenever I needed it.

I realized towards the end of the journey that I was not alone on the journey. My parents, siblings, my wife Dr. Farzana Yasmin, an avid medical school teacher and neonatologist who gave up her dreams to be by my side, and finally, my son, Zafeer Faraz Ullah, who completes me as a human, were always cheering for me from the sidelines, were hurt when I fell down, were screaming my name out when I was successful, and sacrificed thousand folds more than I did, selflessly, hoping to see me cross the finish line. I'll never be able to repay their debts.

THANK YOU ALL

FOR YOUR GUIDANCE, SUPPORT, KINDNESS AND UNCONDITIONAL LOVE

TABLE OF CONTENTS

ABSTRACT ..... *ii*

PREFACE ..... *iv*

ACKNOWLEDGEMENT ..... *vi*

LIST OF TABLES ..... *xv*

LIST OF SUPPLEMENTARY TABLE (APPENDICES) ..... *xvi*

LIST OF FIGURES ..... *xviii*

LIST OF SUPPLEMENTARY FIGURES (APPENDICES) ..... *xx*

LIST OF ABBREVIATIONS ..... *xxi*

CHAPTER 1 ..... *1*

GENERAL INTRODUCTION *1*

1.1 Thesis overview *2*

1.2 Introduction *3*

1.3 The Urinary system *5*

1.3.1 The Kidney **6**

1.3.1.1 The Nephron 7

1.3.3 Ion homeostasis and blood pressure **16**

1.3.4 pH Homeostasis **17**

1.3.4.1 In the Proximal tubule 19

1.3.4.2 In the collecting duct 22

1.4 Tight junctions *24*

1.4.1 Junctional Adhesion Molecules (JAMs) **24**

1.4.2 Tight-Junction Associated Marvel Domain-containing proteins (TAMPs) **25**

1.4.3 Claudins **25**

1.4.3.1 Physiological consequences of claudins loss 29

1.4.3.1 Claudin-4 29

1.5 Chloride-bicarbonate exchanger in the CD *32*

1.5.1 kAE1 interactome **34**

1.5.1.1 Amino-terminal cytosolic domain interactors 34

1.5.1.2 Carboxyl-terminal cytosolic domain interactors 34

1.6 SLC26A7 ..... *35*

1.7 Distal renal tubular acidosis (dRTA) *38*

1.8 Calcium homeostasis *40*

1.8.1 Calcium homeostasis in the kidney 42

1.8.2 Paracellular transport and claudins in calcium renal transport **42**

1.8.2 Calcium handling in the intestine **47**

1.8.3 Hormonal regulation of calcium absorption **47**

1.9.1 Thyroid hormones and erythropoietin 48

1.9.2 Hormonal regulation of the CD cells **49**

2.1 Hypotheses and Research questions *51*

Our general hypothesis is that altering proteins involved in either the transcellular (SLC26A7) or the paracellular pathway (Claudin-4) will affect electrolyte homeostasis.51

2.1.1 Hypothesis 1 ..... **51**

2.1.1.1 Research questions 51

2.1.2 Hypothesis 2 ..... **51**

2.1.2.1 Research questions 51

CHAPTER TWO ***53***

SLC26A7 PROTEIN IS A CHLORIDE/BICARBONATE EXCHANGER AND ITS ABUNDANCE IS OSMOLARITY- AND pH-DEPENDENT IN RENAL EPITHELIAL CELLS ***53***

Abstract ***54***

2.1 Introduction ***55***

2.2 Methods ***57***

2.2.1 Materials **57**

2.2.2 Constructs, cell lines, transfections and viral infection **57**

2.2.5 Bicarbonate transport assay **60**

2.2.6 Statistical analysis **61**

2.3 Results ***62***

2.3.1 In MDCK cells, SLC26A7 exchanges Cl^- for HCO_3^- in HCO_3^- containing buffer .. **62**

2.3.2 The abundance of both kAE1 and SLC26A7 is upregulated in MDCK cells grown in hyper-osmotic medium **66**

2.3.4 The proportion of cell surface SLC26A7 is unchanged in control or hyper-osmotic growth media **71**

2.3.5 SLC26A7 is not more functional in hyper-osmotic conditions than in control conditions **74**

2.3.6 When SLC26A7 protein is co-expressed with kAE1, the Cl^-/HCO_3^- exchange is not osmolarity-sensitive **78**

2.3.7 SLC26A7 protein is less abundant in cells grown in an extracellular medium below pH 7.2 **81**

2.4 Discussion *84*

LOSS OF INTERCALATED CELL CLAUDIN-4 CAUSES URINARY SODIUM WASTE .. *90*

ABSTRACT *91*

3.1 Introduction *92*

3.2 Materials and Methods *94*

3.2.1 Generation of IC cldn-4 KO mice **94**

3.2.2 Collecting duct isolation and protein extraction **95**

3.2.3 Diets and metabolic cage experiments **95**

3.2.4 Plasma electrolytes measurements **96**

3.2.5 Urine, serum, and feces collection and analysis, and blood pressure measurements **96**

3.2.6 Plasma and Urine Creatinine and plasma calcium assays **97**

3.2.7 Protein extraction and Western Blot **97**

3.2.8 RNA isolation and Quantitative RT-PCR **98**

3.2.9 Statistical Analysis **98**

3.3 Results ***98***

3.3.1 IC-cldn-4 KO mice generation, and KO confirmation 98

3.3.3 Abundance of IC-specific transcellular ion transporters is elevated in clnd-4 KO mice 104

3.3.4 Cldn-4 KO mice fed a low NaCl diet are wasting urinary sodium 107

3.3.5 Abundance of kAE1 and pendrin IC markers is elevated after a NaCl-depleted diet 110

3.3.6 There is no difference in RAAS-triggering between cldn-4 KO and WT mice 110

3.3.7 Cldn-4 KO mice maintain a normal acid-base balance 114

3.3.8 Cldn-4 KO mice have a normal calcium homeostasis 116

3.4 Discussion ***118***

CHAPTER FOUR ***123***

4.1 Summary ***124***

4.2 Characterization of SLC26A7: Summary, limitations and future directions ***124***

4.2.1 Summary 124

4.2.2 Limitations of the study 126

4.2.3 Future Directions 127

4.3.1 Proposed mechanism **129**

4.3.2 Summary 131

4.3.3 Limitations of the study 132

4.3.4 Future directions **133**

4.3.4.1 Generation of CD specific KO mouse 133

4.3.4.2 Micro-perfusion studies on isolated CD from WT and cldn-4 KO mice 134

4.3.4.3 Pharmacological inhibition of transport proteins 134

BIBLIOGRAPHY ***136***

APPENDICES ***171***

LIST OF TABLES

Table 3. 1 Plasma electrolytes levels in WT and Cldn-4 KO mice at basal state on normal diet…….....101

Table 3. 2 Plasma electrolytes levels in WT and Cldn4 KO mice on low NaCl diet.....108

Table 3. 3 Fractional Excretion levels in WT and KO mice on low NaCl diet 109

Table 3. 4 Plasma electrolytes levels and fractional excretion in WT and Cldn4 KO mice after an acid challenge (0.28 M NH_4Cl H_2O).....115

Table 3. 5 Plasma electrolytes levels and fractional excretion in WT and Cldn4 KO mice after a low Calcium diet (0.01%).....117

LIST OF SUPPLEMENTARY TABLE (APPENDICES)

Table A 1 List of primer and probe sequences used for qRTPCR in chapter 3.....172

Table A 2 Physical parameters of WT and Cldn-4 KO mice with long term acid load 3 Month age…… 174

Table A 3 Physical parameters of WT and Cldn-4 KO mice at steady state on normal diet at 6 months…….....177

Table A 4 Plasma electrolytes levels in WT and Cldn-4 KO mice at steady state on normal diet at 6 Month age.....177

Table A 5 Physical parameters of WT and Cldn-4 KO mice on low NaCl diet at 6 month age…….. 178

Table A 6 Plasma electrolytes levels in WT and Cldn-4 KO mice on low NaCl diet at 6 month age…… 178

Table A 7 Physical parameters of WT and Cldn-4 KO mice with long term acid load 6 month age…….. 179

Table A 8 Plasma electrolytes levels in WT and Cldn-4 KO mice with long term acid load 6 month age…….....179

Table A 9 Physical parameters of WT and Cldn-4 KO mice with 0.01% Ca2+ diet at 6 Month age…… 182

Table A 10 Plasma electrolytes levels in WT and Cldn-4 KO mice with 0.01% Ca2+ diet at 6 Month age…… 182

Table A 11 Physical parameters of WT and Cldn-4 KO mice at steady state on normal diet at 12 months…….....183

Table A 12 Plasma electrolytes levels in WT and Cldn-4 KO mice at steady state on normal diet at 12 Month age.....183

Table A 13 Physical parameters of WT and Cldn-4 KO mice on low NaCl diet at 12 Month age…… 184

Table A 14 Plasma electrolytes levels in WT and Cldn-4 KO mice on low NaCl diet at 12 Month age……. 184

LIST OF FIGURES

Figure 1. 1 The Nephron 10

Figure 1. 2 The collecting duct cells 15

Figure 1. 3 HCO_3^- reabsorption in the PT cells 21

Figure 1. 4 Acid-base homeostasis in the Type-A IC cells in the collecting duct. 23

Figure 1. 5 Schematic diagram of claudin protein 28

Figure 1. 6 AE1 topological model deduced from the crystal structure. 33

Figure 1. 7 Schematic diagram of the topology of SLC26A7 protein 37

Figure 1. 8 Schematic diagram of calcium homeostasis in the human body. 41

Figure 1. 9 Schematic diagram of calcium reabsorption along nephron segments. 44

Figure 1. 10 Calcium reabsorption in the TAL. 45

Figure 1. 11 Calcium reabsorption in the DCT/CNT 46

Figure 2. 1 SLC26A7 is stably expressed in clone 3 and 8 MDCK cells. 64

Figure 2. 2 Hyper-osmotic extracellular medium up-regulates both SLC26A7 and kAE1. 67

Figure 2. 3 Incubation in hyper-osmotic medium increases the half-life of SLC26A7 protein. 69

Figure 2. 4 Hyper-osmotic extracellular medium does not increase SLC26A7 cell surface/total expression ratio. 72

Figure 2. 5 Hyper-osmotic growth conditions do not increase SLC26A7-mediated Cl^-/HCO_3^- exchange……. 76

Figure 2. 6 Co-expression of SLC26A7 with kAE1 and kAE1 R901X in various conditions 79

Figure 2. 7 Effect of pH on kAE1 and SLC26A7 protein expression 82

Figure 3. 1 Validation of IC cldn-4 KO mouse model 100

Figure 3. 2 Relative abundance of tight junction proteins and corresponding mRNA at basal state……. 103

Figure 3. 3 Relative abundance of selected intercalated cell membrane proteins and corresponding mRNA at basal state. 105

Figure 3. 4 Relative abundance of tight junction proteins and corresponding mRNA after a low NaCl diet……. 111

Figure 3. 5 Relative abundance of selected intercalated cell membrane proteins and corresponding mRNA after a low NaCl diet. 112

Figure 4. 1 Schematic proposed mechanism of normochloremia and hypernatriuria 130

LIST OF SUPPLEMENTARY FIGURES (APPENDICES)

Figure A 1 BCECF-AM based functional assay principal.....172

Figure A 2 Urine pH in WT and KO mice at 3 month age.....175

Figure A 3 Urine osmolarity in WT and IC cldn-4 KO mice after acid load at 3 month age……...…….176

Figure A 4 Urine pH in WT and KO mice at 6 month age.....180

Figure A 5 Urine osmolarity in WT and IC cldn-4 KO mice after acid load at 6 month age181

LIST OF ABBREVIATIONS

ANOVA- Analysis of variance

AQP-Aquaporin

BCA- Bicinchoninic acid

BCECF-AM- 2′,7′-Bis-(2-Carboxyethyl)-5-(and-6)-Carboxyfluorescein, Acetoxymethyl Ester

CAII-Carbonic anhydrase II

CCD-Cortical collecting duct

CD- Collecting duct

Cldn- Claudins

CNT-Connecting tubule

DCT-Distal convoluted tubule

dRTA-Distal renal tubular acidosis

eAE1- Erythrocyte anion exchanger 1

ECF- Extracellular Fluid

e.g.- exempli gratia (Latin), for example

ENaC-Epithelial Sodium Channel

ER-Endoplasmic Reticulum

ER-Endoplasmic Reticulum

FE- Fractional excretion

GAPDH- Glyceraldehyde 3 phosphate dehydrogenase

HEK- Human embryonic kidney

HRP- Horseradish peroxidase

i.e.- id est (Latin), that is

IC-Intercalated cell

IMCD-Inner medullary collecting duct

JAMs- Junctional adhesion molecules

JG- Juxtaglomerular

kAE1- Kidney anion exchanger 1

MDCK- Madine-Darby Canine Kidney

MM- Metanephric mesenchyme

MMLV- Mouse Moloney Leukemia virus

MR- Mineralocorticoid receptor

NO-Nitric oxide

OMCD- Outer medullary collecting duct

PC-Principal cell

PDVF- Polyvinylidene difluoride

PDZ- Post-Synaptic-Density-95/Discs-large/Zona-Occludens-1

pRTA- Proximal renal tubular acidosis

PTI- Photons Technologies International

RAAS- Renin-angiotensin-aldosterone system

ROMK-Renal outer medullary potassium channel

RPKM- Reads Per Kilobase of transcript, per Million mapped

SDS-PAGE- Sodium Dodecyl Sulfate-Poly Acrylamide gel electrophoresis

SEM- Standard error of mean

STAS- Sulfate transporter anti-sigma factor antagonist

TAMPs- Tight junction-associated Marvel domain-containing proteins

TJ- Tight Junctions

TPM- Transcripts per million

UB-Ureteric Bud

ZO- Zona occludens

CHAPTER ONE

GENERAL INTRODUCTION

1.1 Thesis overview

The principal objective of this thesis is to decipher the role of 2 intercalated cell proteins, SLC26A7 and Claudin-4 (cldn-4) in the collecting duct. We generated and characterized intercalated cell specific cldn-4 KO mice upon a standard, low NaCl, acid or low calcium diet. Additionally, we also showed that SLC26A7 is a chloride/bicarbonate exchanger in MDCK cells and the expression of the protein is upregulated in hyperosmotic condition and downregulated in acidic condition.

The first chapter of this thesis introduces the kidneys, role of kidneys in ion and pH homeostasis, structure and functions of intercalated cells, tight junctions, chloride/bicarbonate exchangers kAE1 and SLC26A7 and calcium homeostasis in the kidneys as they are relevant to the thesis topics discussed later in Chapters 2 and 3.

Chapter 2 describes the characterization of the chloride/bicarbonate exchanger SLC26A7. The acid-secreting intercalated cells express both kAE1 and SLC26A7 proteins. We show that in MDCK cells the abundance of heterologously expressed SLC26A7 protein increases in hyper-osmotic growth media that mimics the medullary osmolality. In acidosis condition *i.e.* in lower pH condition, co-expression with kAE1 WT and kAE1 R901X results in decreased SLC26A7 abundance .

Chapter 3 describes the characterization of the role of tight junction protein cldn-4 in salt and acid/base homeostasis in an IC specific cldn-4 KO mouse model.

Overall, this Thesis has examined the IC-specific roles of a transcellular ion transporter and a paracellular tight junction protein in acid-base and ion homeostasis. This work contributed to improved knowledge on essential proteins in the CD physiology.

1.2 Introduction

Every human being starts from a single cell, which then differentiates to develop multiple cellular entities which eventually specialize in performing a set of functions required for the body, such as energy generation, electrical signals, movement, etc[1]. Cell differentiation is the key to this transformation process by which a simple cell generates a specialized cell cluster that constitutes a tissue. There are four general types of tissues in the body, namely, muscle, nervous, epithelial and connective tissues[1]. In a larger scale, one or more tissue combines physically and functionally to form organs (*e.g.,* heart, lung, liver, kidney)[1]. The human body is the home of a number of organ systems working simultaneously and synchronously with each other to carry out a variety of tasks aiming to maintain a perfect combination of bodily pH, water and electrolyte balance (*i.e.,* homeostasis)[2]. The rudimentary idea of homeostasis dates back to the early days of physiology, when physicians were able to associate well-being of an individual with the balance of "life sustaining forces"[1]. Chronologically, the advent of science, technology and tools like microscopes guided the discovery of numerous amounts and types of cells in the body and the movement of ions through these cells. Centuries later, these observations generated knowledge about physiological variables such as blood pressure, body temperature and subcellular ions and the role of molecules such as oxygen, glucose and sodium ions that are maintained within a narrow range to preserve a balance required for energy production and thriving[1,2]. The idea of homeostasis was not only confined to energy generation but also to elimination of waste and undigested elements from the body by concurrent action of multiple organs. For example, the respiratory system brings oxygen to the body, which will eventually be used to generate energy and break down nutrients, the circulatory system transports and delivers these to various regions in the body and carry the waste material generated by metabolic processes to the excretory systems to expel them out of the

body. The kidneys not only perform as one of the excretory systems, but also take part in homeostasis by aiding hormonal regulation of blood pressure, and reabsorbing critical ions like Na^+, Cl^-, Ca^{2+}, HCO_3^- and Mg^{2+}, and secreting H^+ and K^+. Hence, kidneys play a critical role in homeostasis by regulating the blood pressure, electrolyte concentration, and maintaining physiological pH and many others[1,2].

For this dissertation, we focused on the renal system and its role in acid-base and ion homeostasis in cellular and model organisms.

1.3 The Urinary system

The urinary system is the hub for a number of physiologic processes, such as osmoregulation, blood pressure and volume maintenance, erythrocyte production, calcium homeostasis and finally excretion of toxins and other molecules[3]. The array of these functions is carried out by two organs consecutively: the paired kidneys and the ureter[4]. The kidneys perform most of the functions here, whereas the ureters deliver the urine that is produced in the kidneys to the bladder. The bladder is the repository of the final waste, urine, before excreting through the urethra[4].

The development of the urogenital system begins in the human fetus as early as 22 days of gestation along the posterior wall of the abdomen[4,5]. The development of the nephron takes place in three distinct and subsequent stages through the generation of the pronephrons, the mesonephrons and the metanephrons. The pronephrons are composed of pronephric tubules and pronephric duct (precursor of Wolffian duct), however, they are not involved in kidney formation or in function[5]. The mesonephrons develop posterior to the pronephric tubules along the midsection of the urogenital ridge during the embryonic life and possibly participate in filtering function. The mesonephrons degenerate and move to the adrenogonadal primordia, where they become the adrenal gland and gonads[6]. The metanephrons, that form the kidneys in the further developed stage, originate through successive interactions between the metanephric mesenchyme (MM) and the epithelial ureteric bud (UB) posterior end of the urogenital ridge[4]. The UB, after subsequent changes and interaction, transverses on the MM, which branches out dichotomously and forms the urinary collecting duct system. Concurrently, signals sent from the UB to the MM result in a condensation of the mesenchyme on the surface of the bud, followed by aggregation of MM cells to the apex of the branching UB, known as pretubular aggregates. This aggregation,

which is a cluster of cells, transforms from mesenchyme to epithelia before becoming a renal vesicle.[4].

Successive patterned segmentation of the renal vesicles recruits mesenchymal progenitors to form the glomerulus and parts of nephrogenic tubules subject to undergo morphologic changes to form the proximal convoluted tubules, the loop of Henle and the distal tubule[4].

1.3.1 The Kidney

Mammalian kidneys are paired and located at the back of the abdominal wall, but not in the abdominal cavity. Both of them are retroperitoneal, one on the twelfth thoracic vertebrae and other on the third lumber vertebrae, across the sides of the vertebral column[1,4]. The surface of the kidneys is protected by a fibrous layer of connective tissue named the renal capsule[4]. The bean shaped organ is indented in the middle region which is called the hilum, through which the renal artery and renal vein perfuse and drain blood, respectively[1]. The innervations of the kidney also go through the hilum. The funnel shaped calyces (singular calyx) drain urine into the renal pelvis, and then drains to the ureter[1].

Cross-section of the kidneys reveals two distinct layers: striated inner layer named "medulla" and granular outer region named renal "cortex"[4]. The medulla consists of renal pyramids, at the base of which there are conical tissue masses at the corticomedullary junction. The tip of the pyramids extends toward the renal pelvis and forms the papilla. Renal papillae have 10-25 opening which are the end of the CDs and are folded by funnel shaped minor calyces. Multiple minor calyces merge to form a major calyx, which joins with one another to form the renal pelvis to drain the urine from the kidney to the ureter. The renal blood vessels and nerves along with the ureter exit through the indented side of the kidney, hilum, as previously mentioned[4].

By filtering the blood, the kidneys remove (or in fewer cases, adds) ions and molecules that the body does not need and excrete waste through urine. These processes are carried out by several functions of the kidneys[4]. Firstly, the core of the kidney functions is to regulate plasma osmolarity, plasma inorganic ion composition, acid-base balance and fluid volume. The kidneys function by excreting just enough water, secreting and reabsorbing inorganic ions and other molecules to maintain their optimal concentration range[1]. Second, the kidneys excrete urea from protein catabolism, uric acid from nucleic acids, creatinine from muscles, hemoglobin breakdown products and other metabolic wastes in the urine, which otherwise would accumulate in the body as toxic substances[1]. Third, the excretory function of the kidneys is not limited to bodily waste substances, but they also excrete foreign substances like metabolites of drugs, pesticides and food additives. Fourth, as the kidneys also release hormones such as erythropoietin, 1,25-dihydroxymitamin D (Vitamin-D3), and renin, they can be described as an endocrine gland. Last but not least, kidneys perform gluconeogenesis, synthesizing glucose from amino acids and precursors while the body is in prolonged fasting and delivering them to blood[1,4].

1.3.1.1 The Nephron

The functional units of the kidneys are the nephrons, which are approximately 1 million in number in each kidney. The nephrons originate from the metanephric blastema[4]. Each nephron is formed by a sequential series of tubular segments with distinct functions (Figure 1.1)[7]. The segments of the nephrons follow a specific sequence starting with the Malpighian corpuscle (glomerulus and Bowman's capsule), proximal tubule, the loop of Henle composed of the thin descending limb, the thin ascending limb, the thick ascending limb, the distal convoluted tubule, the connecting tubule, and the CD. Depending on the length of the loop of Henle, the nephrons are coined in short or long loop of Henle. The number of short and long loops of Henle varies among

species, *e.g.*, humans and rodents have shorter loops than other species with longer loops of Henle (e.g. kangaroo rat, *Dipodomys merriami)*[1,4,8]. The segments along the nephrons are defined by the structure and function of the epithelial cells.

The renal corpuscle filters the blood excluding cells, large polypeptides and proteins and then exits the corpuscle to the tubule. The corpuscle is composed of interconnected loops of the efferent capillaries, named glomerulus or glomerular capillaries. The arteries that supply blood to glomeruli are called the afferent arteriole. The glomerulus is encapsulated by fluid-filled Bowman's capsule which in combination with the glomerulus filters 20% of blood volume before leaving through the efferent arteriole[1,4]. The separation of blood from the fluid in the glomerulus to the Bowman's capsule takes place through three layers of barriers; the capillary endothelium, basement membrane or basal lamina and specialized epithelial lining of the Bowman's capsule known as podocytes[1,4].

The filtrate from the Bowman's capsule drains into the proximal tubule that begins from the urinary pole of the glomerulus. The initial proximal tubule is convoluted (pars convolute) and then straightens down (pars recta) as it enters the medullary region. The proximal tubule is characterized by well-developed brush border membrane, viewed under scanning electron microscope[4].

The following portion is the loop of Henle, which is first composed of a descending limb followed by a U-shape or hairpin loop that lies in the medulla. The descending limb of the loop dips from the cortex to the medulla and the ascending limb of the loop rises back to the cortex. The ascending limb then returns close to the glomerulus, passes the afferent and efferent arteriole forming a specialized formation called the juxtaglomerulus apparatus, which plays a significant role in kidney function. The tubular segment then coils to form distal convoluted tubule, residing

entirely in the cortex. The distal convoluted tubule delivers the fluid into the CD. The CD carrying the fluid (converted into pre-urine at this point) dips down into the medullary region to empty out in the renal pelvis[1,4,9].

The functions of the nephron segments are very distinct based on a number of characteristics such as the morphology of the epithelial cells, the location of the segment in the kidney structure, the proteins expressed in the apical or basolateral side of the cells etc. The primary focus of this thesis is the proteins expressed in the CD; therefore, the following sections will focus on CD cells and proteins in detail.

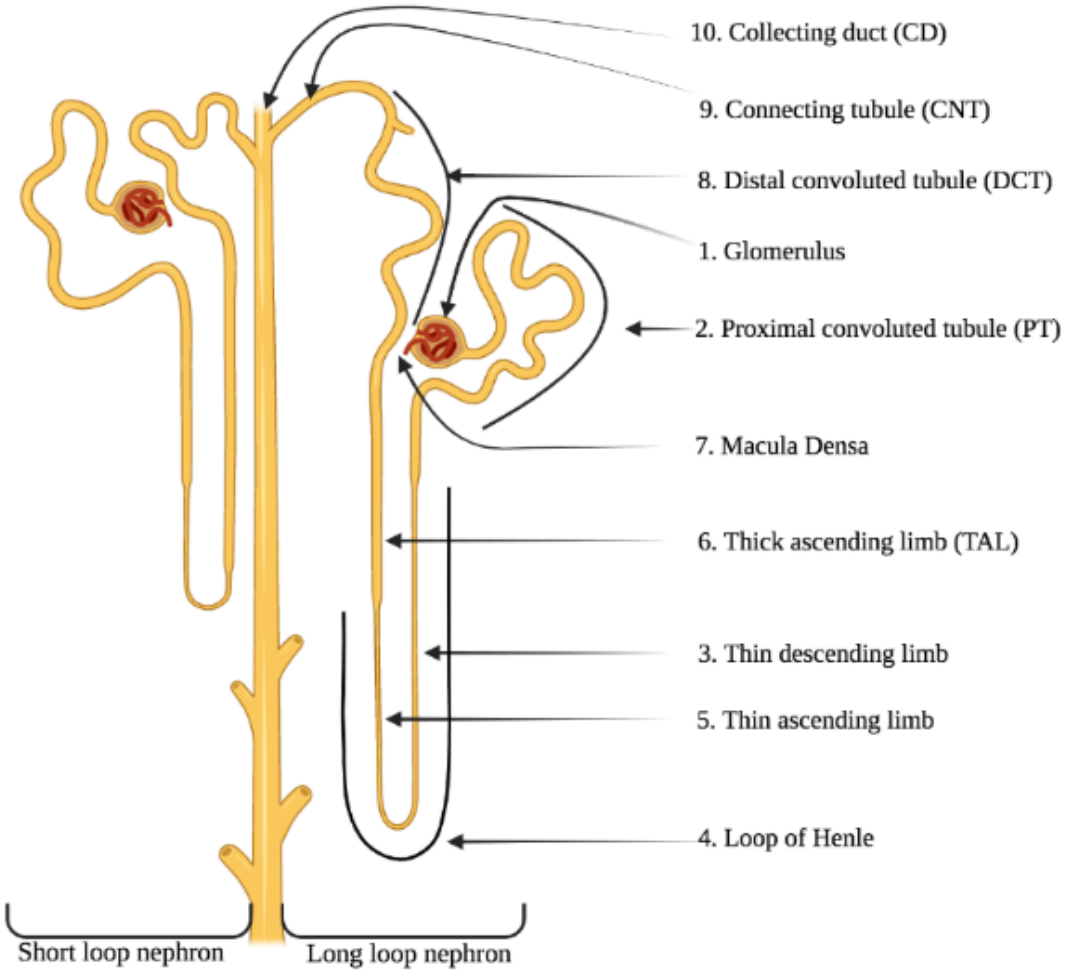

Figure 1. 1 The Nephron

The nephron starts with the glomerulus followed by the proximal convoluted tubule (PT). The tubule then descends as the thin descending limb and loops back up as thin ascending limb, together they are the loop of Henle. The tubule then becomes thick and named Thick ascending limb (TAL). It then convolutes again and comes in close contact to the glomerulus, named macula densa. The distal convoluted tubule (DCT) then becomes connecting tubule (CT) and falls into the collecting duct (CT). There are two types of nephrons, the short and long loop nephrons. The segments are numbers as they descends from glomerulus to CD. This figure was created in BioRender.com.

1.3.1.1.1 The Collecting duct cells

The CD is the last site of urine preparation where reabsorption and secretion take place to fine-tune the urine composition and hence, urine acidification[10]. The CD regulates the transport of water, sodium, potassium, chloride, and bicarbonate by the simultaneous action of transcellular (through the cells) and paracellular (between cells) proteins that are themselves regulated by several stimuli such as hormones[11]. Collecting duct proteins are present in at least two distinct types of cells: principal cells (PCs) and intercalated cells (ICs, subdivided into Type A or α-IC and type B or β-IC).

1.3.1.1.1.1 Principal cells

Various cell types of heterogeneous structural composition have been identified by electron microscopy in the embryonic CD epithelium[12]. "Light PCs" and "dark ICs" were distinguished based on these morphological observations. In cortical rat[13,14], mouse[14,15], and rabbit[16] CDs, two third of the cells were found to be PCs. These cells are simple cuboidal epithelial cells that carry fewer organelles and mitochondria than the dark ICs. The mitochondria also appear to be smaller in size and randomly distributed in the cytoplasm. Lysosomes, autophagic vacuoles, multivesicular bodies, and both rough and smooth endoplasmic reticulum are also evident by transmission electron microscopy[17]. The major role of the PCs in the CD is to reabsorb sodium and water from primary urine and to excrete potassium to the urine. They achieve this by the concomitant action of specific transporters including the epithelial sodium channel ENaC, aquaporin 2 (AQP2), the renal outer medullary potassium channel (ROMK) (Fig. 1.2), and to a lesser extent the Ca^{2+} activated K^+ channel[17]. In the PCs, aldosterone and arginine vasopressin play a key role for regulation of ENaC, ROMK, and AQP2 to facilitate sodium, potassium, and water transport,

respectively[11]. The amiloride-sensitive sodium channel ENaC is expressed at the apical membrane of the PC. Via the action of aldosterone, arginine vasopressin, and other hormones[18,19], high and low sodium diets result in low and high apical expression of ENaC, respectively[20]. Potassium secretion through the apical membrane of the PC is mediated by ROMK and is regulated by mineralocorticoids. In rabbit isolated perfused cortical collecting ducts (CCDs), mineralocorticoids stimulate potassium secretion and sodium reabsorption[21,22]. The Na^+/K^+-ATPase activity is also enhanced by mineralocorticoid stimulation in the CCD of rat[23] and rabbit[24]. Apical expression of ROMK in the DCT, CNT, or CD can be increased in a high-potassium diet[25]. Water molecules in the PC follow the lumen-to-interstitium osmotic gradient and their reabsorption is mediated by the synchronized expression and activity of apical AQP2 and basolateral AQP3 and AQP4[11,26,27].

1.3.1.1.1.2 The Intercalated cells

The other cell types found in the CD are ICs or "dark cells". In comparison with the PCs, ICs have a high density of mitochondria, a dark cytoplasm, and microprojections at the apical membrane and they do not have a central cilium[28]. All ICs are positive for carbonic anhydrase II (CAII) and H^+-ATPase protein expression.

ICs can be subdivided into three subtypes: type-A, type-B, and non-A and non-B IC. The location of the H^+-ATPase expression in addition to the expression of other key proteins define the IC subtype[15,29].

Type-A ICs express H^+-ATPase at the apical membrane and the kidney anion exchanger 1 (kAE1) at the basolateral membrane (Figure 1.2). These cells significantly contribute to acid–base balance by secreting protons via the apical H^+-ATPase and reclaiming bicarbonate via

basolateral kAE1, both ions being generated from hydrolysis of CO_2 and water by the CAII. On the other hand, by expressing H^+-ATPase at the basolateral membrane, and pendrin and NDCBE at the apical membrane, type-B ICs secrete bicarbonate and reclaim protons in the case of alkalosis. In addition to contributing to acid–base balance, type-B ICs also contribute to electrolyte homeostasis, as they are involved in chloride reabsorption[15,29]. Although ICs can be morphologically, structurally, and functionally distinguished from the PCs, experimental evidence supports that both cell types originate from the same precursor[30]. Immortalized type-B ICs plated at a high density were able to convert to type-A ICs and secrete acid instead of alkali[31]. This ability to convert from one cell type to the other was due to the secretion of the extracellular matrix hensin protein by type-B ICs[32]. In support of these findings, a hensin knockout mouse model displayed a predominant abundance of type-B ICs, the absence of type-A ICs in the CD, and development of metabolic acidosis[32].

Lastly, non-A and non-B ICs express both V-H^+-ATPase and pendrin at the apical membrane. The function of non-A and non-B IC is still unclear. However, the fact that both V-H^+-ATPase and pendrin are at the apical membrane suggests that these cells are not involved in acid–base balance but instead may be involved in electrolyte homeostasis. It is also thought that these cells may represent a transition state between the other two types depending on diet and plasma pH[29]. A very recent publication showed that the mouse CD contains a third type of cells in addition to PCs and ICs. These cells have features characteristic of PCs and ICs, as they were positive for both AQP2 and H^+-ATPase, indicating that they may represent a previously unidentified transitional state between the two main cell types[33]. The distribution of the different IC types in the distal nephron varies among species. In mouse, type-A ICs make up 40%, 60%, and 100% of the ICs in CNT, CCD, and OMCD/IMCD, respectively. On the other hand, type-B and non-A and

non-B ICs make up 10% and 50%, 20% and 20%, and 0% of the ICs in CNT, CCD, and OMCD/IMCD, respectively[14]. Recent years of research have demonstrated a clear interplay between PCs and ICs. Indeed, in a similar finding to what was observed in renal tubular acidosis (RTA) patients[34], mice knockout on the B1 subunit of the H^+-ATPase displayed a defective conservation of sodium and chloride due to altered function of ENaC and decreased abundance of pendrin[35]. Thus, a knockout in ICs results in functional defects of not only ICs but also PCs. These animals displayed elevated levels of urinary ATP and prostaglandin E2 (PGE2) originating from type-B ICs but acting on PCs in a paracrine process. Thus, these findings highlight that the function of one cell type is linked to that of its neighbor cells in the CD.

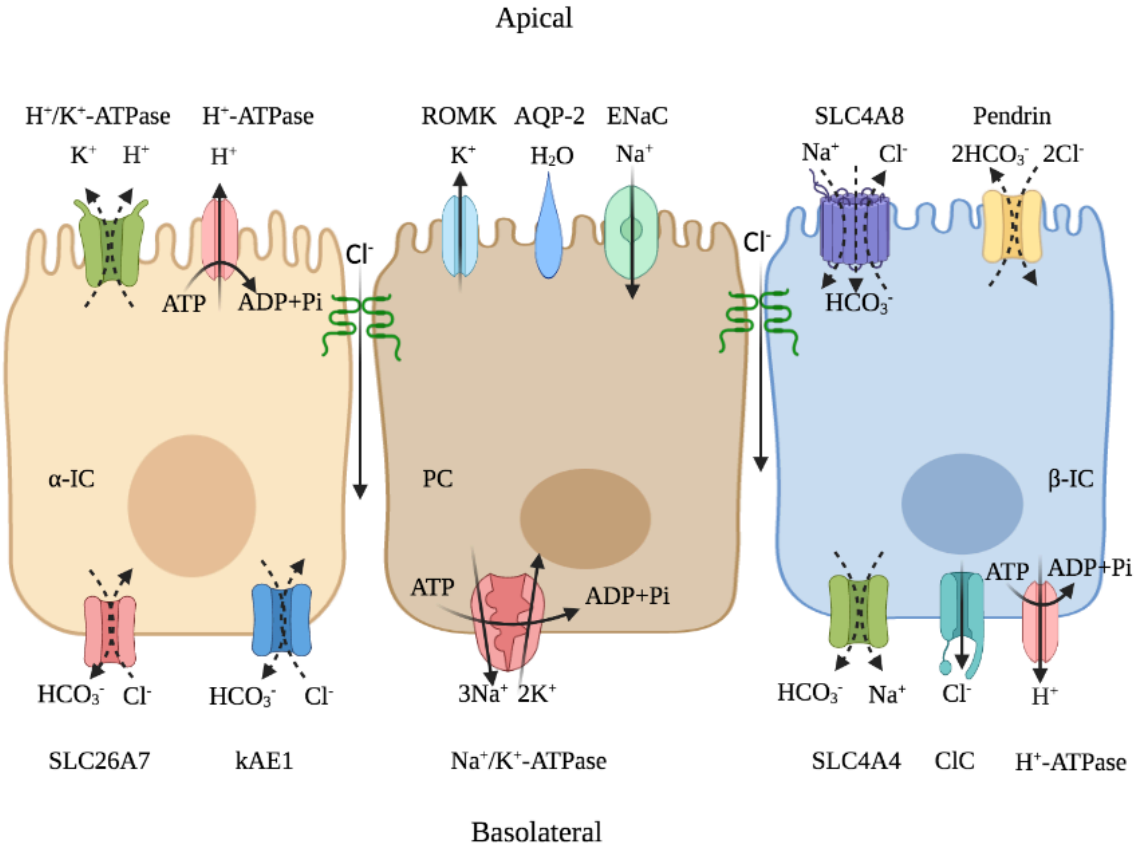

Figure 1. 2 The collecting duct cells

The principal cells (PC), and type-A (α-IC) and Type-B (β-IC) intercalated cells in the CD. The major proteins expressed in the apical membrane in the PCs are ROMK (secretes K^+), AQP-2 and ENaC (reabsorbs H_2O and Na^+ respectively), in the basolateral membrane Na^+/K^+-ATPase (exchanges 3 Na^+ for 2 K^+). The apical membrane of the type-A IC cells expresses H^+ /K^+ -ATPase (secretes K^+ and H^+) and H^+ATPase (secretes H^+), the basolateral membrane express SLC26A7 (in the mouse) and kidney anion exchanger (kAE1) both functions as Cl^-/HCO_3^- exchanger. The apical membrane of the type-B IC cells expresses SLC4A8 (also known as Na^+ dependent Cl^-/HCO_3^- exchanger -NDCBE) and pendrin functions as Cl^-/HCO_3^- exchanger. The basolateral membrane express SLC4A8 (functions as Na^+/HCO_3^- exchanger), chloride channel (ClC) transports Cl^- and H^+ATPase transports H^+ to the interstitium. The figure was created in BioRender.com.

1.3.3 Ion homeostasis and blood pressure

The extent of renal excretion and reabsorption of ions varies to maintain an appropriate extracellular fluid volume and acid–base balance[11]. In the CDs, ICs and PCs regulate acid–base, fluid, and electrolytes homeostasis, respectively[7,35]. Interestingly, in this segment, reabsorption of sodium is partially separated from that of chloride. In PCs, sodium reabsorption takes place via ENaC[36], which results in the generation of a lumen-negative transepithelial potential (Fig. 2). This potential generates the driving force for potassium secretion via the apical channel ROMK and favors proton secretion from the ICs[11].

As detailed above, variations in blood pressure or an increase in plasma pH trigger the release of various hormones including aldosterone, insulin, and angiotensin II, which in turn regulate the function of ENaC[37,38]. Upon aldosterone stimulation, the serine-threonine kinase (SGK1) phosphorylates and thereby inhibits Nedd4-2, an ubiquitin ligase that normally ubiquitinates ENaC to initiate its degradation[39,40]. Thus, SGK1 activation results in increased abundance of ENaC at the apical membrane and further sodium reabsorption[41]. SGK1 has a small regulatory effect on ROMK as well[42]. Aldosterone also triggers the activity of basolateral Na^+/K^+-ATPase in PCs[43].

Chloride reabsorption takes place partially in a paracellular way through the tight junctions and transcellularly via type-B ICs[35,44]. The transepithelial potential generated by ENaC-mediated electrogenic sodium reabsorption is enough to promote lumen-to-blood flux of chloride ions, despite the unfavorable chloride concentration gradient[45]. Claudin-4 and -8 form the paracellular pathway for chloride permeation, which is regulated by a number of proteins including Cap1 and Kelch-like 3 (KLHL3)[46].

The transcellular chloride reabsorption pathway takes place through type-B ICs and is coupled with the electroneutral reabsorption of sodium in the mouse model. This process requires the concomitant action of apical pendrin and SLC4A8 and the basolateral SLC4A9 (although the stoichiometry of this transporter remains a matter of debate) and ClC-Kb in a process energized by the basolateral H^+-ATPase[35,47](Figure 1.2). Bicarbonate apically excreted in exchange for chloride uptake through pendrin is recycled back into the cells by SLC4A8 together with import of a sodium ion and in exchange for a chloride ion. Basolaterally, the sodium and bicarbonate ions are transported to the interstitium via SLC4A9 together with a chloride ion via ClC-Kb. This functional coupling of apical and basolateral transporters/channels results in the net and electroneutral transepithelial absorption of both sodium and chloride ions. This process is amiloride resistant, thiazide sensitive, and regulated by the Nedd4-2 ubiquitin ligase[48] . Of note, although SLC4A8 has been represented at the apical membrane of type-B ICs in Figure 1.2, its precise location remains to be confirmed and further studies confirming the location and contribution of each transporter need to be performed.

In parallel to ion reabsorption, water is also passively reabsorbed in PCs in a process regulated by arginine vasopressin[49]. An increase in plasma arginine vasopressin concentration activates the arginine vasopressin receptor 2 gene (AVPR2) , which triggers a cAMP-dependent cytosolic signaling cascade to relocate intracellular vesicles containing AQP2 to the apical membrane. The apical membrane then becomes more water permeable.

1.3.4 pH Homeostasis

With our acid-generating western diet, type-A IC is the predominant cell type that contributes to urinary acid secretion. In these cells, CO_2 diffuses into type-A IC and is hydrolyzed

via cytosolic CAII to produce H_2CO_3, which in turn dissociates to proton and bicarbonate. The bicarbonate ions are transported to the interstitial fluid in exchange for chloride via kAE1 at the basolateral membrane. On the other hand, the protons are secreted to the lumen via the apical proton pump H^+-ATPase and the H^+/K^+-ATPase. Both the pH difference across the apical membrane and the potential difference across the epithelium affect the function of the H^+-ATPase[50]. In the lumen, the secreted protons bind either to ammonia (NH_3) and generate ammonium (NH_4^+) or to phosphate ions (HPO_4^{2-}) to generate titratable acids that are excreted in the urine. The extent of urinary acidification is regulated by the ratio of type-A versus other CD cell types and by aldosterone[51]. Any malfunction of either of the three main contributors to pH acidification (CAII, kAE1, or H^+-ATPase) leads to defective pH homeostasis.

Acid-base homeostasis is a critical process for normal physiologic function[52]. The physiologic pH of the arterial blood ranges from 7.35-7.45, depending on the intracellular and the interstitial pH. Deviation from normal pH hinders the pH dependent pathways and associated proteins resulting in acidemia (pH lower than 7.35), arterial vasodilation, insulin resistance, compromised immune function and reduced neuronal excitability or alkalosis (pH higher than 7.45), myocardial blood flow and seizures[52].

The production of $[H^+]$ is triggered by the daily metabolism of carbohydrates, lipids, and proteins. Oxidative degradation of these biomolecules produce energy as ATP, CO_2 and water. Partial oxidation, ATP hydrolysis and acidic diet produce H^+ and HCO_3^-[53]. At a physiologic condition, the proportion of HCO_3^- and H^+ is equal, resulting in HCO_3^- binding to free H^+, thus reducing H^+ concentration and increasing pH[54]. The reaction of HCO_3^- and H^+ is reversible and forms carbonic acid (H_2CO_3), which dissociate to CO_2 and H_2O:

$$H^+ + HCO_3^- \Leftrightarrow H_2CO_3 \Leftrightarrow CO_2 + H_2O$$

In this reaction, bicarbonate serves as a buffer, protecting the physiologic processes from pH changes. The buffer system works both intracellularly and extracellularly[54]. The equation above is an example of an extracellular buffer system. During acidosis, when the plasma pH is less than 7.35, the buffer system will increase the pH by engaging more [H^+], thus moving the reaction to the right. However, in case of pH 7.45, the reaction will shift to the left, increasing [H^+] and lowering the pH[54]. Intracellular buffer systems rely on the intracellular buffer capacity of the cells. The excess [H^+] ions will bind to the amine or carboxyl group of intracellular proteins, and therefore will have a dwindled effect of the increased [H^+] or cytosolic acidic pH[53,54].

A change in physiological pH triggers a secondary response in the respiratory system. In comparison to the urinary system, this reaction to pH shift occurs quickly, between minutes to hours (may take up to few days). In case of acidosis, the lungs increase CO_2 excretion by rapid breathing, and reduce CO_2 excretion by slowing it down in alkalosis[54]. In addition to the respiratory system, the urinary system corrects pH shifts by allowing acids to be excreted by the kidneys, which helps to rectify acidosis. Both of these systems complement each other, with respiratory acidosis or alkalosis resulting from a disrupted respiratory system and metabolic acidosis or alkalosis resulting from a disturbed urine system[55].

1.3.4.1 In the Proximal tubule

The proximal tubules of the nephrons reabsorb the vast majority (80-85%) of the filtered HCO_3^- and maintain the acid-base balance[56]. The procedure is carried out in a roundabout method (Figure 1.3). In the presence of CAIV, the [H^+] released by the PT cells is buffered by HCO_3^- in the lumen, resulting in H_2CO_3. CO_2 and H_2O are formed when carbonic acid dissociates. CO_2 diffuses back into the cytosol across the plasma membrane, and in the presence of CAII, H_2O

forms H^+ and HCO_3^-[57]. The apical Na^+/H^+ exchanger (NHE3) secretes H^+ into the pre-urine, while the basolateral Na^+/HCO_3^- exchanger NBC1 secretes HCO_3^- into the interstitium in a 3:1 stoichiometric ratio. Through the basolateral $Na^{+/}K^+$-ATPase, reabsorbed Na^+ is released into the bloodstream.

The H^+ reaches the luminal fluid and is buffered by HCO_3^-, either in exchange for a Na^+ through NHE3 or by direct secretion, and the cycle continues. In contrast, cytosolic HCO_3^- is absorbed into the interstitium together with Na^+[57]. Several membrane proteins are involved in the whole process; for example, H^+ secretion is carried out by V-H^+-ATPase, while HCO_3^- reabsorption to the interstitium is facilitated by Na^+ dependent HCO_3^- co-transporter (NBCe1). Due to reabsorption of HCO_3^- and release of H^+, the pH of the luminal fluid in the distal section of the PT might drop to 6.7 from 7.4. Impaired HCO_3^- reabsorption in the proximal tubule can cause acidosis, known as proximal renal tubular acidosis (pRTA).[56]

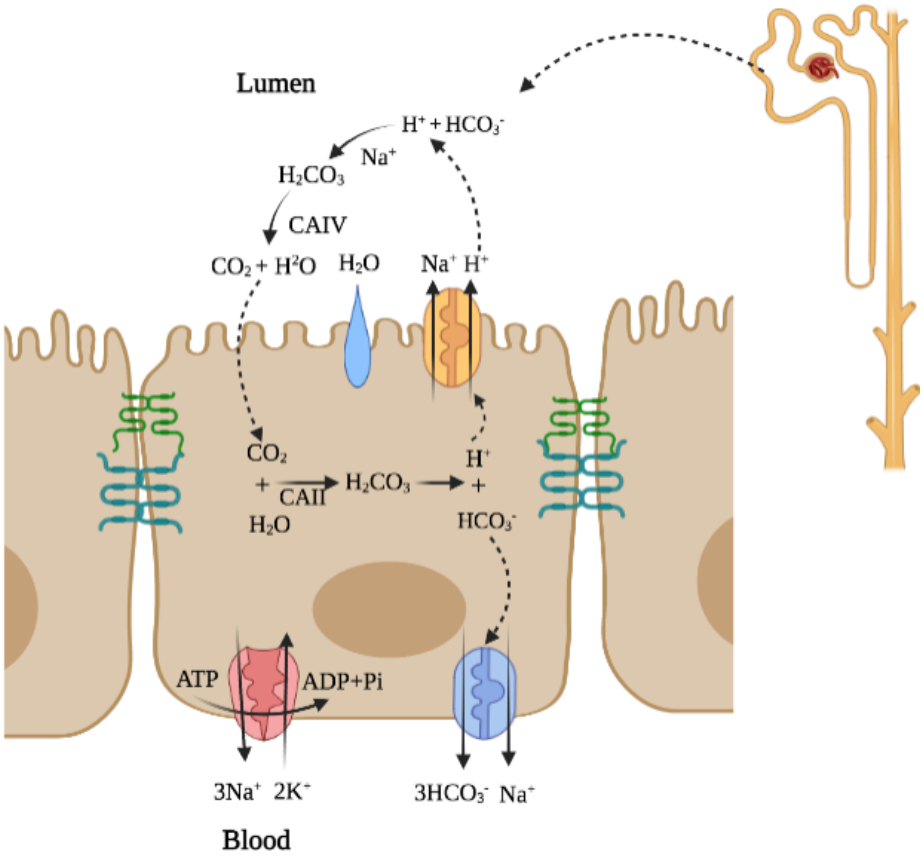

Figure 1. 3 HCO_3^- reabsorption in the PT cells

The epithelial cells in the PT regulate HCO_3^- reabsorption. In the presence of CAIV, H^+ and HCO_3^- produce H_2O and CO_2, which diffuses into the cells. Cytosolic CAII catalyzes H_2O and CO_2 and produce H_2CO_3 which dissociates into H^+ and HCO_3^-. The H^+ is secreted into the pre-urine through the apical Na^+/H^+ exchanger (NHE3) and the HCO_3^- is secreted into the interstitium through basolateral Na^+/ HCO_3^- exchanger NBC1 in a 3:1 stoichiometric ratio. The reabsorbed Na^+ through the NHE3 is secreted into the blood through basolateral Na^+/K^+-ATPase. The figure was modified from[58] and created in BioRender.com.

1.3.4.2 In the collecting duct

With our acid-generating Western diet, type-A IC is the predominant cell type that dictates the final urinary pH. In these cells, CO_2 diffuses into the type-A IC and is hydrolyzed via CAII in the cytosol producing H_2CO_3, which in turn dissociates to proton and bicarbonate (Figure 1.4).

The bicarbonate ions are transported to the interstitial fluid in exchange for chloride via kAE1 at the basolateral membrane. On the other hand, the protons are secreted to the lumen via the apical proton pump H^+-ATPase and the H^+/K^+-ATPase. Both the pH difference across the apical membrane and the potential difference across the epithelium affect the function of the H^+-ATPase[50]. The secreted protons bind to ammonia (NH_3) to produce ammonium (NH_4^+) or phosphate ions (HPO_4^{2-}) to produce titratable acids that are expelled in the urine in the lumen. The amount of acidity in the urine is regulated by the ratio of type-A vs other CD cell types, as well as by aldosterone[51]. Any malfunction of the three main contributors of pH acidification H^+-ATPase results in a disease characterized by a low blood pH called distal renal tubular acidosis (dRTA) (detailed in section 1.7). Various molecules are sensitive to intracellular and extracellular pH variations and affect IC's function and plasma pH. The soluble adenylate cyclase senses cytosolic bicarbonate concentration and indirectly acts on the apical H^+-ATPase[59]. Another example is the G protein-coupled receptor 4 whose deletion results in decreased renal acid excretion and metabolic acidosis in mice[60]. Additional pH sensors identified in the kidney are reviewed elsewhere[61].

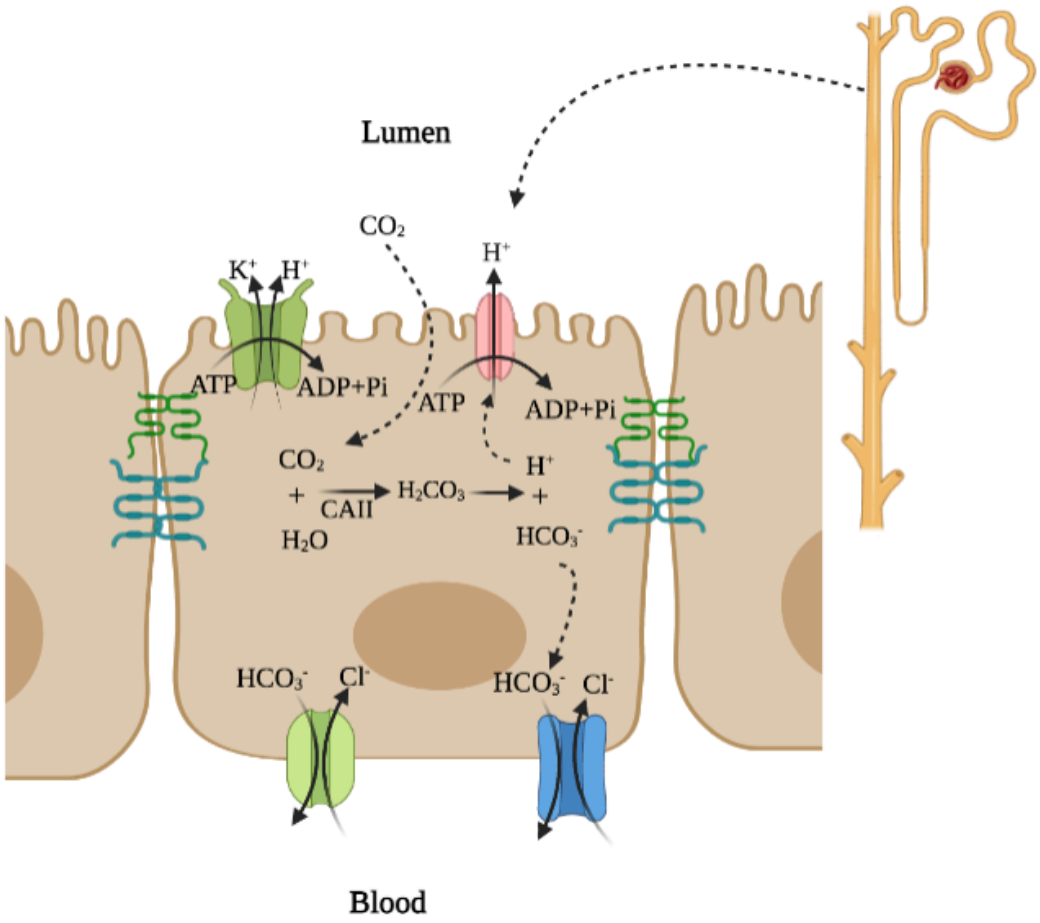

Figure 1. 4 Acid-base homeostasis in the Type-A IC cells in the collecting duct.

By secreting H^+ in the pre-urine, type-A cells in the CD maintain acid-base homeostasis. CO_2 diffuses across the plasma membrane in these cells. CO_2 and H_2O are converted by cytosolic CAII to carbonic acid (H_2CO_3), which is subsequently broken down into H^+ and HCO_3^-. The apical H^+ATPase secretes H^+ into the lumen, while the basolateral Cl^-/HCO_3^- exchangers, kAE1 (green transporter) and SLC26A7 (blue transporter) absorb HCO_3^- into the blood. The blue and green tight junction proteins correspond to claudins and occludins. The image was modified from[10] and created in BioRender.com.

1.4 Tight junctions

Epithelial cells cover the body surface by forming a barrier protecting from the external environment. All surfaces of internal organs such as the lungs, the gastrointestinal tract or the nephrons in contact with the external environment are also protected by an epithelial layer . This epithelial layer protects the internal environment from pathogens and maintains an optimal internal composition. Therefore, its permeability must be tightly regulated, including through the space separating adjacent epithelial cells. This space forms the 'tight junctions' (TJ as mentioned earlier)[62]. Tightness of these junctions varies between organs. For example, in the bladder, the barrier is absolutely impermeable[63]. In the proximal tubule, these junctions are highly permeable to enable optimal ion reabsorption. TJ can either be permeant to anions/cations or barrier to the ions. The transport process through TJ is known as 'paracellular' transport pathway.

Tight junction protein complex is composed of transmembrane proteins, scaffolding proteins and cytoskeletal proteins. There are 3 transmembrane proteins in the TJ complex, namely, the junctional adhesion molecules JAMs, TAMPs and claudins.

1.4.1 Junctional Adhesion Molecules (JAMs)

JAMs are a member of the immunoglobulin superfamily[64]. Structurally, the proteins have two extracellular immunoglobulin-like loops, a transmembrane domain and a cytoplasmic domain consisting of a **PDZ** [**P**ost synaptic density protein (PSD95), ***D****rosophila* disc large tumor suppressor (Dlg1) and **Z**ona Occludens-1 protein (ZO-1)] binding motif[65]. The localization of JAMs is not only limited to epithelial cells, but also in endothelial cells and in leukocytes. JAMs contribute to the TJs, and are involved in the transcytosis process of immune cells across an epithelial cell layer through TJs[64,65].

1.4.2 Tight-Junction Associated Marvel Domain-containing proteins (TAMPs)

There are 3 members in this protein family: occludins, tricellulins and MarvelD3[66–68]. These proteins share a similar structural topology having two extracellular loops, one intracellular loop with cytosolic N and C-termini. The N-terminus of the MarvelD3 protein is longer and C-terminus is shorter than the other two members of this group of proteins. Occludin localizes at the junction between two cells, whereas tricellulin localizes at the junction between 3 cells (hence the name)[67,68]. Co-immunoprecipitation experiments proved that MarvelD3 proteins interact with occludins and tricellulins and immunohistochemistry experiments showed that MarvelD3 protein colocalizes with occludins at the cell-cell junction[66]. *In vitro* studies with non-tight junction-forming fibroblast cells suggested that TAMPs proteins were unable to form tight junctions-like strands[69]. Occludin-null mice did not demonstrate any gross phenotype except for postnatal growth retardation, and electrophysiological studies suggested normal intestinal epithelium barrier function[70]. These studies advised that although the TAMPs are integral part of the TJ complex, their function is not required for tight junction formation or barrier function[69–71].

1.4.3 Claudins

These proteins were first identified in 1998 from the purified junctional fraction of chicken liver[72]. Transmembrane claudins are found in all epithelial and endothelial cells, and play a key role in TJ complexes[73]. The number of members in the claudin family varies between species, *e.g.,* 27 in humans[74] and 56 in pufferfish, *Fugu rubripes*[75]. The size of the claudin proteins also varies between 207 and 305 amino acids and a molecular weight from 20 to 28 kilodaltons. They also vary in sequence similarity and, are divided into ‘classic’ claudins with very common sequence similarity (cldn1-10, 14, 15, 17, and 19) and ‘non-classic’ claudins, not as close in sequence

similarity (cldn11-13, 16, 18, 20-27)[76]. Claudins can also form oligomers, by associating with the same (homotypic interaction) or different (heterotypic interaction) claudins within the same membrane (*cis*-interaction) or from the adjacent cell (*trans*-interaction)[76–78]. Upon exogenous expression in epithelial cells, claudins can either increase or decrease transepithelial electrical resistance (TEER) and can be selective to anions or cations, or act as blockers[74]. Topologically, claudin protein family shares a similar structure with four transmembrane domains, two extracellular loops (ECL1 and ECL2), a short N-terminus and a comparatively longer C-terminus[74,79]. All the claudins contain a conserved GLWCCC motif[80] that functions as Hepatitis C virus receptor, cell-cell contact (*trans* interaction) domain and in trafficking the protein to the plasma membrane[81] (Figure 1.5).

Fifty amino acids ECL1 is bigger in size than ECL2 and plays an essential role in ion selectivity [82]. Cldn-4 ECL1 carries a lysine in amino acid position 65 making it an anion selective pore and cation barrier, while Cldn-15 contains an aspartate at the amino acid position 64, which makes it a cation selective pore and anion barrier[82]. The ECL2 plays a role in *trans* interactions with another claudin from the neighboring cell[74]. Cldn-3 and 4 ECL2 also form a binding site for the *Clostridium perfringens* enterotoxin (CPE) [83,84].

Claudin C-terminus is comparatively longer than the N-terminus, however, its length varies among family members. The C-termini of cldn-12, 22, 25, and 27 have a PDZ binding domain that interacts with scaffolding proteins zona occludens-1, 2, 3 (ZO1-3)[85]. The C-terminus is critical for claudins to traffic to the plasma membrane, for their degradation and posttranslational modifications. Truncation of cldn-1, 5, 6, or 16 C-terminus results in endoplasmic reticulum retention and an inability to reach the plasma membrane supporting the role of this domain in

trafficking[86–88]. In Madin-Darby Canine Kidney II (MDCK II) cells, swapping cldn-4 C-terminus with that of cldn-2 increases the chimeric protein's half-life compared to intact cldn-2 [89].

Post translational modifications such as phosphorylation and lipid modification (palmitoylation) are essential for claudin's function and plasma membrane localization. Mutating cysteine residues from the second and fourth transmembrane domains impaired cldn-14 function. Phosphorylation sites vary between claudins and are not conserved[90,91]. Claudins' phosphorylation can either promote or inhibit their localization to the TJ and hence modulate the permeability function[91]. Claudin-16 localization is regulated by protein kinase A (PKA) phosphorylation at Serine 217, resulting in its delayed degradation[92]. In contrast, cldn-3 phosphorylation by PKA at Threonine 192 disrupts the TJ integrity via its removal from the TJ in ovarian cancer cells[93]. Phosphorylation of cldn-1-4 and 7 by with no –lysine-kinase 4 (WNK4) at Serine 206 causes an increase in Cl^- permeability[94,95].

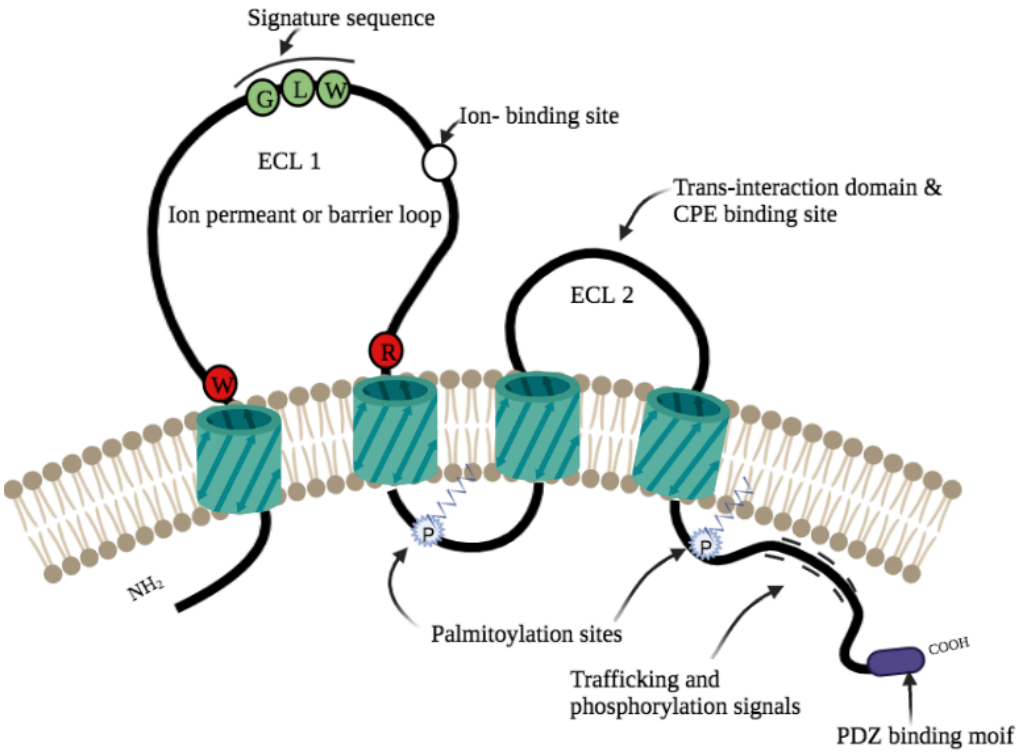

Figure 1. 5 Schematic diagram of claudin protein

The claudin proteins have 4 transmembrane domains (blue barrels) with two extracellular loops (ECL 1 and ECL 2). The N and C termini are intracellular, and the C-terminal have a PDZ domain. Post-translational modification sites (palmitoylation and phosphorylation) are both intracellular. All claudin proteins conserve the GLW (green circles) motifs in the ECL1. The figure is modified from[73] and created in Biorender.com.

1.4.3.1 Physiological consequences of claudins loss

The type and number of claudins expressed in specific tissues determine TJ permeability, as more than one claudin can be expressed in epithelial cells[71,96]. For example, cldn-1 deficient mice did not survive over a day after birth and had wrinkled skin because of the loss of epidermal barrier[71]. In cldn-5 deficient mice, a size-selective blood-brain barrier disruption occurs for small molecules (molecular weight below 800D)[97]. Mutations in cldn-14 causes non-syndromic recessive deafness DFNB29 as it is expressed in the sensory epithelium of the organ of Corti in the ear[98,99]. Cldn-11 knockout mice also showed autosomal recessive deafness resulted from the degeneration of cochlear hair[100]. Oligodendrocyte-specific protein (OSP)/cldn-11 is expressed in the myelin sheath of the central nervous system and Sertoli cells in the testis and lack of this gene results in a neurological and reproductive deficit in mice[101]. Claudin-18 null mice demonstrated atrophic gastritis as early as day 3 postnatal, decreased intragastric pH, and increased production of cytokines, interleukin-1β, cyclooxygenase-2 which collectively resulted in spasmolytic polypeptide-expressing metaplasia[102]. Claudin-15 plays a role in cell proliferation as was seen in cldn-15 null mice that develop mega intestine due to an increase in the epithelial cells in the upper intestine[103]. Cldn-2 knockdown *in vitro* and *in vivo* influenced epidermal growth factor receptor-mediated cell proliferation and tumorigenesis[104,105]. Expression of cldn-4 in thymocytes enhanced T-cell receptor-mediated ERK activation and proliferation in the fetal thymus organ culture model[106]. Cldn-2 deficient mice displayed significantly reduced sodium, chloride, and water reabsorption in the renal proximal tubule compared to the wild-type counterpart[107].

1.4.3.1 Claudin-4

Claudin-4 is localized in the intestine, lungs, skin and distal nephron in the kidneys[108]. Claudin-4 is an anion selective pore (Cl^-) and monovalent cation barrier (Na^+). The positively

charged lysine 65 on ECL1 dictates this selectivity[82].

Claudin-4 forms homotypic trans-interactions with cldn-4 from the neighboring cell but does not form homodimers within the same cells[109]. On the other hand, cldn-4 forms heteromeric *cis*-interactions with cldn-8 which is required for its TJ localization[107]. Cldn-8 knockdown in mouse inner medullary collecting duct (mIMCD3) cells resulted in mis-trafficked cldn-4 along with a reduced paracellular chloride conductance[107]. However, cldn-4 does not seem to be required for cldn-8's TJ localization in IMCD3 cells.

Total cldn-4 KO mice demonstrated urothelial hyperplasia, which resulted in urinary obstruction leading to hydronephrosis[110]. Although most urinary and plasma electrolytes were normal, they demonstrated an increase in Ca^{2+} and Cl^- fractional excretion (FE). Although there was no gross anatomical anomaly in the KO mice at the early stage of their life, the mortality rate was higher at 20 months age compared to WT littermates, due to urothelial hyperplasia and hydronephrosis[110]. Interestingly, in these mice, a decreased expression of cldn-8 at the TJ of the distal nephron was observed[107,110].

A PC-specific cldn-4 KO mouse was generated using the Flox/Cre system, where the PC predominant AQP-2 promoter regulates *Cre* gene expression[111]. These mice developed hypochloremia with increased luminal Cl^- leading to ENaC inhibition and increase of urinary Na^+. In addition, the KO mice displayed renal loss of water and hypotension. As plasma [Cl^-] was reduced, a compensatory increase in plasma HCO_3^- resulted in metabolic alkalosis[111].

Together, these studies highlight the significant role of cldn-4 in acid-base and electrolyte homeostasis in the distal nephron.

1.4.3.2 Acid/base, electrolyte homeostasis and tight junctions

The proteins expressed in both the apical and basolateral membranes of the distal nephron play an important role in acid/base and electrolyte regulation. However, until recently, the importance of TJ proteins in acid/base and electrolyte homeostasis and the possible interplay with apical/basolateral transporters remained unclear. A first evidence of a functional relationship between TJ and the kAE1 came from a serendipitous observation[112]. When polarized MDCK I cells expressing kAE1 wild type or kAE1 R901X mutant were apically biotinylated, a biotin leakage to the lateral membrane was observed in kAE1 wild type-expressing cells while cells expressing mislocalized kAE1 R901X did not. This observation suggested an increased permeability of the paracellular barrier when functional and properly located kAE1 was expressed. The TEER was also lower in the cells expressing kAE1 compared to the kAE1 R901X mutant[112]. Recently, our lab showed that in polarized mIMCD3 cells, inducibly expressing functional kAE1 increased paracellular permeability and lowered TEER through a cldn-4 dependent effect[113]. This effect was abolished when a functionally-dead mutant was expressed. Epithelial permeability to both Na^+ (P_{Na}) and Cl^- (P_{Cl}) was higher in cells expressing kAE1 protein compared to non-induced cells. A membrane yeast two-hybrid assay conducted by Dr. Reinhart Reithmeier (personal communication, University of Toronto, 2013) showed that kAE1 and cldn-4 physically interact with each other. Proximity ligation assay and immunohistochemistry exhibited co-localization of kAE1 and cldn-4[113]. Since ICs and PCs are functionally intertwined to regulate electrolytes homeostasis, and since kAE1 and cldn-4 are functionally and physically interacting, the role of IC cldn-4 in acid-base and electrolytes was questioned. Moreover, the loss of urinary calcium in total cldn-4 KO mice[110] remains un-explained.

1.5 Chloride-bicarbonate exchanger in the CD

Erythrocyte anion exchanger 1 (eAE1) is a prominent component of the erythrocyte membrane proteins, accounting for approximately 1.2 X 10^6 copies per cell[114]. On an electrophorogram of blood membrane fractions, the third band from the top corresponds to eAE1 hence its historical name as 'band 3' protein.[114]. There are 911 amino acids in this protein, with the first 360 comprising the cytosolic N-terminus, and the remainder crossing the lipid membrane and forming the short cytosolic C-terminus[115]. The eAE1 N-terminus interacts with the cytoskeletal proteins ankyrin[116], protein 4.1[117], protein 4.2[118] and GAPDH[119]. The kidney isoform of eAE1, kAE1 contains 846 amino acids, missing the first 65 amino acids of the eAE1 N-terminus. A promoter sequence located in the third intron of the 20 exon gene induces the expression of kAE1 in kidney cells[120]. A crystal structure of the AE1 protein has recently been published[121]. The structure revealed that the protein contains 14 transmembrane domain (TMDs). The TMDs are arranged into two sub-domains; the gate domain (TMD 5-7 and 12-14) and the core domain (TMD 1-4 and 8-11). Among these, the TMD 3 and 10 spanned half of the lipid bilayer and form two half helices (Figure 1.6)[121]. Kidney anion exchanger 1 (kAE1) is localized at the basolateral membrane of type A IC cells in the CD[122]. This protein is also expressed in podocyte cells in the outer layer of glomerular capillaries[123]. kAE1 function is synchronized with H^+-ATPase and CAII to maintain acid-base homeostasis[122] as previously described (Section 1.3.4.2).

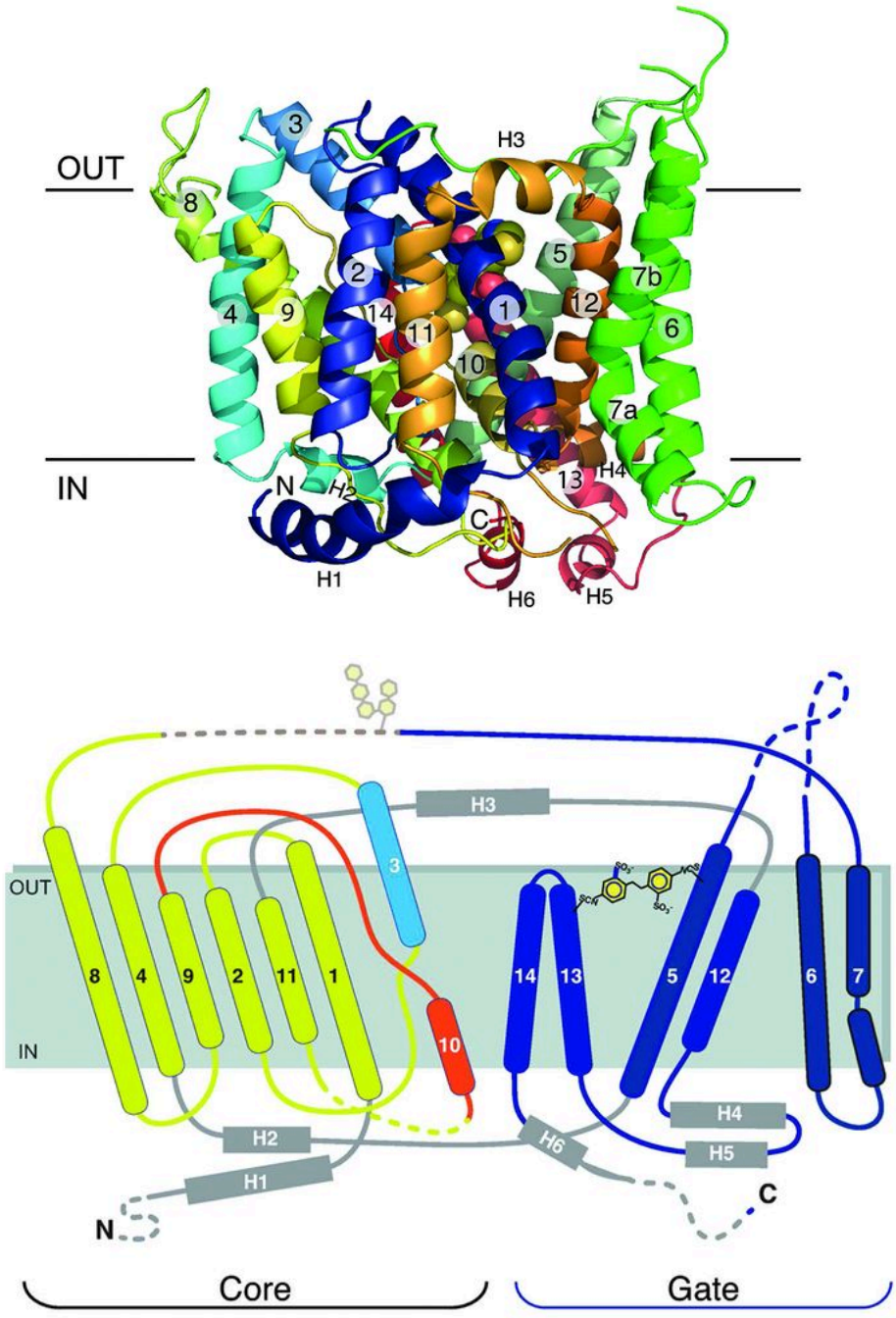

Figure 1. 6 AE1 topological model deduced from the crystal structure.

A) Structural details of the AE1 protein viewed from the membrane plane. B) Topological structure of the AE1 protein postulated from the crystal structure. The figures are adopted from[121] with permission.

1.5.1 kAE1 interactome

1.5.1.1 Amino-terminal cytosolic domain interactors

The N- and C-termini cytoplasmic domains of kAE1 carry binding motifs essential for membrane trafficking, localization and interactions with other proteins[123]. An N-terminal kAE1 interactor[124], the integrin-linked kinase (ILK) binds with the cytoplasmic domains of β-integrins and cytoskeleton associated proteins[125,126]. Although the interaction is required for kAE1 trafficking in HEK293 cells[124], deleting ILK interaction site within kAE1 sequence did not affect its trafficking in MDCK cells[127]. A component of the podocyte slit diaphragm, the single-spanning transmembrane protein nephrin interacts with the ILK/integrin complex[128,129]. In *Xenopus* oocytes co-expressing nephrin and kAE1 did not increase kAE1 function, however, in conditionally immortalized human podocyte cells, expression of kAE1 was dependent on nephrin. Yeast two hybrid assay, colocalization and immunoprecipitations confirmed that nephrin interacts with kAE1 in podocyte cells[123]. The kAE1 N-terminus also binds with ankyrin-G with 3 specific motifs and this interaction is required for its localization to the cell membrane[130].

1.5.1.2 Carboxyl-terminal cytosolic domain interactors

In line with the co-ordinated action of CAII, H^+ATPase and kAE1 in acid-base homeostasis, an interaction of kAE1 C-terminus with CAII was shown to increase kAE1 activity[122] although this concept has since been challenged[131]. A member of the peroxiredoxin protein family, peroxiredoxin 6 (prdx 6) co-localizes and interacts with kAE1 C-terminus, and is required for kAE1 function[132]. A prdx 6 KO mice demonstrated baseline acidosis with increased kAE1 expression. Upon an acid diet, prdx 6 abundance increased in WT mice, suggesting a strong interaction between these two proteins' expression, localization and function. However the

physiological role of this interaction remains unclear[132]. Glyceraldehyde 3 phosphate dehydrogenase (GAPDH) also interacts with kAE1 C-terminus and is essential for its membrane localization in mammalian kidney[133]. kAE1 C-terminus is also a binding site for the B1 subunit of the Na^+/K^+-ATPase and the interaction is required for both proteins‘ membrane localization and abundance[134]. The C-terminus of the kAE1 is also a docking site for adaptor proteins AP-1 μ1A, AP-3 μ1 and AP-4 μ1[135–138]. Adaptor proteins' binding is important for kAE1 trafficking intracellularly[136] and to the basolateral membrane[137]. Clathrin is another kAE1 interactor, a protein that interacts with adaptor protein complexes. Clathrin knockdown perturbs basolateral proteins polarity[137,139]. Finally, PDZ and LIM domains proteins 5 (PDLIM5) binds N-terminal interactor ILK as described above and is essential for its membrane targeting[140]. PDLIM5/ILK complex connects kAE1 N and C termini, thereby creating a multiprotein complex essential for kAE1 abundance and basolateral membrane localization[140].

1.6 SLC26A7

Solute-Linked Carrier (SLC) gene families contribute to CD's role in maintaining acid-base and electrolyte homeostasis. The sections above thoroughly described SLC4A1 gene encoding AE1 proteins and its role in electrolyte homeostasis in the CD. However, SLC26A gene family has also been reported to play a role in acid-base balance in intercalated cells[141]. Members of the SLC26 family that are involved in Cl^-/HCO_3^- are SLC26A4 (pendrin) and SLC26A7[142].

The SLC26 family is composed of 10 members, SLC26A1-11, SLC26A10 is considered as a pseudogene[143]. The expression of these genes is restricted to polarized epithelial cells and is tissue specific to organs such as the intestine, pancreas, thyroid gland and kidney[144]. The family members transport various substrates (ions or molecules) and vary in their mode of transport by acting either as exchangers or Co-transporter) for Cl^-, HCO_3^-, I^-, SO_4^-, oxalate, formate and

glyoxylate[142,145–147]. This thesis focuses on SLC26A7, the role of which is controversial based on the system tested. This protein either acts as a chloride channel in *Xenopus* oocytes[148] or as a Cl^-/HCO_3^- exchanger in mouse kidney OMCD cells[150]. The SLC26A7 protein is also expressed in gastric parietal cells[151] and in Reissner's membrane epithelium in the murine cochlea[152]. In the mouse kidney, SLC26A7 expression is detected the proximal tubule[149], basolateral membrane of the thick ascending limb[153], distal tubule[154], and in the medullary CDs after vasopressin induction[155]. In humans, the protein is localized in the ICs and colocalize with AE1[156]. This protein has 12 transmembrane domains with intracellular N- and C-termini (Figure 1.7). The second extracellular loop contains two N-linked glycosylation sites, at Arginine 125 and 131 positions. The C-terminus carries a sulfate transporter anti-sigma factor antagonist (STAS) domain[157]. Mutations in the SLC26A7 gene result in goitrous congenital hypothyroidism supporting a role of this gene in the thyroid gland[158].

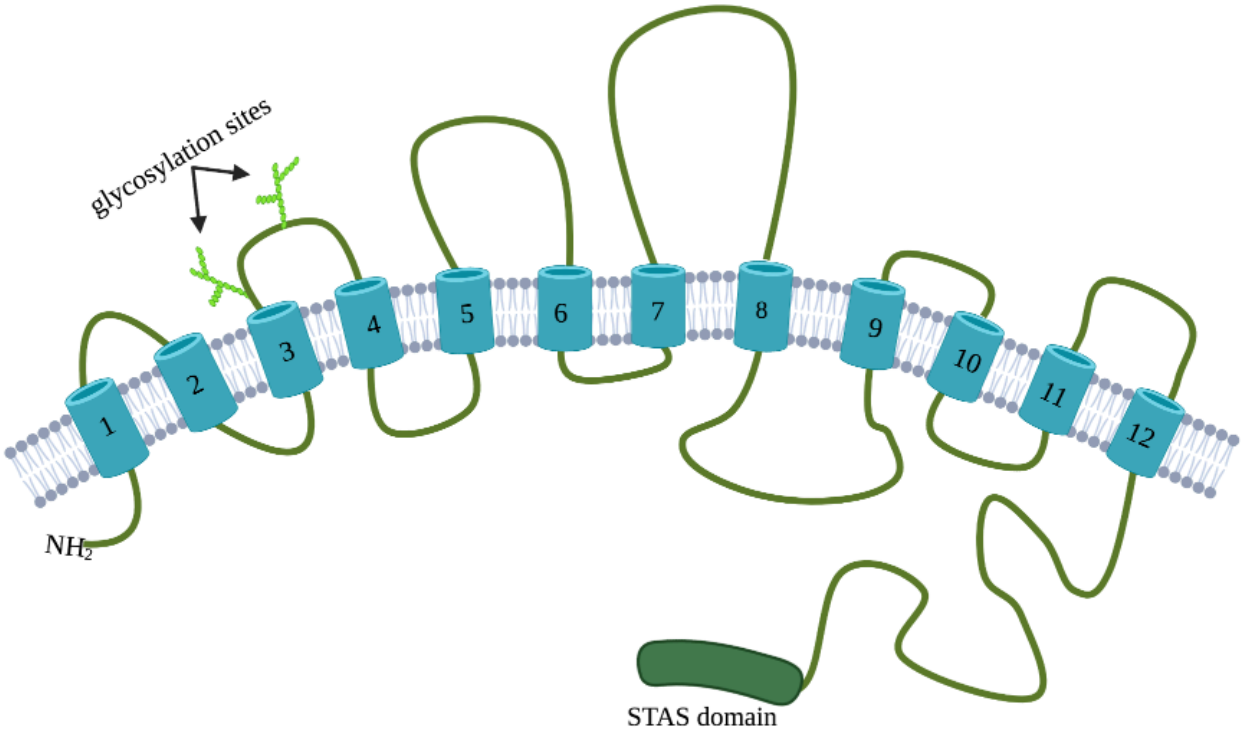

Figure 1. 7 Schematic diagram of the topology of SLC26A7 protein

The protein contains 12 transmembrane domains (blue), 6 extracellular and 5 intracellular loops with intracellular N and C- termini (green). Two glycosylation sites are between the 3rd and 4th TMD (green branch). The C-terminus contains a STAS domain. The figure was modified from[157] and created in Biorender.com.

1.7 Distal renal tubular acidosis (dRTA)

SLC26A7 or SLC4A1 gene mutations can lead to several diseases including blood and gastric disorders[159]. In this thesis, we will focus on a disease that is common between these two genes: distal renal tubular acidosis (dRTA). Type 1 dRTA results from a renal defect in acid secretion[160] and consequently in bicarbonate reabsorption in tubules of the distal nephron[161]. Mutations in the genes encoding either kAE1[162–164], the H^+-ATPase[165], or CAII[166] can result in dRTA. dRTA patients carrying dominantly or recessively inherited mutations develop renal stones, hypokalemia, hyperchloremia, nephrocalcinosis, metabolic acidosis, and a defective urine acidification in addition to facing difficulties to thrive[30]. Until now, 23 point or frameshift mutations in the SLC4A1 gene encoding kAE1 protein are reported to cause dRTA, in a homozygous, heterozygous, or compound heterozygous state[142,167–169]. Investigations in Madin–Darby canine kidney (MDCK) cells showed that dRTA-causing kAE1 mutants were either nonfunctional or mistrafficked to the apical membrane, the Golgi, or the endoplasmic reticulum[112,170,171]. Coexpression of dominant dRTA mutants with the wild-type (WT) kAE1 protein, thereby mimicking the situation found in patients with a dominant form of the disease, showed that the mutant affected the trafficking of the WT protein in these cells[172]. In contrast, coexpression of recessive mutants with kAE1 WT, as found in parents of patients with recessive dRTA, showed that the WT protein rescued the mutant's trafficking. These findings provided a molecular mechanism for development of dRTA.

However, recent *in vivo* findings challenged our understanding of dRTA pathophysiological mechanisms. Indeed, when expressed in mouse inner medullary collecting duct (mIMCD3) or mouse cortical collecting duct M1 cells, the dominant mutant kAE1 R607H (corresponding to the human dominant kAE1 R589H dRTA mutation) showed a normal function

and proper targeting of the protein to the basolateral membrane[173]. This mutant was previously reported to be retained in the ER in MDCK cells[112,171]. Moreover, in a kAE1 R607H knockin mouse model that developed dRTA upon acid challenge, the protein was properly targeted to the basolateral membrane, although its expression level was lower compared with WT mice[173]. In fact, these mice had a lower amount of H^+ATPase and were unable to relocate this protein to the apical membrane upon acid challenge. The number of type-A ICs in these mice was significantly lower in comparison with the WT mice. A recent study investigating the interactome of the H^+-ATPase identified the nuclear receptor coactivator 7 as an interactor[174]. A targeted deletion of this protein in mice resulted in incomplete dRTA[175]. These recent findings may be the first step towards deciphering the functional link between basolateral kAE1 and apical targeting of the H^+ATPase. Therefore, our understanding of the pathophysiology associated with dRTA remains obscure and further studies will be necessary to fully understand the molecular mechanisms of this complex disease.

The CAII enzyme is found in the cytosol of the PT cells, loop of Henle, and the ICs of the CD[176]. CAII converts CO_2 and water into bicarbonate and protons in PT cells and ICs. Accordingly, the lack of or dysfunction of CAII results in an impaired bicarbonate reabsorption and acid secretion[177], defined as type 3 RTA. Patients with type 3 RTA have acidemia, alkaline urine, osteopetrosis, cerebral calcification, and mental retardation. Beside the kidney, tissues, and organs affected in type 3 RTA correlate with tissue expression of the CAII. A recent study of CAII deficient mice showed that CAII also plays a significant role in urine concentration[178]. In addition to type 3 RTA, these mice had polyuria and polydipsia without altered sodium or calcium reabsorption/excretion, indicating that they had a specific defect in water reabsorption.

1.8 Calcium homeostasis

One of the most significant electrolytes, calcium plays a versatile role in direct and indirect signaling pathways in critical cellular reactions[179]. Calcium participates in dispersing action potential, mediating co-factor function and transducing intra- and extracellular signal as a secondary messenger[180]. As a result, calcium homeostasis is highly regulated and approximately 99% of calcium is stored in bone[181]. The remaining 1% is found in the extracellular and intracellular regions in non-ionized and ionized forms[182]. Normal human body contains 1000-1200 g of calcium[183]. Calcium homeostasis in the body involves three organs: 1) the intestine 2) the bones and 3) the kidneys, orchestrated by three major mechanisms: 1) absorption/reabsorption and storage, 2) hormonal regulation of the transport and 3) calcium sensing[181]. Combined action of the intestinal absorption, renal reabsorption and exchange between bone and plasma under the influence of calciotropic hormones Vit-D3 and parathyroid hormone (PTH)[183] regulate the amount of calcium in the body (Figure 1.8). Upon ingestion, 20-25% dietary calcium is absorbed along the small intestine by active transcellular (through the cell) and passive paracellular (between the cells) routes. The amount of calcium absorbed depends on the age of the individual, the amount of calcium and vit-D intake, and circulating levels of calciotropic hormones (Vit-D3 and PTH)[181–183].

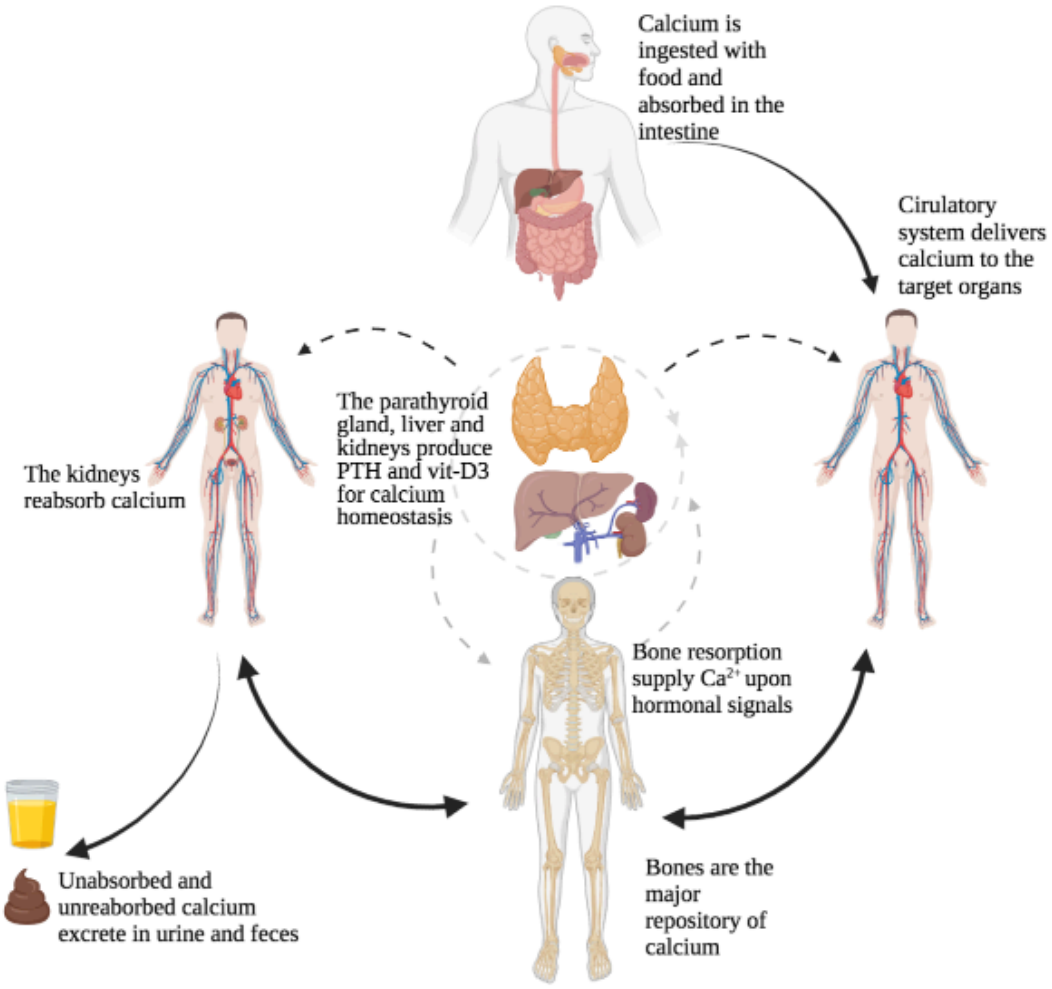

Figure 1. 8 Schematic diagram of calcium homeostasis in the human body.

Calcium homeostasis involves three major organs in the body: the intestine, the bones and the kidneys with the hormonal control from blood. Calcium is ingested with food and after being absorbed by the intestine the unabsorbed portion leaves the body with feces. Vit-D3 and PTH (with the involvement of the liver, kidneys and the parathyroid gland) regulate the calcium level in the blood. A significant proportion of the absorbed calcium is stored in the bones and a portion is reabsorbed in the kidneys. Depending on the requirements of the body, a portion of the non-reabsorbed calcium exits through urine. The figure was created in BioRender.com.

1.8.1 Calcium homeostasis in the kidney

In both the intestine and the kidneys, calcium transport takes place through the transcellular and paracellular pathways[184]. In the intestine, calcium transport occurs through transcellular or paracellular routes[184]. In the kidney, the transport process varies between nephron segments. In the PT, approximately 60-70% and in the TAL approximately 25% calcium is reabsorbed paracellularly (Figure 1.9 A)[182,184]. In the DCT and CT up to 10-15% calcium is reabsorbed through the transcellular pathway[185]. Paracellular transport of calcium in the PT is carried out principally by tight junction protein cldn-2[184]. In the TAL cldns-14, 16, and 19 regulate the transport process[184]. In the DCT and CNT, transmembrane proteins in the apical and basolateral sides TRV5/6, sodium-calcium exchanger (NCX), plasma membrane calcium channel (PMCA) and intracellular protein calbindin mediate the transepithelial transport[184,185]. In the CD the amount of calcium reabsorption is very small to none[185]. Proteins residing in the CD epithelial cells are mainly involved in maintaining acid-base homeostasis by acidifying urine[186]. However, defects in urinary acidification, such as in dRTA, is often associated with hypercalciuria via an unknown mechanism[185]. As total cldn-4 knockout (KO) mice demonstrated hypercalciuria[110], calcium homeostasis and regulation are detailed in the next section.

1.8.2 Paracellular transport and claudins in calcium renal transport

Paracellular transport of ions is facilitated by highly regulated tight junction proteins[187]. In the isolated and perfused PT of cldn-2 KO mice, cation, NaCl and water[188] permeability was reduced and the mice became hypercalciuric which suggests that cldn-2 mediates paracellular transport of calcium in the PT (Figure 1.9 B)[103,184,187]. Recent studies suggest that, both cldn-2 and 12 facilitate paracellular Ca^{2+} transport independently yet complementing each other[189]. In the TAL, calcium reabsorption is facilitated by the lumen positive transepithelial voltage gradient

generated by the concerted action of the apical potassium channel (ROMK), sodium potassium chloride cotransporter (NKCC2), and basolateral chloride barttin channel[184,187]. Cldn-16 and 19 facilitate transepithelial permeability to calcium (Figure 1.10 A)[184]. However, upon hypercalcemia, activation of the calcium-sensing receptor (CaSR) results in cldn-14 expression and localization at the tight junction, which then inhibits paracellular calcium flux from lumen and sodium flux from blood (Figure 1.10 B)[190,191]. In the DCT and CNT, calcium transport (~10%) is transcellular which is carried out in three consecutive steps: 1) entry through apical TRPV5/6 channels[192,193], processing by calbindin proteins intracellularly[194], and 3) exit through the basolateral PMCA1 and NCX1 channels (Figure 1.11)[188,195]. Vitamin-D and PTH regulate the plasma level of calcium [196].

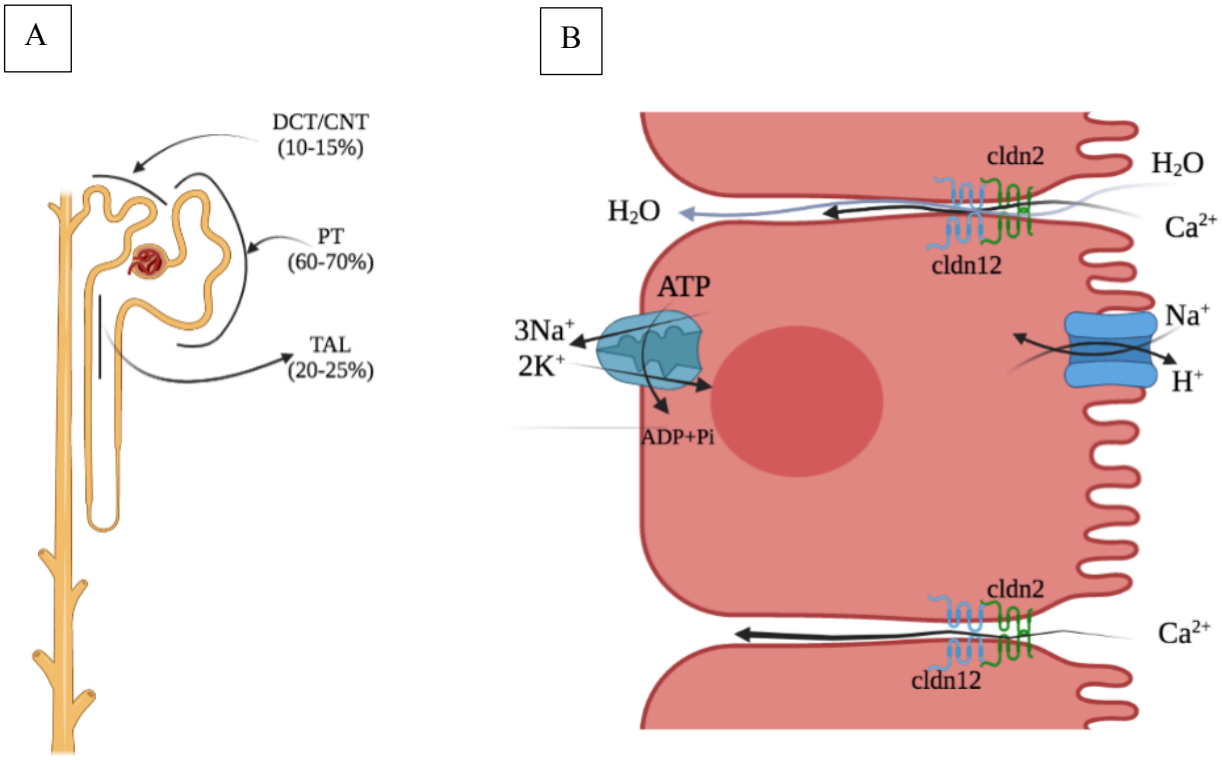

Figure 1. 9 Schematic diagram of calcium reabsorption along nephron segments.

A, schematic diagram of the nephron with corresponding amounts of calcium reabsorbed along the tubule. B, schematic diagram of PT cells with key proteins involved in calcium reabsorption. The blue apical protein is Na^+/H^+ exchanger is NHE3. The basolateral blue protein is Na^+/K^+-ATPase. Paracellular passage of Ca^{2+} is facilitated by both cldn-2 and cldn-12.The figure is modified from[184] and created in Biorender.com.

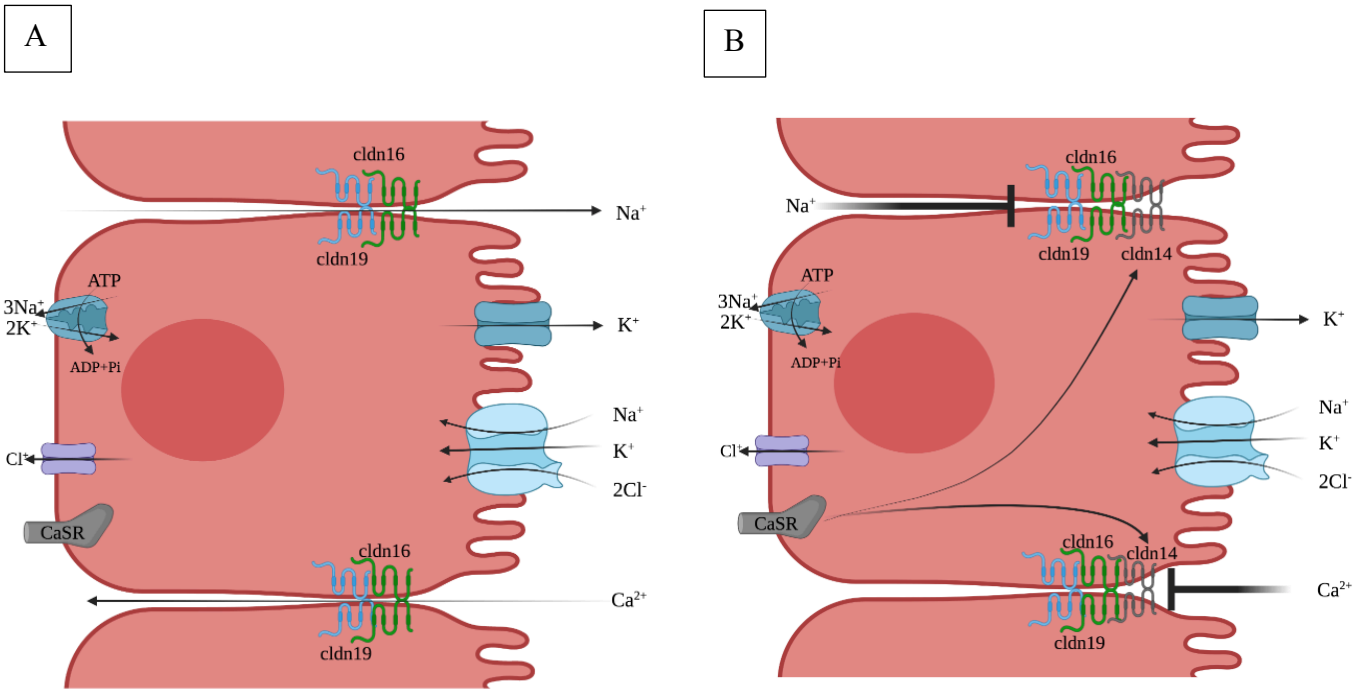

Figure 1. 10 Calcium reabsorption in the TAL.

A) Schematic diagram of calcium reabsorption in the TAL at normocalcemia condition. Paracellular calcium flux is mediated by the pores created by cldn-19 and cldn-16. B) In hypercalcemic condition, the Ca^{2+} sensing receptor (CaSR) is activate and signals to increase the cldn-14 expression in the tight junction along with cldn-16 and 19. Cldn-14 blocks the paracellular transport of Ca^{2+}, (also prevents back flux of Na^{+}) which result in increased calcium in the urine. The figure was modified from[184] and created in Biorender.com.

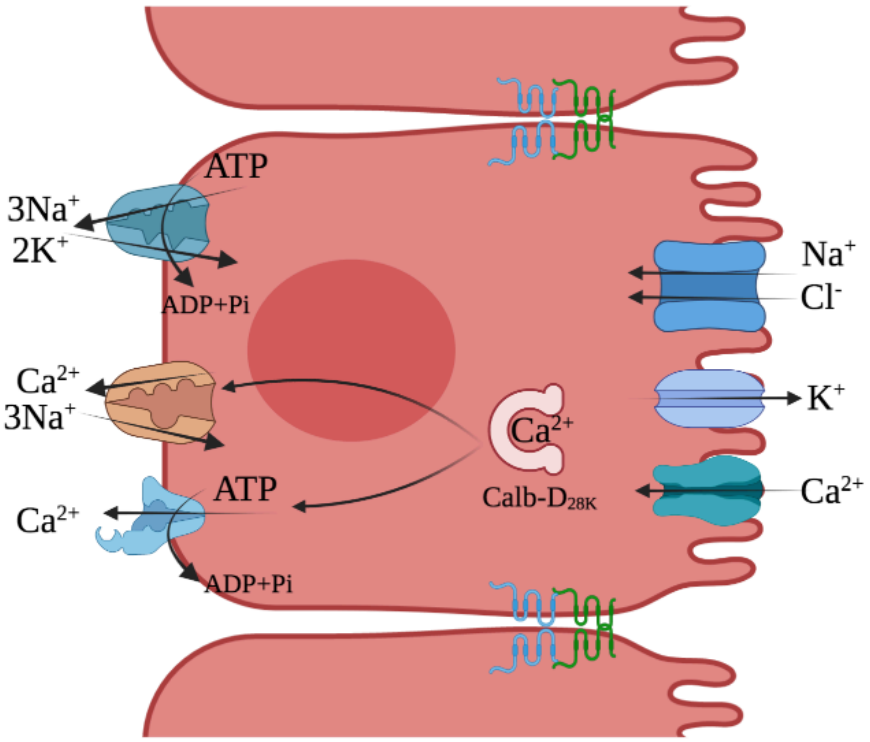

Figure 1. 11 Calcium reabsorption in the DCT/CNT

In the DCT/CNT, calcium reabsorption takes place via transcellular route. At the apical membrane calcium is reabsorbed by the TRPV5 protein (turquoise). Intracellular Calbindin-$D_{28}K$ ferries the calcium to the basolateral side of the cell. On the basolateral membrane calcium is transported to the interstitium via PMCA1 (ATP driven plasma membrane calcium channel, light blue protein) and NCX (Na^+ Ca^{2+} exchanger, orange protein). The Na^+ exchanged for Ca^{2+} is recycled via the Na^+/K^+-ATPase (blue protein). The image is modified from[185] and created in Biorender.com.

1.8.2 Calcium handling in the intestine

Daily dietary intake of calcium is reabsorbed through the intestine via transcellular and paracellular routes[184,197]. The transcellular route is active and takes place if dietary intake is low[198]. On the other hand, the paracellular route is passive and happens when dietary calcium intake is high[198]. The extent of calcium reabsorption depends on several factors, such as the "intraluminal calcium concentration, the solubility of calcium, the permeability of tight junction and sojourn time"[184,199]. The sojourn time varies in different segments. For example, in rats receiving a high calcium diet, sojourn times corresponded to 3 minutes in the duodenum, 43 minutes in jejunum, 141 minutes in ileum, 92 minutes in cecum and 92 minutes in colon[184,198]. Upon a calcium-replete diet, calcium absorption predominantly occurs through a passive paracellular route[200]. *In vivo* and *in vitro* experiments conducted upon various calcium diets suggested that the paracellular transport in different intestinal segments is driven by either transepithelial voltage difference (-5 to -20 mv) or solvent drag (dragging ions paracellularly together with flow of water)[184]. Overall, in the intestine, sodium absorption through the sodium/glucose transporter 1 (SGLT1) and sodium/proton exchanger 3 (NHE3), create an osmotic gradient promoting water reabsorption which allows the paracellular calcium passage in presence of cldn-2 and 12[184]. However, in the duodenum and cecum, transcellular calcium absorption occurs through apical TRPV6, intracellular calbindin D_9-K and basolateral PMCA1[184,201,202].

1.8.3 Hormonal regulation of calcium absorption

The active form of 1α,25-dihydroxy vitamin D, also called calcitriol, is synthesized in the proximal tubule. Calcitriol is produced by converting 25-hydroxyvitamin D3 to 1α,25-dihydroxy vitamin D with the enzyme 1α-hydroxylase[203]. Calcitriol acts on the gastrointestinal system by

increasing calcium absorption, calcium reabsorption in the renal tubule and resorption from bones, thus increasing plasma calcium level. The parathyroid hormone also plays a role in increasing plasma calcium concentration by activating 1α-hydroxylase enzyme, thereby promoting 1α,25-dihydroxy vitamin D production.[204]. The plasma level of calcium is kept in a very narrow range since it is a crucial molecule for many cellular and physiological functions. When plasma calcium level is elevated, calcitriol release inhibits parathyroid hormone production, wanes down intestinal absorption and renal reabsorption and brings plasma calcium level to normal. Together, this hormonal regulation system keeps plasma calcium concentration at a physiologic range of 2.4-2.5 mM (total calcium)[179,203,204]

1.9 Hormonal production by the kidneys and hormones regulating the kidney

1.9.1 Thyroid hormones and erythropoietin

Literature supports a clear interplay between hormones and the kidneys[205]. Thyroid hormones (thyroxine and triiodothyronine) are greatly involved in the development of the kidney in terms of kidney weight, mitotic index and kidney size in young rats[206] as well as during morphologic development in adults[207].

Interstitial cells in the kidneys secrete erythropoietin in the peritubular capillaries which is necessary to produce and mature erythrocytes in the bone marrow[208]. The interstitial cells are able to sense a subtle change in the oxygen levels and as a result, adjust erythropoietin production. In pathological conditions such as upon anemia, heart failure or chronic obstructive pulmonary disease, the interstitial cells sense a drop in oxygen levels, and increase production of erythropoietin. More erythropoietin signals the bone marrows to synthesize more erythrocytes to reinforce oxygen transport function[2,208].

1.9.2 Hormonal regulation of the CD cells

The mineralocorticoid receptor (MR) expressed in the basolateral membrane of CD cells mediates the renin-angiotensin-aldosterone system (RAAS) response in this nephron segment. MR and the glucocorticoid receptor (GR) signal the kidneys to regulate volume depletion and potassium secretion[209–211]. ENaC in the PC is activated by the mineralocorticoid aldosterone, which also increases paracellular transport of Cl^-, H^+ secretion by the H^+ATPase in the intercalated cells and activates basolateral Na^+/K^+-ATPase[212,213]. Aldosterone is also secreted in hyperkalemic conditions and activates ENaC, which in turn creates an electronegative lumen favoring K^+ secretion via the apical ROMK and calcium activated K^+ channel (BK) [212]. In K^+ depleted diet condition, type A IC function increases by increasing maxi-K channel expressed in both PCs and ICs)[214].

The H^+ATPase abundance is increased as a result of angiotensin II secretion[215]. Similarly, aldosterone released during metabolic acidosis also increases pendrin and H^+ATPase activity[216,217]. Additionally, paracrine signals promote the coordination of CD cells' functions[35]. Paracrine factor prostaglandin-E2 (PGE2) secretion increases Na^+ reabsorption and osmotic water permeability in rabbit CD cells[218].

The renin-angiotensin-aldosterone (RAAS) system regulates blood volume[219]. Decreased blood pressure activates the juxtaglomerular cells (JG) cells that are attached to the afferent arterioles and initiates cleavage of precursor prorenin to active renin. The renal sympathetic nerve activity regulates the production of renin in combination with renal blood pressure and Na^+ concentration in the lumen. Reduced plasma Na^+ concentration activates the renal sympathetic nerves and renin is produced from the stimulated JG cells. Sodium-sensitive macula densa cells that are located at the top of the thick ascending limb, are also activated by low luminal Na^+ levels

and activate the adjacent JG cells to produce renin. Renin synthesis initiates the RAAS cascade: The renin-angiotensin-aldosterone (RAAS) system consists of the compounds renin, angiotensin II and aldosterone, regulates the blood volume[219]. Liver-produced plasma angiotensinogen is converted to angiotensin I by released renin. Angiotensin converting enzyme converts angiotensin I to angiotensin II. Angiotensin II induces arteriolar constriction and aldosterone secretion to regulate the blood pressure. The mechanism involves the juxtaglomerular (JG) cells residing in the afferent arterioles. Decreased blood pressure activates the JG cells and initiate cleavage of inactive prorenin to active renin and released into blood. Circulating blood carries angiotensinogen which is produced in the liver. Renin cleaves angiotensinogen into angiotensin I which is next catalyzed to angiotensinogen II, the active form of angiotensin, by the angiotensin converting enzyme (ACE). In the PT, angiotensinogen II increases the activity of Na^+/H^+-exchange, thus increasing Na^+ absorption. An elevated concentration of plasma Na^+ increases the plasma osmolarity resulting in an increase of blood volume and extracellular fluid (ECF) volume and high blood pressure. Angiotensin II also stimulate the adrenal cortex to release aldosterone. Aldosterone acts on the CNT/CD cells by increasing luminal sodium channel ENaC and basolateral Na^+/K^+-ATPase leading to increased Na^+ reabsorption and K^+ secretion. Angiotensin II also stimulates the pituitary gland to release antiduretic hormone (ADH), also called vasopressin, that acts on the CD to increase AQP-2 protein abundance, water reabsorption and the ECF volume. The interplay between all these hormones thus helps the body to maintain optimal sodium concentration, water and blood pressure[219].

2.1 Hypotheses and Research questions

Our general hypothesis is that altering proteins involved in either the transcellular (SLC26A7) or the paracellular pathway (Claudin-4) will affect electrolyte homeostasis.

2.1.1 Hypothesis 1

Chloride/bicarbonate exchangers SLC26A7 and kAE1 are both expressed in type-A intercalated cells in the CD. However, when kAE1 is unable to maintain pH homeostasis as in dRTA, SLC26A7 is not able to correct the acidosis. We hypothesize that *SLC26A7 expression is downregulated in acidic condition and is therefore unable to compensate for the acidosis. .*

2.1.1.1 Research questions

1. Is SLC26A7 a chloride/bicarbonate exchanger in renal epithelial cells at the basal state?
2. What is the role of SLC26A7 in renal epithelial cells in relation to kAE1 in normal, hypertonic and acidic conditions?
3. Why SLC26A7 is unable to compensate the loss of kAE1 in dRTA situation?

2.1.2 Hypothesis 2

Total KO of murine cldn-4 results in hydronephrosis, hypocalcemia and hypercalciuria and elevated urinary chloride[110]. PC-specific cldn-4 KO mice display increased urinary volume and higher fractional excretion of sodium and chloride[111]. Together, these studies suggest that cldn-4 plays a significant role in the collecting duct in sodium, chloride and calcium reabsorption. However, its role in the intercalated cells is still unknown. We hypothesize that *intercalated cells cldn-4 plays a significant role in pH homeostasis and salt balance.*

2.1.2.1 Research questions

1. What is the role of cldn-4 in the intercalated cells?

2. Are the IC specific cldn-4 KO mice able to reabsorb sodium and chloride as efficiently as the wild type mice?
3. Does IC cldn-4 participate in calcium and acid/base homeostasis?

CHAPTER TWO

SLC26A7 PROTEIN IS A CHLORIDE/BICARBONATE EXCHANGER AND ITS ABUNDANCE IS OSMOLARITY- AND pH-DEPENDENT IN RENAL EPITHELIAL CELLS

Abstract

Acid-secreting intercalated cells of the CD express the chloride/bicarbonate kidney anion exchanger1 (kAE1) as well as SLC26A7, two proteins that colocalize in the basolateral membrane. The latter protein has been reported to function either as a chloride/bicarbonate exchanger or a chloride channel. Both kAE1 and SLC26A7 are detected in the renal medulla, an environment hyper-osmotic to plasma. Individuals with mutations in the SLC4A1 gene encoding kAE1 and mice lacking *Slc26a7* develop distal renal tubular acidosis (dRTA). Here, we aimed to (i) confirm that SLC26A7 can function as chloride/bicarbonate exchanger in Madin-Darby canine kidney (MDCK) cells, and (ii) examine the behavior of SLC26A7 relative to kAE1 wild type or carrying the dRTA mutation R901X in iso- or hyper-osmotic conditions mimicking the renal medulla. Although we found that SLC26A7 abundance increases in hyper-osmotic growth medium, it is reduced in low pH growth conditions mimicking acidosis when expressed at high levels in MDCK cells. In these cells, SLC26A7 exchange activity was independent from extracellular osmolarity. When SLC26A7 protein was co-expressed with kAE1 WT or the R901X dRTA mutant, the cellular chloride/bicarbonate exchange rate was not additive compared to when proteins are expressed individually, possibly reflecting a decreased overall protein expression. Furthermore, the cellular chloride/bicarbonate exchange rate was osmolarity-independent. Together, these results show that (i) in MDCK cells, SLC26A7 is a chloride/bicarbonate exchanger whose abundance is up regulated by high osmolarity growth medium and (ii) acidic extracellular pH decreases the abundance of SLC26A7 protein.

2.1 Introduction

Type-A intercalated cells in the CD of the kidney regulate the amount of acid excreted in urine, via the concerted action of cytosolic carbonic anhydrase II, apical v-H^+-ATPase and the basolateral kidney anion exchanger 1 (kAE1)[161]. Mutations in the genes encoding these proteins can lead to distal renal tubular acidosis (dRTA)[220], a dominantly or recessively inherited disease characterized by metabolic acidosis, hypokalemia, hyperchloremia and failure to thrive[142]. In addition to kAE1, SLC26A7 protein is also expressed at the basolateral membrane of the same cells in the hypertonic medullary CD of rat and mouse kidneys[150,220]. SLC26A7 is a 14 transmembrane domain-containing protein[157] with two N-linked glycosylation sites at positions N125 and N131, in its second extracellular loop and a cytosolic carboxyl (C)-terminal STAS (sulfate transporter anti-sigma factor antagonist) domain. In addition to the kidney, SLC26A7 is also expressed in gastric parietal cells[151], mouse cochlea[152] and plays an important role in enamel maturation[221] and in thyroid hormones synthesis[158,222]. SLC26A7 protein behaves as an osmolality-sensitive chloride/bicarbonate exchanger in rat kidney outer medullary CD cells and either as a chloride/bicarbonate exchanger or a chloride channel in *Xenopus* oocytes and human embryonic kidney (HEK) cells[148,150]. When heterologously expressed in *Xenopus* oocytes and in polarized MDCK cells exposed to a hypertonic extracellular environment, SLC26A7 relocated from endosomes to the plasma membrane in a MAP kinase dependent pathway[150,223]. Although a role of SLC26A7 in renal acid excretion was unveiled in *Slc26a7* knockout animals which developed dRTA[220], individuals carrying a mutated *SLC26A7* gene have a normal acid-base status but develop a goitrous congenital hypothyroidism[158,222]. An isoform of the erythroid Band 3, kAE1 is a 14 transmembrane dimeric glycoprotein[121]. It participates in urine acidification via physical and functional coupling to cytosolic carbonic anhydrase II[224], which produces protons and bicarbonate

from water and carbon dioxide, and to the apical v-H^+-ATPase. Mutations within the kAE1 transmembrane domain, or its short C-terminal domain cause dRTA[164,225]. It has been proposed that in heterozygous individuals carrying recessive mutations, the wild-type (WT) allele rescues trafficking or function of the mutated protein, while in dominant cases, the mutant prevents normal trafficking of the WT protein, thereby causing the disease[172]. A number of dominant dRTA mutations are located within the short cytosolic C-terminal domain of kAE1, which appear to cause mis-trafficking of the protein[112,167,168,226–229]. Among these, the dominant C terminally truncated kAE1 R901X mutant, is partially functional but mis-traffics either to the apical membrane or both apical and basolateral membranes of polarized Madin-Darby canine kidney (MDCK) cells[112,170], while being partially retained intracellularly in non-polarized cells[228]. Although the cause of the mis-trafficking remains unclear, this truncation removes a potential Post-Synaptic-Density-95/ Discs-large/Zona-Occludens-1 (PDZ) binding site, a phosphorylatable tyrosine (Y904) and a µ1A adaptor protein binding site (Y904DEV907) from the protein[127,135,136,144,230]. Patients with mutations within the SLC4A1 gene and Slc26a7 knockout mice develop dRTA[220,231,232], but human patients with mutated SLC26A7 do not[158]. Recent evidence supports a loss of type-A intercalated cells in dRTA patients' or mouse kidneys, in an un-explained mechanism[173,233]. Although the two proteins are reported to act as chloride/bicarbonate exchangers, the relative roles of SLC26A7 and kAE1 proteins in the medullary CD cells are unknown. While expression of SLC26A7 in human type-A intercalated cells remains unknown, both Human Protein Atlas (https://www.proteinatlas.org/ENSG00000147606-SLC26A7) and Nephroseq database (https://www.nephroseq.org/resource/login.html) report the presence of mRNA encoding SLC26A7 protein in the human kidney and the renal cortex and medulla, respectively. Therefore, assuming that SLC26A7 is expressed in human type-A intercalated cells, we aimed to clarify the

role of SLC26A7 protein in renal epithelial cells relative to kAE1 in normal, hypertonic (mimicking the hypertonic renal medulla) or acidic (mimicking acidosis) growth conditions. We examined the abundance, localization and function of SLC26A7 in control MDCK cells grown in normal or hypertonic conditions to mimic the extracellular environment of the outer medullary CD. As untreated dRTA patients are acidotic, we also investigated the behavior of SLC26A7 expressed in cells grown at pH lower than 7.2. Finally, we assessed the abundance of SLC26A7 protein and the level of chloride/bicarbonate exchange in MDCK cells co-expressing SLC26A7 and kAE1 WT or the kAE1 R901X dRTA mutant.

2.2 Methods

2.2.1 Materials

The following is a list of materials and their suppliers used in this study: mouse anti-myc antibody (Cell Signalling Technology), mouse anti-FLAG antibody (Sigma Aldrich), rabbit anti-FLAG (Cell Signalling), mouse anti-HA antibody (hemagglutinin, Covance), rat anti-HA antibody (Sigma Aldrich), mouse anti-actin antibody (Sigma Aldrich), rat anti-E-cadherin (Sigma Aldrich), mouse anti-Na^+/K^+-ATPase (Santa Cruz), goat anti-mouse antibody horseradish peroxidase conjugated (HRP; Cell Signalling Technology), Alexa 488-conjugated goat anti-mouse antibody (Invitrogen Molecular Probes), Cy3-conjugated donkey anti-mouse antibody (Jackson Immunoresearch), X-treme GENE HP DNA transfection reagent (Roche).

2.2.2 Constructs, cell lines, transfections and viral infection

MDCK (CCL-34) and HEK-293 (CRL-11268) cells were obtained from the American Type Culture Collection (ATCC, Manassas, USA) and grown in DMEM-F12 or DMEM, respectively, supplemented with 10% Fetal bovine serum (v/v), 0.5% penicillin and 0.5%

streptomycin under 5% CO_2 at 37 °C. A pCDNA3 vector with human SLC26A7 cDNA containing an amino-terminal FLAG epitope was kindly provided by Dr. Reinhert Reithmeier (University of Toronto). Additionally, a new construct containing a hemagglutinin (HA) epitope 3′ to the N-terminal FLAG epitope and 5′ of the first methionine of SLC26A7 cDNA was prepared to facilitate detection by immunofluorescence. MDCK cells stably expressing SLC26A7 with either a FLAG or both HA and FLAG epitopes were obtained by transfection of MDCK cells by electroporation using the NEON transfection system according to the manufacturer's instructions. Forty-eight hours later, transfected cells were selected and maintained with medium containing 1 mg/ml of G418. Clones originating from a single cell resistant to the drug were isolated and clones 3 and 8 expressing SLC26A7 FLAG, and clone 4 expressing SLC26A7 HA/FLAG were selected as the highest expressors of SLC26A7 protein. Importantly, no difference in SLC26A7 chloride/bicarbonate exchange was found between clone 3 expressing SLC26A7 FLAG and clone 4 expressing SLC26A7 carrying FLAG and HA epitopes (data not shown), indicating that the epitopes do not alter SLC26A7 function. MDCK cells stably expressing kAE1 WT or R901X with a myc or HA epitope in position 557 were obtained by mouse Molony leukemia viral (MMLV) infection as previously described[171,234]. For cells co-expressing both kAE1 and SLC26A7 proteins, clone 3 cells stably expressing SLC26A7 FLAG were infected with MMLV enclosing pQCXIH viral vector (Clontech) containing kAE1 WT or R901X myc or HA cDNA and the hygromycin resistance gene. Cells resistant to both G418 and hygromycin co-expressed both proteins for 2 to 3 weeks and were therefore used during this period. After the third week, kAE1 expression gradually declined until un-detectable, despite maintenance of the antibiotic selection pressure, as previously described[172]. MDCK cells expressing kAE1 R901X expressed the lowest amount of kAE1 protein for the shortest time compared to kAE1 WT expressing cells.

2.2.3 Treatments, lysate preparations and immunoblots

MDCK cells stably expressing SLC26A7 with an N-terminal FLAG or HA and FLAG epitopes were either kept under control conditions or treated for 16–18 h with growth medium supplemented with either 100 mM sodium chloride, sodium gluconate or 200 mM mannitol. Additionally, for cycloheximide experiments, cells were either maintained un-treated or incubated with 10 μg/ml cycloheximide in complete growth medium to block protein synthesis. For lysate preparations, MDCK cells expressing kAE1 and/or SLC26A7 proteins were lysed in PBS supplemented with 1% Triton X-100 and protease inhibitors (aprotinin 1 μg/ml, leupeptin 2 μg/ml, pepstatin A 1 μg/ml, PMSF 100 μg/ml). Protein content was measured by BCA protein assay using bovine serum albumin as a standard. Proteins diluted in 2× Laemmli sample buffer (Bio-Rad) were resolved on 8% SDS-PAGE gels, then transferred to PVDF membranes (Bio-Rad). The membranes were blocked with 3% skim milk in TBST (5 mM Tris base, 15 mM NaCl, 0.1% Tween-20), incubated in 1% skim milk in TBST containing mouse anti-FLAG, -HA or myc antibodies depending on the protein expressed, followed by HRP-coupled anti-mouse antibody. Probed proteins were detected with Clarity Western ECL kit (Bio-Rad) and using a Kodak Image station 440CF (Kodak, Rochester) or film. For relative quantification of SLC26A7 protein upon cycloheximide incubations, we considered both upper and lower bands detected for SLC26A7 protein and used ImageJ software.

2.2.4 Immunofluorescence imaging by confocal microscopy

MDCK cells expressing SLC26A7 HA-FLAG protein were either grown on coverslips or on semi-permeable filters for 12 days to confluence and kept in control conditions or treated with the various hyper-osmolar growth media for 16 h. Cells were fixed with 4% paraformaldehyde

(Canemco Supplies) in PBS, then quenched with 100 mM glycine (pH 8.5) in PBS. After permeabilization with 0.2% Triton X-100 in PBS, non-specific binding sites were blocked by incubation with 1% BSA in PBS. Samples were then incubated with mouse anti-HA antibodies followed by a secondary Alexa 488 antibody. Rat anti-E-cadherin or rabbit anti- Na^+/K^+-ATPase antibodies were also used as markers for the basolateral membrane or plasma membrane, respectively. Nuclei were stained with DAPI. Samples were examined using an Olympus IX81 microscope equipped with a Nipkow spinning disk optimized by Quorum Technologies (Guelph, ON, Canada) and a 63X oil objective. Note that in Fig. 4, we kept the same microscope settings between each condition to provide a comparison of the relative amount of SLC26A7 between conditions. For calculating the ratio of plasma membrane/total SLC26A7 protein, Volocity software (Quorum Technologies) was used to measure the mean fluorescence intensities of regions of interest corresponding to the plasma membrane (segmented using E-cadherin as a cell surface marker) and the cytosol (the remainder of the cell area outside the membrane E-cadherin staining). For each cell, we divided the mean fluorescence from plasma membrane SLC26A7 by total mean fluorescence intensity (=membrane + cytosol). Each dot on Fig. 4 represents the average ratio calculated from a field of approximately 40 cells.

2.2.5 Bicarbonate transport assay

The procedure was performed as previously described[234–236]. Briefly, MDCK cells expressing kAE1 WT, kAE1 R901X, SLC26A7 or combinations of SLC26A7 and kAE1 proteins grown under control or hyper-osmotic conditions for 16 h, were incubated with 10 μM BCECF-AM (2′,7′-Bis-(2-Carboxyethyl)-5-(and-6)-Carboxyfluorescein, Acetoxymethyl Ester, Thermo Scientific) for 10 min at 37 °C. Coverslips were then placed in fluorescence cuvettes and the cells

perfused at room temperature with Ringer's buffer (5 mM glucose, 5 mM potassium gluconate, 1 mM calcium gluconate, 1 mM magnesium sulfate, 10 mM HEPES, 2.5 mM sodium dihydrogen phosphate, 25 mM sodium bicarbonate) supplemented with 140 mM sodium chloride for 5 to 10 min. The perfusing solution was then switched to a chloride free medium containing 140 mM gluconate to induce intracellular alkalization. BCECF-AM intracellular fluorescence being next calibrated with buffers at pH 6.5, 7.0 or 7.5, supplemented with 100 μM nigericin sodium salt (Calbiochem, Millipore). The Ringer's buffers were continuously bubbled with an air: CO_2 mixture (19: 1), providing 5% CO_2. We used a Photon Technologies International (PTI) (London, Ontario, Canada) fluorimeter to record BCECF fluorescence fluctuations. Excitation wavelengths (440 and 490 nm) and emission wavelength (510 nm) were used (calibrated to the fluorimeter). Transport rates of the cells were determined by linear regression of the initial fluorescence variations (over the first 60 s), normalized to pH calibration measurements. All measurements were done using PTI FelixGX software. Baseline intracellular pH values measured for 60 s prior to switching from the chloride-containing to a chloride-free solution in the various cell lines used in this project are: MDCK: 7.28 ± 0.06 (n = 14), kAE1 WT: 7.45 ± 0.06 (n = 19), SLC26A7: 7.49 ± 0.10 (n = 11), SLC26A7 +kAE1 WT: 7.47 ± 0.07 (n=6), SLC26A7+kAE1 R901X: 7.12 ± 0.03 (n = 4), kAE1 R901X: 7.40 ± 0.08 (n = 7), with values indicating mean cytosolic pH ± SEM (number of replicates). The differences of baseline intracellular pH between the various cell lines did not reach statistical significance. Please refer to Figure A 1 (appendices) for detailed explanation of this experiment.

2.2.6 Statistical analysis

All the experiments were independently repeated a minimum of three times. Experimental results are summarized as mean ± SEM. All statistical comparisons were made using unpaired

Student's t-test or one-way ANOVA with a post-hoc test as indicated. A P value<0.05 was considered statistically significant.

2.3 Results

2.3.1 In MDCK cells, SLC26A7 exchanges Cl^- for HCO_3^- in HCO_3^- containing buffer

SLC26A7 has been characterized as both a chloride channel and a chloride/bicarbonate exchanger in HEK293 and *Xenopus* oocytes[148,150]. We compared the ability of either human SLC26A7 or kAE1 WT to exchange chloride for bicarbonate under normal growth conditions, using MDCK cells that are devoid of endogenous kAE1[237] or SLC26A7 proteins (our own unpublished observation), but that contain endogenous carbonic anhydrase II and proton ATPase[238,239]. We prepared MDCK cells stably expressing SLC26A7 protein carrying an N-terminal FLAG epitope to facilitate protein detection[157]. Immunoblot analyses showed that two highest expressing clones (3 and 8) had a similar migration profile displaying two main bands that were absent in un-transfected MDCK cells (Fig. 1A), reflecting core (white circle) and complex (black circle) glycosylated SLC26A7 proteins as previously described[157]. The subsequent experiments were chosen to be conducted using clone 3 (protein hereafter called SLC26A7). Immunostaining results confirmed that although SLC26A7 looked predominantly intracellular in non-polarized cells, it colocalized with the basolateral membrane marker E-cadherin in polarized cells, with some visible intracellular staining (Figs. 2.1B & 4B). To confirm that SLC26A7 is present at the plasma membrane in non-polarized cells, we performed a functional assay based on 2′,7′-Bis(2-carboxyethyl)-5(6)-carboxyfluorescein-acetoxymethyl ester (BCECF-AM) pH-sensitive fluorescence variations upon switching the bathing solution from one containing chloride to one chloride-free as previously described[223,232,235,236,240]. The rate of intracellular pH change, reflecting bicarbonate-chloride transport rate in the initial 60s of activity was measured. We found

that it reached 0.10 ± 0.02 ΔpH/min (n = 7, ± SEM) in MDCK cells expressing SLC26A7 protein, a value that was significantly higher than un-transfected cells, but lower than that of kAE1 WT transport rate 0.16 ± 0.02 ΔpH/min (n = 8, ± SEM), when the experiment is performed in buffers at pH ranging from 7.35 to 7.45 (Fig. 2.1C–E). These experiments support that in MDCK cells bathed in a buffer at physiological plasma pH, a fraction of SLC26A7 protein is present at the plasma membrane and behaves as a chloride/bicarbonate exchanger, in agreement with previous data obtained in *Xenopus* oocytes expressing SLC26A7 protein[150,223].

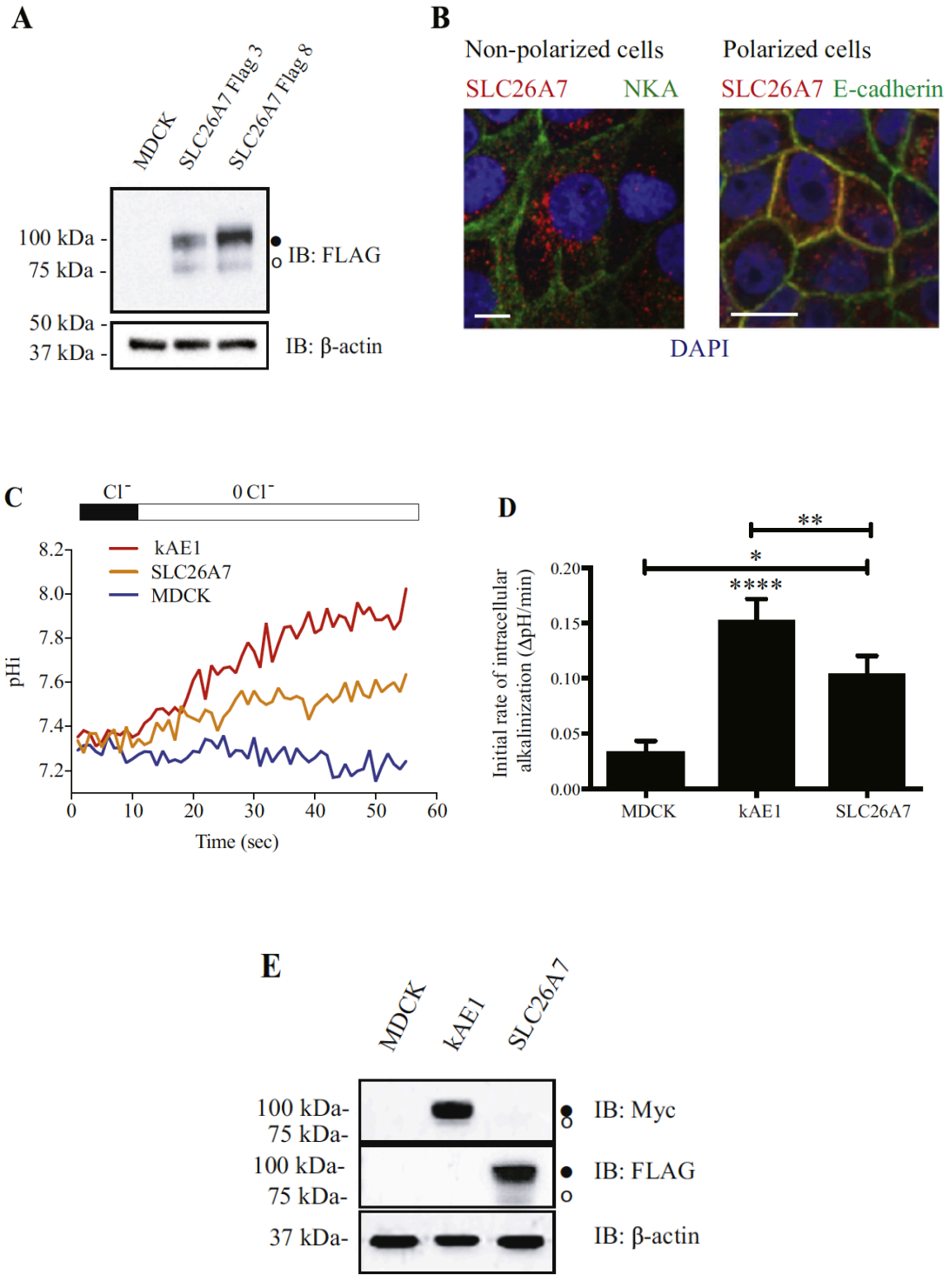

Figure 2. 1 SLC26A7 is stably expressed in clone 3 and 8 MDCK cells.

SLC26A7 is stably expressed in clone 3 and 8 MDCK cells (A, B & E), and exchanges chloride for bicarbonate to a lower extent than kAE1 (C & D). A, Two MDCK clones (SLC26A7 FLAG 3 & 8) that expressed the highest amount of SLC26A7 proteins were isolated and together with untransfected cells ("MDCK" lane), were analysed in an immunoblot using an anti-FLAG antibody. SLC26A7 migrates as two main bands of 72 and ~100 kDa, the upper, most abundant corresponding to complex glycosylated protein (black circle), and the lower molecular weight band corresponding to core glycosylated SLC26A7 protein (white circle) [5]. The SLC26A7 FLAG 3 (hereafter called SLC26A7) was used for subsequent experiments. B, Immunostaining showing that SLC26A7 (red) is perinuclear in non-polarized cells (left image) but both intracellular and basolateral in polarized MDCK cells (right image). DAPI (blue) stained nuclei, NKA stands for the plasma membrane marker Na^+/K^+-ATPase, E-cadherin is a basolateral membrane marker. Bars correspond to 10 μm. C, Traces representing intracellular pH variations over 60 s for untransfected MDCK cells (blue) or MDCK cells expressing kAE1 (red) or SLC26A7 protein (orange), upon switching from a chloride-containing solution to a gluconate-containing solution. D, Initial rates of intracellular alkalinization (first 60 s) were measured in control, SLC26A7-, or kAE1-expressing MDCK cells incubated with pH-sensitive fluorescent dye BCECF-AM upon switching from a chloride-containing to a chloride-free bicarbonate medium. * Indicates $p < 0.05$, ** indicates $p < 0.01$, **** indicates $p < 0.0001$, $n = 7$ at minimum using one-way ANOVA, error bars correspond to standard error of the mean. E immunoblots showing expression of kAE1 (carrying a myc epitope) or SLC26A7 (carrying a FLAG epitope) proteins in cells used for the PTI assay.

2.3.2 The abundance of both kAE1 and SLC26A7 is upregulated in MDCK cells grown in hyper-osmotic medium

SLC26A7 is expressed in acid-secreting intercalated cells of the renal medulla[150]. These cells are constantly bathed in a hyper-osmotic environment compared to plasma. We therefore determined what effect an extracellular hyper-osmotic environment has on SLC26A7 and kAE1 abundance. To do so, we incubated non-polarized polyclonal MDCK cells stably expressing SLC26A7 (Fig. 2A–B), kAE1 WT (Fig. 2C–D) or kAE1 R901X dRTA mutant (Fig. 2E–F) in growth media supplemented with either 100 mM sodium chloride, sodium gluconate or 200 mM mannitol (to maintain the same osmolality as the other solutions) for 16 h at 37 °C, prior to analysis by immunoblot. All hyper-osmotic media induced a significant increase in both SLC26A7 and kAE1 protein abundance in MDCK cells (Fig. 2A–D). Actin abundance was unchanged in the hyper-osmotic conditions. Interestingly, the abundance of kAE1 R901X dRTA mutant showed a trend towards an increase in hyper-osmotic conditions but it did not reach statistical significance (Fig. 2E–F).

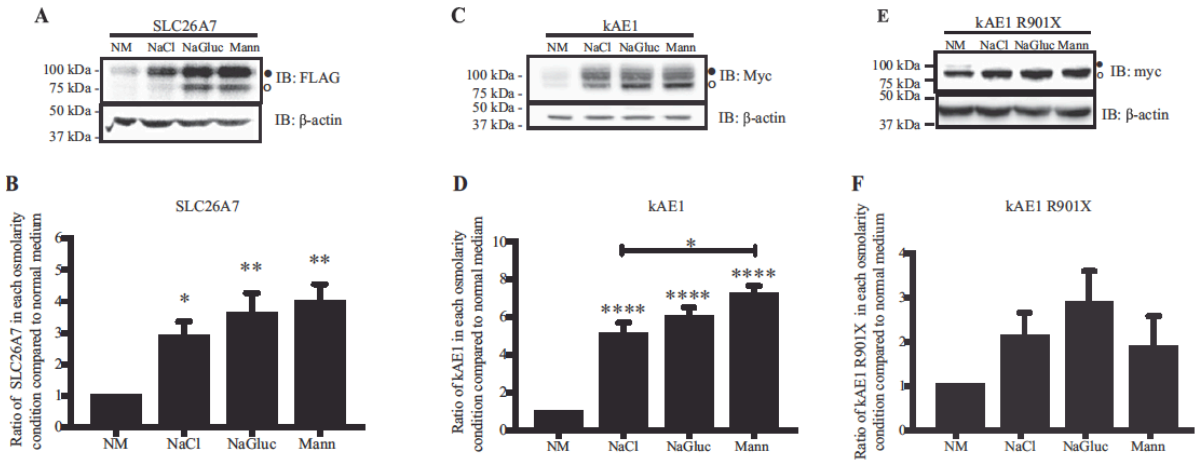

Figure 2. 2 Hyper-osmotic extracellular medium up-regulates both SLC26A7 and kAE1.

Hyper-osmotic extracellular medium up-regulates both SLC26A7 and kAE1 abundance in MDCK cells. MDCK cells stably expressing SLC26A7 protein (containing a FLAG epitope) (A), kAE1 WT (kAE1, C) or kAE1 R901X (E) (both containing a myc epitope) were incubated for 16 h at 37 °C in either normal growth medium (NM) (DMEM-F12 supplemented with 10% FBS and penicillin/streptomycin), growth medium supplemented with 100 mM sodium chloride (NaCl), 100 mM sodium gluconate (NaGluc) or 200 mM mannitol (Mann). Cells were then lysed prior to analysis by immunoblot with a mouse anti-FLAG antibody (A, upper blot), mouse anti-myc antibody (C & E, upper blots) or a mouse anti-actin antibody (A, C & E, bottom blots). Black circles correspond to SLC26A7 or kAE1 carrying complex oligosaccharide, white circle to proteins carrying high mannose. The bar graphs show quantification results by densitometry analysis of SLC26A7 (B), kAE1 WT (D) or kAE1 R901X (F) of a minimum of 3 independent experiments using ImageJ freeware (National Institute of Health). * Indicates $p < 0.05$, ** indicates $p < 0.01$, **** indicates $p < 0.0001$ versus NM, using one-way ANOVA, error bars correspond to standard error of the mean. There was no significant difference observed for kAE1 R901X between the various conditions (F).

2.3.3 Increased SLC26A7 abundance is due to a longer half-life in hyperosmotic medium

The increased abundance of SL26A7 protein in hyper-osmotic medium could be due to a prolonged half-life. To test this hypothesis, we quantified the relative amount of SLC26A7 protein in cells under normal or hyper-osmotic conditions over time in the presence of the protein synthesis inhibitor cycloheximide (Fig. 2. 3). We observed that in cells incubated with regular growth medium, the half-life of SLC26A7 protein was approximately 4 h. Although a statistical difference was only found between NM and mannitol treatment at 6 h and 12 h, nonlinear regression fit curves for each treatment support that the half-life of SLC26A7 in cells grown in hyper-osmotic conditions was higher than in normal growth conditions, reaching approximately 12 h, 7 h and 12 h after sodium chloride, sodium gluconate and mannitol-supplemented incubations, respectively. This result suggests that the higher abundance of SLC26A7 protein is due to a decreased degradation in some hyper-osmotic conditions, although this experiment does not exclude that hyper-osmolarity induces an increased synthesis as well.

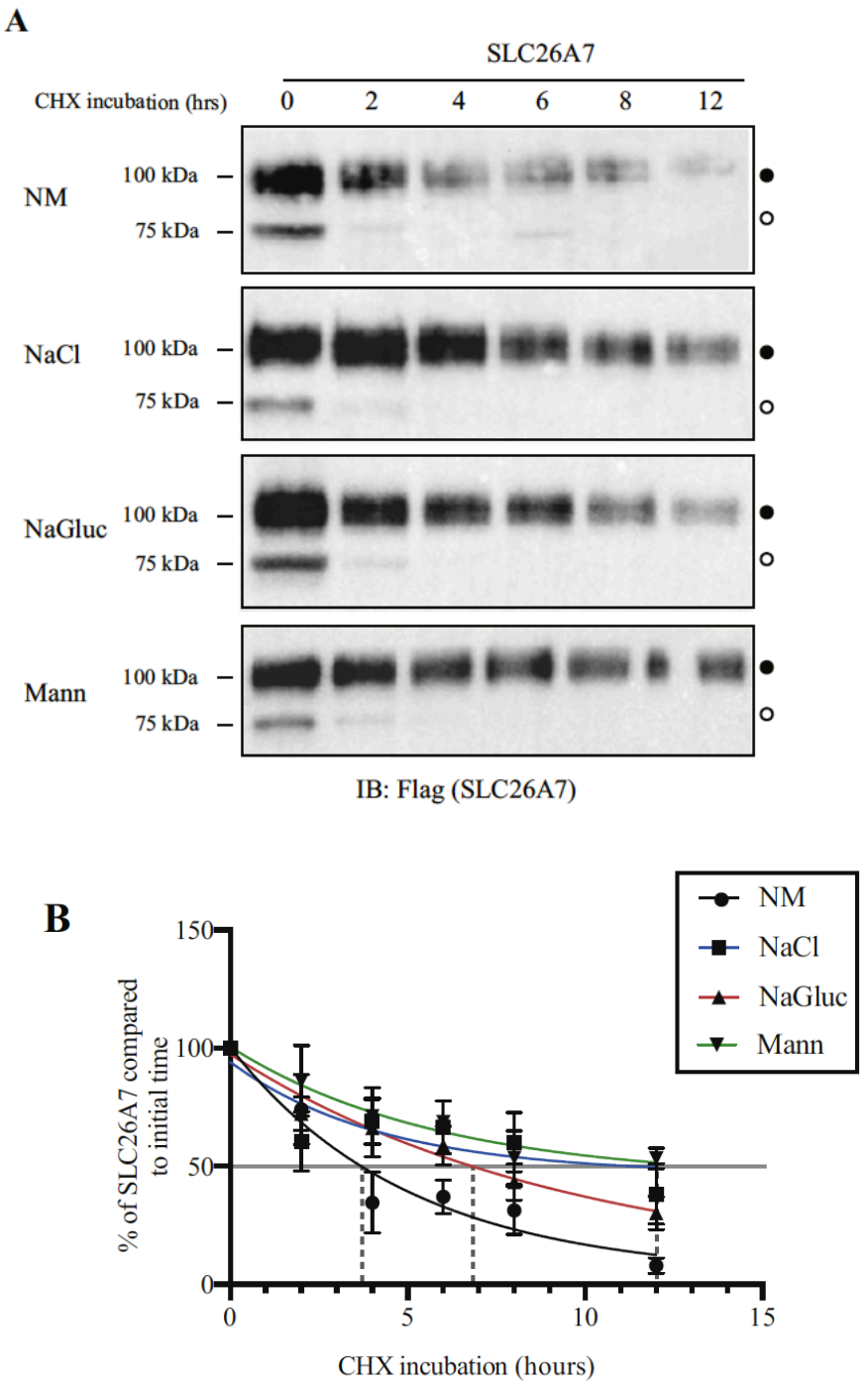

Figure 2. 3 Incubation in hyper-osmotic medium increases the half-life of SLC26A7 protein.

Incubation in hyper-osmotic medium increases the half-life of SLC26A7 protein. A, MDCK cells stably expressing SLC26A7 protein containing an N-terminal FLAG epitope were incubated for 16 h at 37 °C in normal growth medium (NM) (DMEM-F12 supplemented with 10% FBS and penicillin/streptomycin), growth medium supplemented with either 100 mM sodium chloride

(NaCl), 100 mM sodium gluconate (NaGluc), or 200 mM mannitol. In addition to these treatments, 10 μg/ml of cycloheximide was added to the growth medium 0, 2, 4, 6, 8 or 12 h prior to lysing the cells. Cells were then lysed and SLC26A7 protein content compared by immunoblot using an anti-FLAG antibody. The white circles correspond to SLC26A7 carrying high mannose oligosaccharide, and the black circles to protein carrying complex oligosaccharide. B, Quantification of the relative amount of SLC26A7 protein by band densitometry analysis. The graph shows quantification of 3 independent experiments using ImageJ freeware. Dotted lines indicate the half-life of SLC26A7 in each growth condition. Error bars correspond to the standard error of the mean. One-way ANOVA analysis of SLC26A7 percentage between conditions at each time point revealed a statistically significant difference between NM and Mann at 6 and 12 h ($p < 0.05$) (not shown on graph to avoid overcrowding).

2.3.4 The proportion of cell surface SLC26A7 is unchanged in control or hyper-osmotic growth media

As SLC26A7 protein abundance is increased in hyper-osmotic conditions, we aimed to determine whether this rise correlates with higher cell surface expression. Several attempts to perform cell surface biotinylation did not produce robust results and were not included in this manuscript. Immunofluorescence was then performed on non-polarized (Fig. 2.4 A) or polarized (Fig. 2.4 B) SLC26A7-expressing MDCK cells treated in control or hyper-osmotic conditions. As indicated with arrowheads in Fig. 2.4A, hyper-osmotic growth conditions allowed us to detect SLC26A7 at the plasma membrane. The protein remains however predominantly intracellular. In polarized cells (Fig. 2.4 B), although hyper-osmotic growth medium incubation seemed to result in more intense fluorescence levels at the basolateral membrane, the cells still showed a significant amount of intracellular staining for SLC26A7, specifically in mannitol-supplemented growth medium. Comparing the proportion of plasma membrane fluorescence versus total cell fluorescence on polarized cells showed no significant difference in the plasma membrane/ total abundance ratio of SLC26A7 protein in any condition compared to normal medium (Fig. 2.4 C). Although our immunoblot results suggest that hyper-osmotic growth media increase the overall abundance of SLC26A7, immunofluorescence results indicate that the protein reaches the cell surface in the same proportion as in cells grown in normal medium.

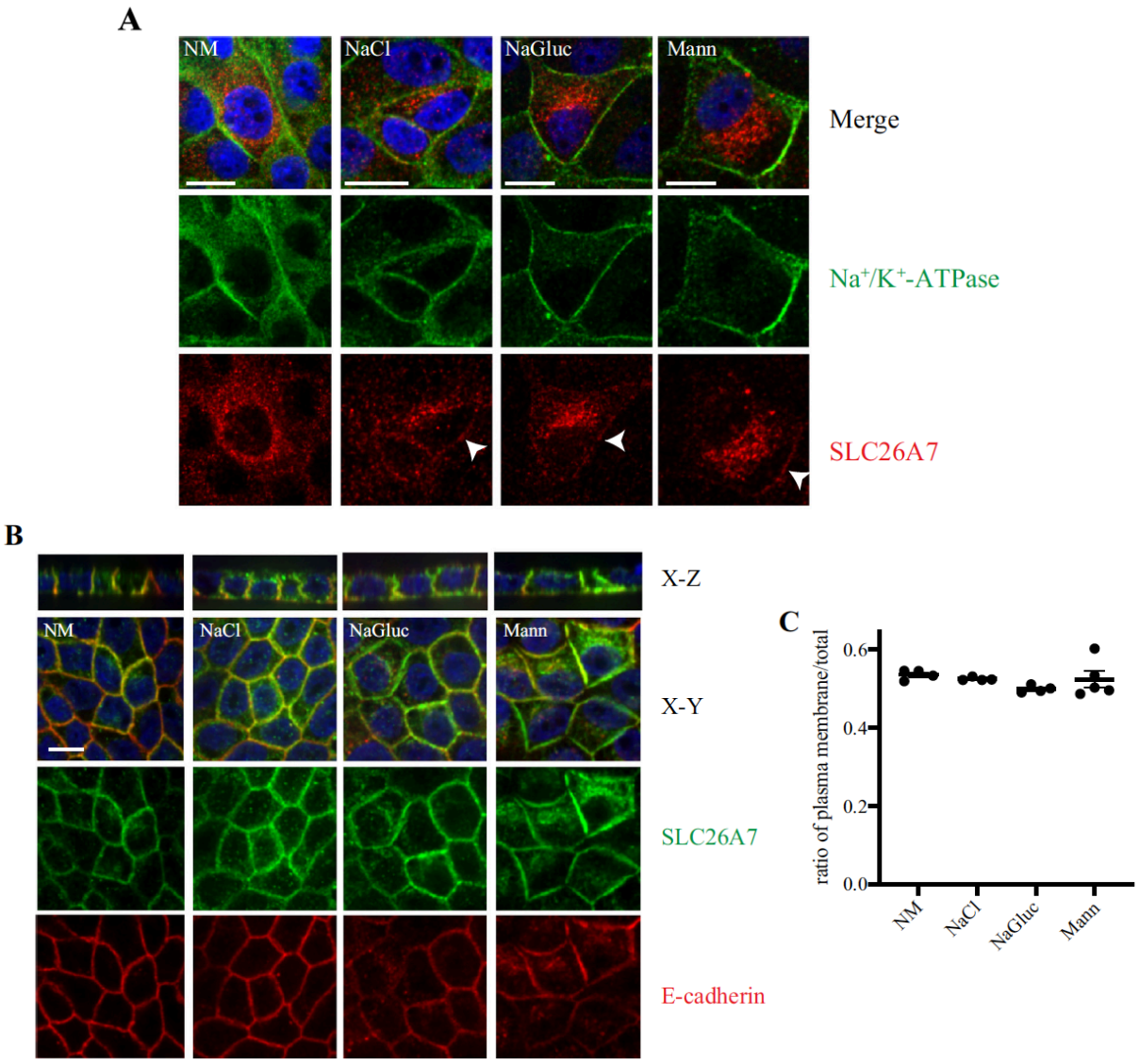

Figure 2. 4 Hyper-osmotic extracellular medium does not increase SLC26A7 cell surface/total expression ratio.

Hyper-osmotic extracellular medium does not increase SLC26A7 cell surface/total expression ratio. Nonpolarized (A) and polarized (B) MDCK cells (clone 3) stably expressing SLC26A7 protein carrying N-terminal FLAG epitope were incubated for 16 h at 37 °C in normal growth medium, growth medium containing 100 mM sodium chloride (NaCl), 100 mM sodium luconate

(NaGluc) or 200 mMmannitol (Mann) prior to immunofluorescence staining. After the various osmotic treatments, the cells were fixed, permeabilized and incubated with mouse anti-FLAG antibody followed by either Cy3-coupled secondary antibody (A, red) or Alexa 488-coupled secondary antibody (B, green). In panel A, cells were also incubated with an anti-Na^+/K^+-ATPase antibody (green) and in B panel, with an anti-E-cadherin antibody (red). DAPI (blue) stained nuclei. Bars correspond to 10 μm. C, Ratio of mean fluorescence intensities from plasma membrane SLC26A7 versus total SLC26A7 protein in each condition, measured using Volocity software (See Methods for experimental details) on polarized cells. Each dot represents the ratio calculated from a field of approximately 40 cells. Error bars correspond to standard error of the mean. There was no significant difference between the ratio of plasma membrane SLC26A7 in the various conditions.

2.3.5 SLC26A7 is not more functional in hyper-osmotic conditions than in control conditions

Petrovic and colleagues reported that when expressed in *Xenopus* oocytes, SLC26A7 protein alkalinized the intracellular environment in a more efficient way when cells were acutely bathed in a hyper-osmotic extracellular environment[150]. In agreement with these data, type-A intercalated cells from micro-perfused outer medullary collecting duct cells (OMCD) alkalinized the intracellular pH less efficiently in *Slc26a7* knockout animals[220]. We next asked whether high osmolarity growth medium affects the activity of SLC26A7 in renal epithelial cells. We repeated the bicarbonate transport assay using SLC26A7-, kAE1 WT- (kAE1) or kAE1 R901X-expressing MDCK cells incubated for 16 h in normal, sodium chloride-, sodium gluconate- or mannitol-containing growth medium (Fig. 2.5). We observed that the activity of SLC26A7 increased NaCl and NaGluc hyper-osmotic conditions compared with MDCK cells (Figs. 2.1D & 2.5A) but did not differ from the normal medium in any of the growth condition (Fig. 2.5A). The lack of apparent significant difference between NM or Mannitol and MDCK cells is likely due to the statistical analysis performed here. As this experiment is testing several hypotheses, the type-II errors would be very high in Fig. 2.5A compared to Fig. 2.1D. The type-II adjustment factor would also be very high, which makes the p-value higher and the difference between groups insignificant. Indeed, SLC26A7 activity was found significantly different from MDCK cells in Fig. 2.1, panel D. Similarly, the activity of kAE1 WT proteins did not significantly change under the various growth conditions except when kAE1 WT cells were grown in mannitol containing growth medium (Fig. 2.5B), a result that will need further investigations to be fully understood.

In dRTA patients carrying the kAE1 R901X mutation, SLC26A7 does not compensate for the malfunctioning kAE1 mutant[164], although our data and previous results[150] support that

SLC26A7 exchanges chloride for bicarbonate. We, therefore, next aimed to compare the contribution of SLC26A7 protein expressed by itself or in cells co-expressing kAE1 WT or kAE1 R901X dRTA mutant. However, prior to this, we examined kAE1 R901X dRTA mutant activity when expressed in MDCK cells incubated in the three hyper-osmotic media. As shown on Fig. 2.5C, kAE1 R901X mutant activity was significantly lower than kAE1 WT in these cells and similar to the MDCK cells, although the protein was expressed in these cells (Fig. 2.2E–F). We conclude that hyper-osmotic cell culture media neither increased SLC26A7 nor kAE1 R901X protein chloride/anion exchange activity compared to normal medium, despite an increase in protein abundance.

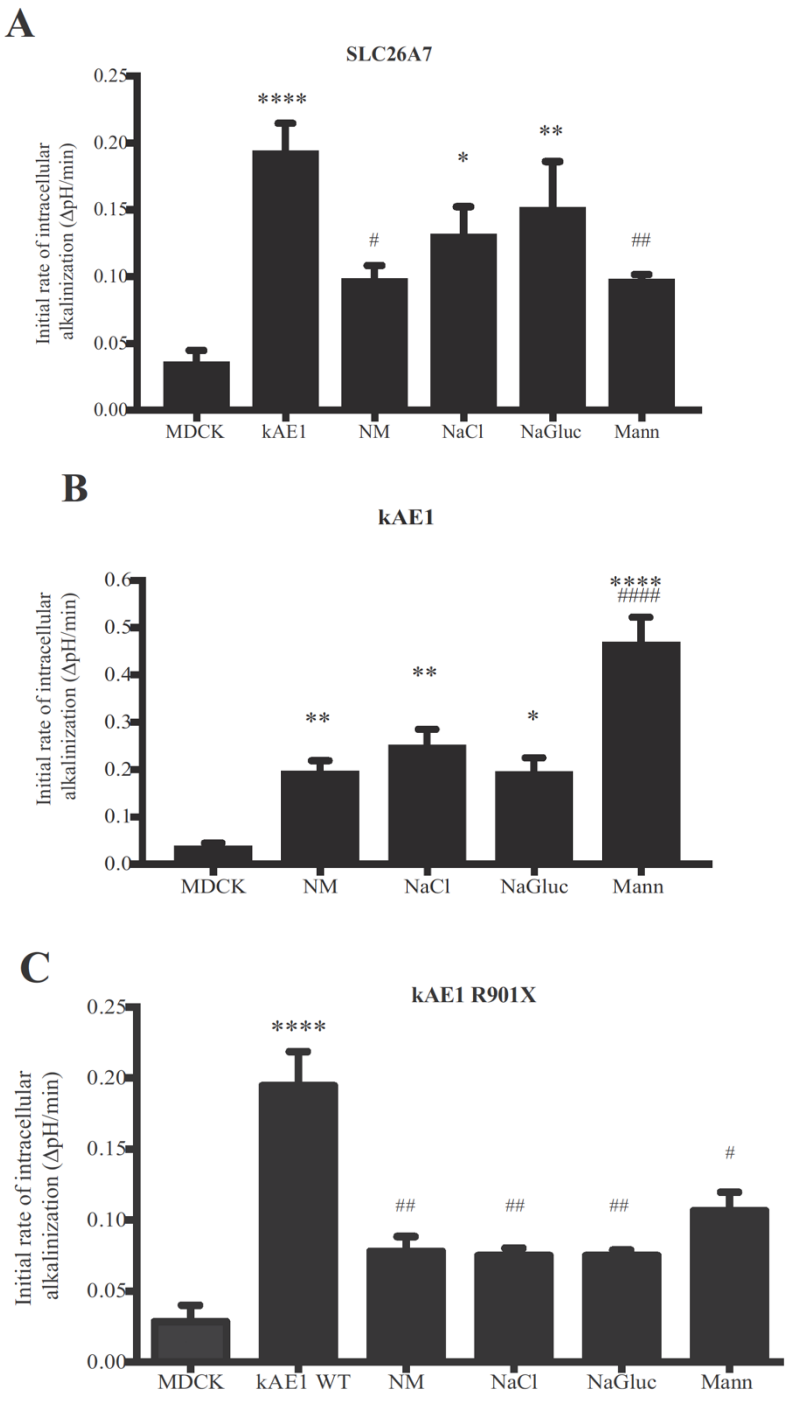

Figure 2. 5 Hyper-osmotic growth conditions do not increase SLC26A7-mediated Cl-/HCO_3^- exchange.

Hyper-osmotic growth conditions do not increase SLC26A7-mediated chloride/bicarbonate exchange. MDCK cells stably expressing SLC26A7 protein (A) containing an N-terminal FLAG epitope or kAE1 WT (B) or R901X (C) carrying a myc epitope were incubated for 16 h in normal (NM) or hyper-osmotic media prior to loading with the pH-sensitive fluorescent probe BCECF-AM. Fluorescence variations were measured upon switching perfusing solution from a Ringer's buffer containing sodium chloride to one without chloride. If the exchanger is at the plasma membrane and functional, an alkalinization of intracellular pH is observed over time. After fluorescence calibration using high-potassium pH solutions supplemented with nigericin, initial fluorescence rates were calculated over the first 60 s. *indicates $p < 0.05$, ** indicates $p < 0.01$, **** indicates $p < 0.0001$ versus MDCK cells; # indicates $p < 0.05$, ## indicates $p < 0.01$, #### indicates $p < 0.0001$ versus kAE1 in normal medium using one-way ANOVA, $n = 5$ to 12. There was no significant difference between kAE1 R901X and MDCK cells under various growth conditions, and no significant difference between NM, NaCl, NaGluc and mannitol conditions for SLC26A7 protein. Error bars correspond to standard error of the mean.

2.3.6 When SLC26A7 protein is co-expressed with kAE1, the Cl^-/HCO_3^- exchange is not osmolarity-sensitive

Intercalated cells express both SLC26A7 and kAE1 proteins[150]. We therefore aimed to mimic the physiological situation by generating MDCK cells co-expressing both kAE1 and SLC26A7 proteins, using viral constructs carrying different resistance genes (see Methods section). kAE1 WT (carrying a myc epitope) and SLC26A7 (carrying a FLAG epitope) proteins were co-expressed in the cells as verified by immunoblot (Fig. 2.6A) albeit kAE1 was less abundant than in cells expressing kAE1 only despite our best efforts to obtain equal protein abundance. Note that lane 3 was loaded with half the amount of protein compared with lane 2. kAE1 R901X was also less abundant than kAE1 WT as previously reported[241] therefore, we loaded 5 times more proteins in lane 6 than lane 2. Thus, we were unable to obtain cells expressing similar amounts of SLC26A7 or kAE1 proteins and therefore unable to truly compare transport activities between cell lines. Despite this limitation, we next performed a functional assay to assess whether osmolarity affects transport function in these cell lines. As shown on Fig. 2.6B, neither cells co-expressing SLC26A7 and kAE1 WT nor SLC26A7 and kAE1 R901X displayed a significantly different chloride/ bicarbonate exchange function upon incubation with hyper-osmotic media. This data indicates that notwithstanding an increase in individual protein abundance upon incubation with a hyper-osmotic medium, the transport function of the proteins when individually or co-expressed is not affected by these media. However, the low abundance and variable expression levels of SLC26A7 and kAE1 may have prevented us from detecting a significant effect.

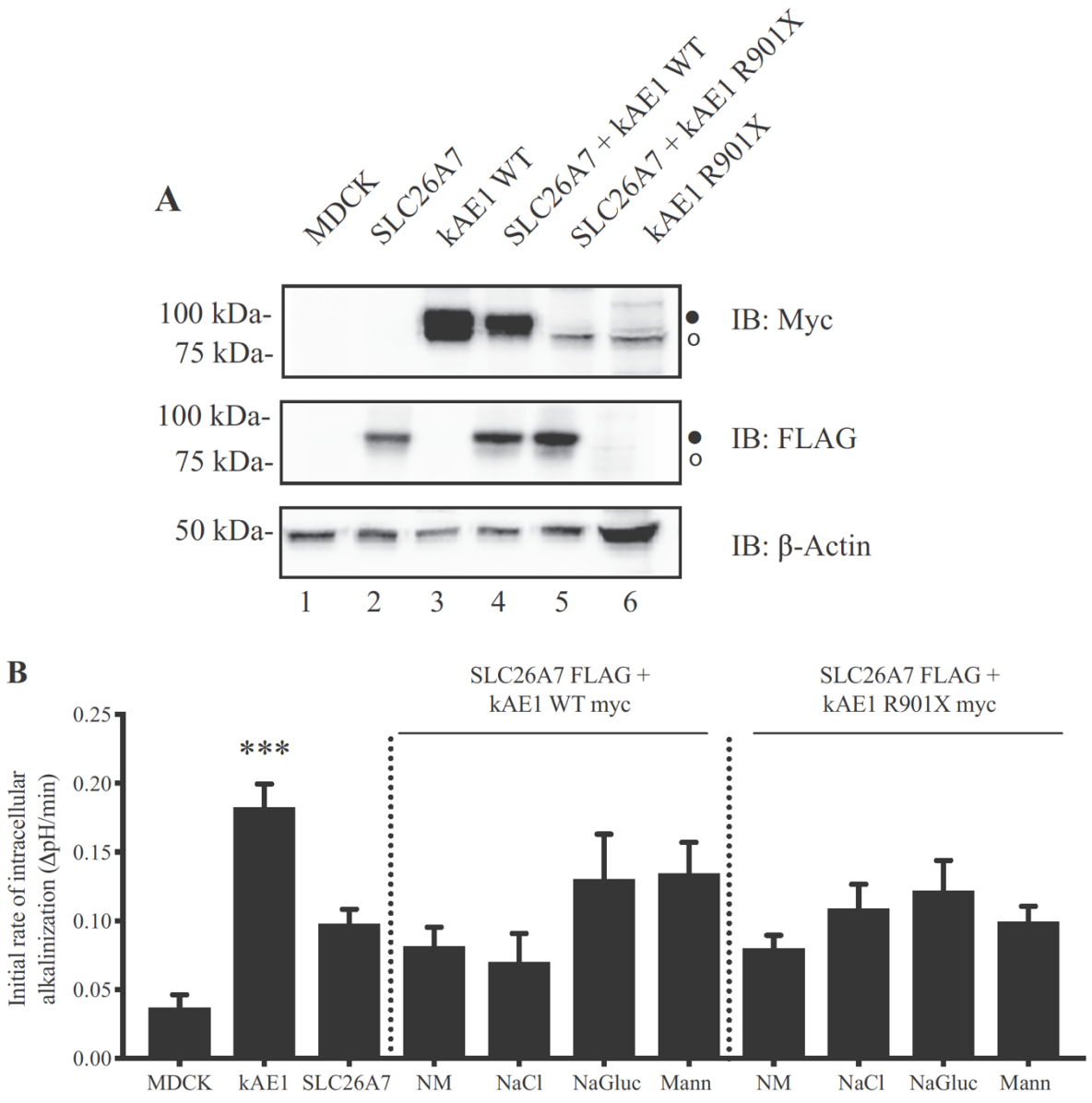

Figure 2. 6 Co-expression of SLC26A7 with kAE1 and kAE1 R901X in various conditions

When SLC26A7 is co-expressed with kAE1 WT or R901X dRTA mutant, the chloride/bicarbonate exchange is not osmolarity-sensitive. MDCK cells expressing kAE1 WT only, SLC26A7 only, kAE1 WT and SLC26A7 or kAE1 R901X and SLC26A7 were grown on glass coverslips and incubated for 16 h with various growth media prior to incubation with BCECF-AM. Cells were

lysed and subjected to immunoblot using anti-FLAG, anti-myc or anti-actin antibodies to verify the respective protein expression and loading. Black and white circles indicate proteins carrying complex and high mannose oligosaccharide, respectively. Note that (i) kAE1 R901X migrates slightly further than kAE1 WT due to the truncation of the last 11 amino acids, and (ii) this mutant is also less abundant than kAE1 WT as previously reported [43], therefore while 15 μg of proteins were loaded on each lane, only 7.5 μg were loaded for kAE1 WT and 75 μg were loaded for kAE1 R901X. B, Fluorescence variations were recorded upon switching perfusing solution from a Ringer's buffer containing sodium chloride to one with sodium gluconate. After fluorescence calibration using high-potassium pH solutions supplemented with nigericin, initial rates of intracellular alkalinization were calculated over the first 60s. *** indicates $p < 0.001$versus MDCK cells using one-way ANOVA (non-parametric) followed by a Kruskal-Wallis post hoc test, n=5 to 12; error bars correspond to standard error of the mean.

2.3.7 SLC26A7 protein is less abundant in cells grown in an extracellular medium below pH 7.2

Untreated dRTA results in systemic metabolic acidosis, characterized by low plasma bicarbonate concentration and abnormally low plasma pH (pH < 7.35)[231]. To determine what impact a low extracellular pH could have on SLC26A7 or kAE1, we incubated MDCK cells expressing either or both proteins at pH 7.0, 7.2 or 7.7 in HEPES buffered CO^2-independent growth medium at 37 °C for 16–18 h. Immunoblot analysis and quantification data (Fig. 2.7) indicate that in both cell lines individually expressing SLC26A7 (panels A & B) or co-expressing it with kAE1 (panels C & D), SLC26A7 is significantly less abundant at pH 7.0 than at a more alkaline pH.

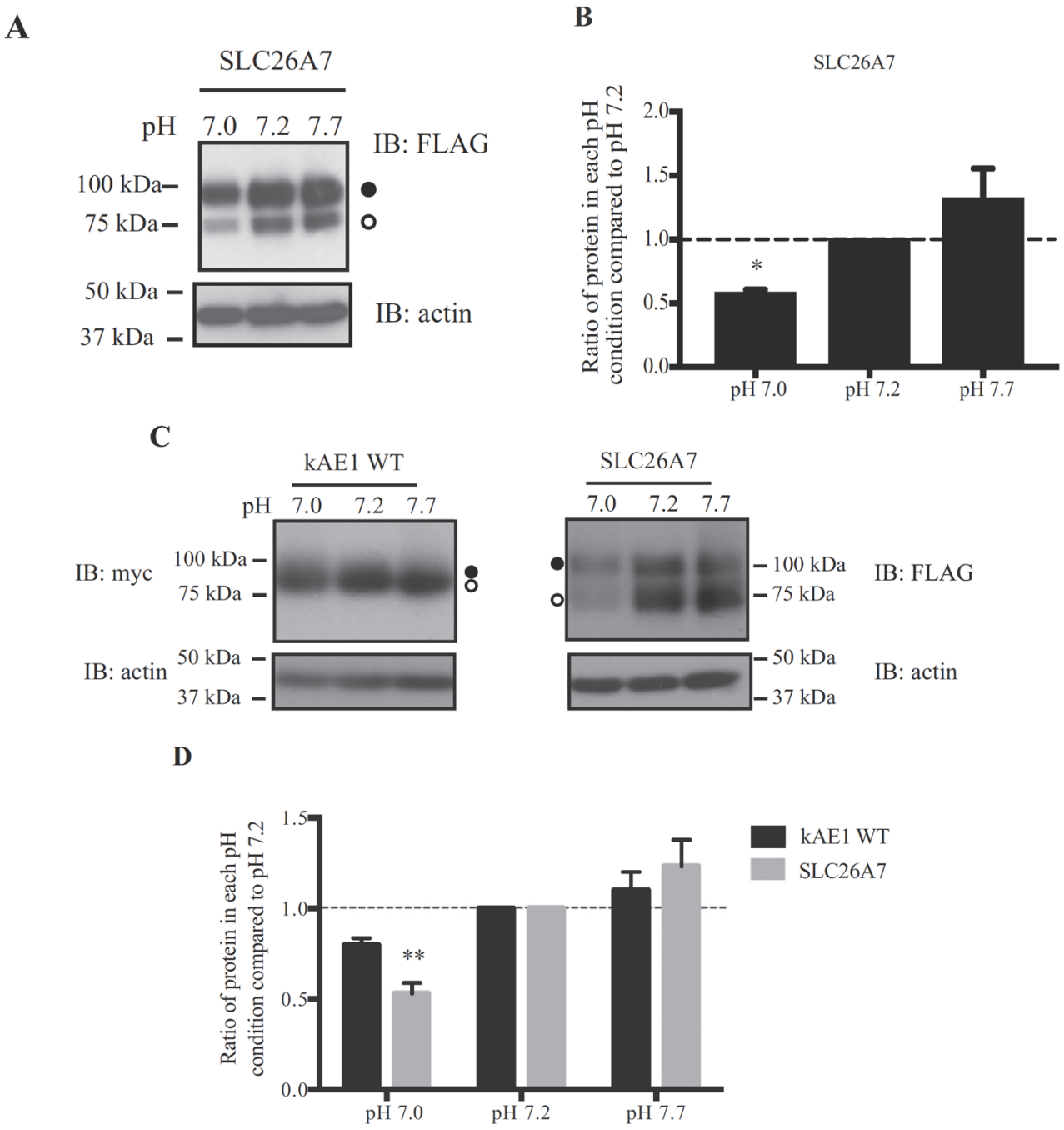

Figure 2. 7 Effect of pH on kAE1 and SLC26A7 protein expression

When individually (A & B) or co-expressed with kAE1 WT (C & D), SLC26A7 is less abundant when cells are incubated in acidic medium. MDCK cells expressing SLC26A7 protein (A) or co-expressing both kAE1 WT and SLC26A7 proteins (C) were incubated in a CO2-independent

HEPES buffered medium for 16 h at 37 °C at pH 7.0, 7.2 or 7.7. After cell lysis, the abundance of SLC26A7 or kAE1 proteins was compared in the various media by immunoblotting using anti-FLAG, anti-myc or anti-actin antibodies. The white circle corresponds to SLC26A7 carrying high mannose oligosaccharide, and the black circle to protein carrying complex oligosaccharide. bar graphs show densitometry quantification of SLC26A7 (B) or kAE1 and SLC26A7 (D) for 3 independent experiments using ImageJ freeware. * Indicates $p < 0.05$, ** indicates $p < 0.01$ versus pH 7.2 using one-way ANOVA, $n = 4$. Error bars correspond to the standard error of the mean.

2.4 Discussion

In this work, we report that in MDCK cells, SLC26A7 protein behaves like a chloride/bicarbonate exchanger. Although mostly detected intracellularly by immunofluorescence, the protein displays a choride/bicarbonate exchange activity, which indicates that at least a portion of this protein is at the plasma membrane. We also observed an increase in SLC26A7 protein abundance in cells incubated in hyper-osmotic media. However, using immunofluorescence staining, we show that hyper-osmotic media incubation did not increase SLC26A7 plasma membrane/total ratio. In agreement with this finding, the functional activity of SLC26A7 protein did not increase upon incubation with hyper-osmotic medium. Our results show that in cells expressing SLC26A7 alone or with kAE1 WT, the bicarbonate transport rate is not significantly affected by hyper-osmotic media incubation. Finally, we show that a low extracellular pH incubation decreases SLC26A7 protein's relative abundance when expressed individually or with kAE1 protein. Although our aim was to assess SLC26A7 and kAE1 protein transport activities when co-expressed, we have not been able to obtain robust results due to the low abundance (kAE1 R901X) and variability (kAE1 WT) in protein expression in the various cell lines. Indeed, as the transport activity was low in cells co-expressing SLC26A7 and kAE1 WT or R901X, we are unable to dissect whether the lack of effect of osmolarity on function is due to low abundance of the proteins or to a loss of function of the proteins when co-expressed. A better expression system allowing equivalent SLC26A7 and kAE1 protein abundance would be necessary to definitely answer this question. Currently, the function of SLC26A7 is not clearly understood, with data supporting that SLC26A7 is a chloride channel while other evidences suggest it functions as a chloride/bicarbonate exchanger. When expressed in *Xenopus* oocytes, SLC26A7 protein behaves as a chloride channel[148] or as a chloride/bicarbonate exchanger[150], however, in acid secreting cells

in the outer medullary collecting duct, it exchanges chloride for bicarbonate, in an osmolarity-dependent pathway[220]. It was proposed that the function of SLC26A7 is differentially regulated depending on the intracellular pH, whereby alkaline pH promotes bicarbonate transport as opposed to acidic pH which switches its function to a chloride channel[152]. Prior to this work, no SLC26A7 functional data was available from model renal epithelial cells due to limited protein expression[223], thus, leaving a doubt about the ion exchange activity of this protein. Although we have not directly tested whether SLC26A7 functions as a chloride channel when expressed in MDCK cells, our results are consistent with SLC26A7 mediating chloride/bicarbonate exchange similarly to the other chloride/bicarbonate exchanger expressed in intercalated cells, kAE1 protein (Fig. 1). As the function of SLC26A7 is reported to be regulated by intracellular pH[148], we asked whether extracellular pH could also affect the abundance or function of this protein, as would happen in untreated dRTA patients. Incubation of MDCK cells expressing SLC26A7 protein in CO_2-independent, HEPES-buffered growth medium at pH 7.0, 7.2 or 7.7 for 16 h revealed a significant reduction in SLC26A7 abundance at pH below 7.2, indicating that this protein's stability or synthesis is sensitive to extracellular pH. kAE1 abundance was not significantly altered. The mechanisms that down-regulate SLC26A7 expression upon a change in extracellular pH is not known and will require further studies. As dRTA patients have metabolic acidosis, this reduction in SLC26A7 protein abundance provides a possible explanation for the lack of compensatory chloride/bicarbonate exchange activity of SLC26A7 when kAE1 is mutated and non-functional[232]. However, the loss of SLC26A7 at acidic pH seems irreversible as patients who temporarily stop their plasma pH-normalizing bicarbonate treatment become acidotic again. This fact emphasizes that at neutral extracellular pH, SLC26A7 expression cannot sustain a physiological plasma pH in the absence of kAE1 protein. Importantly, in RNA-seq analysis of micro-dissected rat kidney

tubules, the RPKM values for SLC26A7 mRNA is 5.5 in OMCD and no value was reported in CCD, while for kAE1 mRNA, the values reached 182 in OMCD and 103 in the CCD[242]. Similar analysis conducted in isolated mouse CCD cells showed a mean TPM of 8.08 for SLC26A7 but 290 for kAE1 mRNA[243]. Thus, assuming the mRNA abundance parallels the protein abundance, this data suggests that SLC26A7 protein is far less abundant than kAE1 in the CD, which provides an alternative explanation for the inability of SLC26A7 to compensate the loss of kAE1 protein. However, data from micro-perfused kidneys from *Slc26a7* knockout mice show approximately 75% reduction of exchange activity in hypertonic conditions[220], supporting that in this setting, SLC26A7 protein is the predominant exchanger, which must therefore be sufficiently abundant to perform this large amount of activity in mouse kidneys. Importantly, although AE1 mRNA was increased in *Slc26a7* knockout animals[220], SLC26A7 mRNA abundance was unchanged in AE1 knockout animals[232]. SLC26A7 is expressed in the outer medullary collecting duct where acid-secreting cells are expected to be bathed in an extracellular hyperosmotic environment relative to plasma. We then examined the abundance and function of the protein in cells grown in normal or growth medium supplemented with either 100 mM sodium chloride, sodium gluconate, or 200 mM mannitol. When cells were grown under control conditions, SLC26A7 was predominantly located intracellularly, in agreement with previous reports[157,223], but its ion-exchange activity could however be detected, indicating that a significant amount of protein was present at the cell surface. The reason for our inability to clearly detect plasma membrane SLC26A7 may originate from a suboptimal ability of the antibody to recognize its epitope by immunofluorescence compared to immunoblots. Immunofluorescence experiments used Triton X-100 to permeabilize the cell membrane, while immunoblots used Triton-X and SDS, which may denature the protein better and result in a more detectable epitope. This hypothesis is supported by our difficulties to detect

SLC26A7 protein at the plasma membrane by immunofluorescence (Figs. 1 & 4), despite detectable functional activity. Incubation in hyper-osmotic media increased the overall abundance of both SLC26A7 and kAE1 proteins 3 to ld (Fig. 2). Similar findings were obtained when SLC26A7 was expressed in *Xenopus* oocytes[141]. This increase was paralleled with a 1.5-to-3-fold lon longer half-life for the SLC26A7 protein (Fig. 3). The difference between the 1.5-to-3-fold increase in half-life and the 3-to-4-fold increase in protein abundance suggests that protein expression may also be up-regulated. Although in intercalated cells the endogenous promoter controlling the translation of SLC26A7 and *SLC4aA1* genes might be regulated differently, we observed that under the control of the CMV promoter present in the pCDNA3 vector, SLC26A7 protein abundance was increased in hyper-osmotic growth media. This finding indicates that the osmotic dependent up-regulation of SLC26A7 occurs either at the level of the transcript stability or the protein. Such up-regulation of proteins may not be unique to SLC26A7 protein as the sodium-potassium ATPase gene expression is also up-regulated in hyper-osmotic conditions in rat inner medullary CD cells[244].

We observed that when individually expressed in MDCK cells grown in standard growth medium, SLC26A7 exchanges chloride for bicarbonate at half the rate of kAE1 protein (Fig. 1B). With several unsuccessful attempts to obtain cells co-expressing similar amounts of both SLC26A7 and kAE1, we have not been able to test whether chloride/bicarbonate exchange was additive in cells co-expressing the two proteins. In these cells, our results show a lack of significant sensitivity of the transport function to hyper-osmolarity, but with such a varying protein abundance between SLC26A7 and kAE1 WT or R901X, we cannot conclude whether this is due to low protein expression or to the co-expression of one protein decreasing the transport activity of the other. Our expression system allows us to select cells resistant to both hygromycin and G418

antibiotics, however, we are not able to modulate expression levels. We and others have previously reported that kAE1 R901X is less abundantly expressed than kAE1 WT protein in renal epithelial cells[112,136], and that in our constitutive expression system, despite constant selection pressure, kAE1 protein expression disappears after 3 weeks post-infection[172]. An alternative expression system where both proteins' expression could be induced would be better suited to assess transport function additivity in cells co-expressing equivalent amounts of kAE1 and SLC26A7 proteins. Our data support that SLC26A7 functions as a chloride/bicarbonate exchanger when expressed in MDCK cells, and that culture of these cells in a hyper-osmotic growth medium promotes SLC26A7 protein upregulation, without a significant increased plasma membrane/total abundance ratio or function. Although our attempts to robustly quantify plasma membrane SLC26A7 by immunofluorescence were not very conclusive as detailed above, the similar exchange activity in iso- and hyper-osmotic conditions points towards a similar abundance of plasma membrane SLC26A7 in these two conditions. The reason for this probable lack of increased cell surface abundance could be due to the overwhelming of the protein synthesis and processing machinery in these cells, resulting in intracellular accumulation of SLC26A7 protein. As both kAE1 and SLC26A7 appear to act as chloride/bicarbonate exchangers at the basolateral membrane of acid-secreting intercalated cells, it is imaginable that the two proteins physically interact as is seen between SLC26A3, SLC26A6 and CFTR proteins[245]. However, we have been unable to observe a physical interaction between the two proteins by co-immunoprecipitation (data not shown), although it is possible that the addition of the N-terminal HA or FLAG epitopes alters their ability to interact. The co-existence of these two redundant chloride/bicarbonate exchangers in the same renal epithelial cell type is however reminiscent to the thyrocytes where both SLC26A4 (pendrin)

and SLC26A7 are co-expressed and necessary for proper cell function and iodide organification[158,222].

Overall, our results support that SLC26A7 acts as a chloride/bicarbonate exchanger in MDCK cells. However, it's function is significantly lower than that of the other chloride/bicarbonate exchanger kAE1, which could be attributed to possible lower relative abundance of total protein or relatively less localization in the plasma membrane. Its abundance is affected by hyperosmolarity but not its relative cell surface amount or function in MDCK cells. Further when incubated in an acidic extracellular medium, cells expressing SLC26A7 display a reduced abundance of the protein. Together, these results provide a better understanding of the individual and collective role of SLC26A7 and kAE1 proteins in renal epithelial cells. The finding that SLC26A7 protein abundance can be increased in hyper-osmotic conditions could provide a conceivable way to up-regulate the chloride/bicarbonate exchange in intercalated cells of dRTA patients.

CHAPTER THREE

LOSS OF INTERCALATED CELL CLAUDIN-4 CAUSES URINARY SODIUM WASTE

ABSTRACT

The collecting duct is composed of several epithelial cell types that collaborate to maintain acid-base (through type-A and -B intercalated cells, IC) and electrolyte homeostasis (through principal cells, PC, and type-B IC). The aldosterone sensitive distal nephron also contributes paracellular reabsorption of chloride through tight junction proteins including claudin-4 (cldn-4). Global cldn-4 knockout (KO) mice display lethal hydronephrosis, hypocalcemia, and increased urinary fractional excretion of chloride and calcium. PC-specific cldn-4 KO mice also display elevated fractional excretion of chloride and sodium. We recently showed that type A IC-specific kidney anion exchanger 1 (kAE1) functionally and physically interacts with Cldn-4. To obtain a complete picture of the role of cldn-4 in the distal nephron, we generated IC-specific cldn-4 KO mice. Although they displayed normal acid-base and calcium balance, the KO mice wasted urinary sodium when fed a NaCl depleted diet. Elevated IC markers transporters including pendrin, kAE1 and NDCBE was observed at baseline and when fed a NaCl-depleted diet, without a change in H^+-ATPase abundance. This study indicates that in IC, cldn-4 is not involved in pH or calcium homeostasis but is essential for sodium conservation.

3.1 Introduction

Fine-tuning of the urine occurs in the collecting ducts (CD). This process includes the combined action of proteins expressed in at least 3 different cell types. Principal cells (PC) harbor the apical epithelial sodium channel (ENaC), the renal outer medullary potassium channel (ROMK), and the water reabsorbing channel aquaporin-2 (AQP-2), which all contribute to maintaining salt and water homeostasis[10]. Apical potassium secretion is coupled to electrogenic sodium reabsorption through apical ENaC and basolateral Na+/K+- ATPase. The second cell type is the intercalated cells (IC) that are responsible for acid/base and salt homeostasis[10]. In type-A ICs, the action of apical v-H+-ATPase, cytoplasmic carbonic anhydrase II (CAII) and basolateral kidney anion exchanger 1 (kAE1) promote acid secretion. In type B IC, apical pendrin, a sodium-driven chloride bicarbonate exchanger (NDCBE, also called SLC4A8), and basolateral H+-ATPase and AE4 promote base secretion and electroneutral salt reabsorption[10,29,35,47,246]. Non-A, non-B intercalated cells and hybrid intercalated-principal cells have also been described although their function is unclear[246].

Contributing to ion and water reabsorption/secretion, are tight junctions (TJ) proteins[108], including claudins (cldn). Claudins are integral membrane proteins that either form paracellular permeant pores or barriers to ions and water[247]. Claudins are composed of 4 transmembrane domains and intracellular N and C termini[96,248,249]. Twenty-seven members have been identified in the claudin gene family in both mice and humans[108,250]. In the CD, cldn-3, -4, -6, -8, -10 and -14 are present in tight junctions[108]. The interplay between the paracellular and transcellular pathways regulates the overall permeability of the epithelium to specific ions and molecules. For example, heterologous expression of kAE1 in polarized Madin-Darby canine kidney (MDCK) cells results in an increase in epithelial monolayer permeability to apically applied fluorescent biotin[112]. We

further recently showed that heterologous expression of kAE1 in mIMCD3 cells alters tight junction properties, via a cldn-4 dependent pathway[113]. Inducible expression of kAE1 in mIMCD3 cells resulted in a lower transepithelial electrical resistance (TEER) compared to control cells, an effect dependent on its chloride-bicarbonate exchange function. Immunoprecipitation and proximity ligation assays showed that kAE1 physically interacts with cldn-4[113].

Detectable in both principal and intercalated cells, cldn-4 acts as a paracellular pore for chloride, a barrier to sodium and interacts with cldn-8[107]. Global cldn-4 knockout mice develop unilateral or bilateral hydronephrosis, and urothelial hyperplasia[110], causing a lower survival rate after 12 months of age. These mice also demonstrate hypocalcemia, hypercalciuria, and increased urinary chloride excretion[110]. PC-specific cldn-4 knockout mice display higher urine volume, hypotension, increased fractional excretion of sodium and chloride compared with control animals at a basal state and after a salt-deficient diet[111]. These studies showed that in PC cldn-4 plays a significant role in salt reabsorption. To provide a complete picture of the role of cldn-4 in the collecting duct, we investigated its role in intercalated cells. We generated IC-specific cldn-4 KO mice and characterized them at the basal state, after an acid diet, a NaCl-, or calcium-deficient diet. Our results show that when fed a NaCl deficient diet, they waste urinary sodium but not chloride, but maintain normal acid-base and calcium balance. The lack of urinary chloride loss may be explained by a compensatory up-regulation of IC markers involved in electroneutral sodium and chloride reabsorption such as pendrin, NDCBE, and surprisingly kAE1. These results suggest that the integrity of IC tight junctions in the collecting duct is important for salt balance but not for acid-base or calcium balance.

3.2 Materials and Methods

3.2.1 Generation of IC cldn-4 KO mice

All animal protocols were approved by the University of Alberta's Animal care and use committee (AUP#1277) and followed the guidelines of the Canadian Council on Animal care. Animals were provided with standard rodent chow (Picolab® Rodent Diet 20 # 5053, LabDiet, ST. Louis, MO, USA) and water ad libitum unless otherwise stated and maintained a 12 hour light and dark cycles throughout.

Claudin-$4^{flox/flox}$ mice (129SvS4 strain) were provided by Dr. Zea Borok (University of Southern California)[251]. For genotyping, DNA was extracted from ear biopsies using PhireThermo™ according to the manufacturer's protocol and were genotyped by polymerase chain reaction using flox-specific primers (5'- CAG TAG GAA AGT TGC TGT TGA GGC- 3' and 5'-CTC CCG TGA GAC AAG AGA ATG AAG- 3').

The β1-Cre mice (C57BL6/CBA strain) were provided by Dr. John Barasch (Columbia University)[252] and contain the Cre reporter gene under the control of the human ATP6V1B1 promoter sequence. Mice were genotyped using Cre-specific primers (5'-GGA CAT GTT CAG GGA TGG CCA GGC G-3' and 5'-GCA TAA CCA GTG AAA CAG CAT TGC TG-3'). Claudin-$4^{flox/flox}$ and β1-Cre mice were bred to generate IC-specific cldn-4 KO mice that are heterozygous for β1-Cre gene and homozygous for Flox. Polymerase chain reaction followed by electrophoresis displaying a 257 bp single band detected with cldn-4 specific primers, was indicative of Cldn-$4^{flox/flox}$ mice (hereafter named "WT"), whereas a 257 bp single band detected with cldn-4 specific primers and a 243 bp band with Cre primers was indicative of β1-Cre cldn-$4^{flox/flox}$ mice (hereafter named "KO").

3.2.2 Collecting duct isolation and protein extraction

Freshly dissected mouse kidneys were decapsulated, sliced in 0.1-0.2 mm thick sections and incubated with a collagenase type II solution (1.33 mg/ml H_2O) containing Trypsin inhibitor and DNAse I (5 mM Glycine, 48 mg/l Trypsin Inhibitor; Sigma Cat# T-9253, 25 mg/l DNAse I; Sigma Cat# DN-25) at 37° C for a total of 20 min under sequential gentle shaking. Supernatant was next visualized under a dissection microscope and 50 to 100 individual collecting ducts from the same animal were pooled into a single Eppendorf tube prior to lysis with 5 X Laemmli buffer for protein detection. A protein assay (BCA) was not performed due to the small amount of sample collected.

3.2.3 Diets and metabolic cage experiments

Metabolic cage studies were done as described previously[144,189]. Briefly, Three-month-old WT and IC-cldn-4 KO mice were placed in metabolic cages for 48 hours and fed a standard 0.49% NaCl containing rodent chow and standard water ad libitum. Bodyweight, food and water consumption, urine volume, and feces mass were measured every 24 hours. To study NaCl-restricted conditions, 3-month-old WT and KO mice were placed in metabolic cages for 48 hours to collect a baseline urine, feces, and physical parameters were measured. After 48 hours they were returned to conventional cages with free access to a sodium deficient diet (0.01-0.02% sodium, 0.07% chloride, Takled Custom diet # TD.08290, Envigo, USA) and water. After 14 days the mice were returned to the metabolic cages, physical parameters were measured (see tables), and samples collected for another 24 hours. To acid load the animals, 3-month-old WT and KO mice were placed in metabolic cages with normal rodent chow and normal water for 48 hours, and samples were collected as before. Drinking water was then replaced with water containing 0.28M NH_4Cl (pH 5.2) for another 24 hours. Bodyweight, food and water consumption were measured, tissue

and urine and feces were collected. For calcium-depleted diet experiments, WT or KO mice fed a standard chow diet were housed in metabolic cages for 48 hours to obtain baseline data. The mice were then returned to their static cages and fed a 0.01% Ca^{2+}-containing chow (Takled custom diet, # TD.95027) for the next 10 days prior to returning to metabolic cages for additional 48 hours for samples and tissue collection.

3.2.4 Plasma electrolytes measurements

On the last day of the metabolic cage studies, mice were anesthetized, blood was collected, and electrolytes were immediately measured using i-STAT Chem8+ cartridge chip (Abott Laboratories, USA) and a VetScan i-STAT 1 Analyzer (Abaxis, Union City, CA, USA). Cardiac perfusion was next performed with 1X PBS supplemented with heparin prior to kidney collection for immunoblot, qRT-PCR and immunohistochemistry.

3.2.5 Urine, serum, and feces collection and analysis, and blood pressure measurements

Urine was collected in metabolic cages under paraffin oil for 24 hours and urine pH was measured immediately using a pH microelectrode (PerpHect® Ross® Micro Combination pH electrode, ThermoScientific, Beverly, MA, USA) attached to a Accumet AR10 pH meter, Fischer Scientific. Urine electrolytes were measured using ion chromatography with a Dionex Aquion Ion Chromatography System (Cat# 22176-60004, ThermoFischer™ Scientific Inc., Mississauga, ON, Canada) as done previously[189]. The anion eluent was composed of 4.5 mM Na_2CO_3 and 1.5 mM $NaHCO_3$ in ddH_2O as per the manufacturer's guidelines. The cation eluent was made of 20 mM Methanesulfonic acid dissolved in ddH_2O. For blood pressure measurements in conscious mice, the computerized tail-cuff measurement method was used after performing 5 consecutive days of training to the machine. At least 10 measurements were recorded every day. The measurements

started 5 days prior to the last day of specific diet, and the values from the last day were the only ones kept for analyses.

3.2.6 Plasma and Urine Creatinine and plasma calcium assays

Plasma creatinine was measured using Diazyme Creatinine liquid reagents assay (Diazyme Laboratories, Poway, CA, USA) as per the manufacturer's instruction and described previously (Beggs et al., 2021) . Urine creatinine was measured by Parameter™Creatinine assay (CAT# KGE005, R&D systems [MN, USA]) according to the manufacturer's instructions. Plasma calcium level was measured using a QuantiChrom calcium assay kit (DICA-500) by BioAssay systems (Hayward, CA, USA) according to the provided instructions.

3.2.7 Protein extraction and Western Blot

Freshly dissected kidneys were decapsulated, mechanically homogenized in ice-cold RIPA lysis buffer (5 mM NaCl, 0.5 M EDTA pH 8.0, 1 M Tris pH 8.0, 1% NP-40, 0.5% Sodium deoxycholate, 10% SDS dissolved in ddH2O supplemented with cOmplete™mini protease inhibitor cocktail and PhosSTOP™ phosphatase inhibitor from Roche), vortexed every 15 mins over 1 hour, and centrifuged at 4°C, 14000 rpm for 15 minutes. Protein concentration was measured using a BCA assay. Standard immunoblot experiments were performed with 8%, 10% or 12% SDS-PAGE, depending on the protein size. PVDF membranes were blocked with 5% milk in TBST (5mM Tris base, 15 mM NaCl, 0.1% Tween 20), incubated in primary antibody overnight at 4°C followed by incubation in secondary antibody conjugated to horseradish peroxidase. Mouse anti-AE1, mouse anti-V-H^+-ATPase and mouse anti-pendrin antibodies are kind gifts from Dr. Sebastian Frische (Aarhus University, Denmark)[253–255]. Proteins of interest on the membrane were visualized using GE Healthcare Amersham™ ECL prime Western blotting detection reagent (Göteborg, Sweden) and images captured by ChemiDoc touch imaging systems (Bio-Rad, CA,

USA). Quantification and densitometric analysis were performed by ImageJ freeware (National Institutes of Health, USA).

3.2.8 RNA isolation and Quantitative RT-PCR

Kidney sections were stored in RNAlater (ThermoFisher Scientific) immediately upon dissection. Total RNA was extracted using TRIzol reagent (Invitrogen, Carlsbad, CA, USA) as previously described[256,257]. Total RNA was quantified using a NanoDrop (NanoDrop 2000C, ThermoFischer, USA) and cDNA was reverse transcribed from 5 μg of total RNA template. The primers used for qRT PCR are listed in Supplementary Table 1. Quantitative reverse transcriptase PCR was performed using TaqMan qPCR mastermix in a QuantStudio 6 Pro RT PCR system (ThermoFisher Scientific). Expression levels of mRNAs from specific genes were normalized to β -Actin, as a housekeeping gene.

3.2.9 Statistical Analysis

All data are presented as mean ± SEM (n). Statistical analysis was performed using an unpaired/paired Student's t-test (wherever appropriate) with either Bonferroni's or Mann-Whitney or Kruskal-Wallis post hoc test using GraphPad Prism software (Ver 7.0e).

3.3 Results

3.3.1 IC-cldn-4 KO mice generation, and KO confirmation

To knockout the cldn-4 gene specifically in IC, we used a Cre-Lox recombination strategy. Heterozygous B1-Cre mice were bred with cldn-$4^{flox/flox}$ mice. Their offspring were bred again with cldn-$4^{flox/flox}$ mice to obtain B1-Cre-cldn-$4^{flox/flox}$ mice (hereafter referred to as "KO" mice). cldn-$4^{flox/flox}$ mice not carrying the ATP6V1B1 promoter-Cre transgene were used as negative control, hereafter referred to as "WT". Successful gene deletion was confirmed by PCR genotyping and immunoblot analysis (Figure 3.1). Immunoblots from 3 independently isolated sets of

collecting ducts showed a 49 ± 6% reduction in cldn-4 protein in the KO compared to the WT mice (Figure 3.1). Both WT and cldn-4 KO animals were viable and no gross difference was noted between the strains. No significant difference was observed in body weight, food or water consumption, urine volume and feces production, plasma electrolytes, urine pH and osmolarity, or fractional excretion (Table 3.1 and 3.2). We conducted similar experiments on mice aged 6 and 12 months. Please refer to Table A3 and A4 for 6 month age group and A11 and A12 for 12 month age group mice in the appendices.

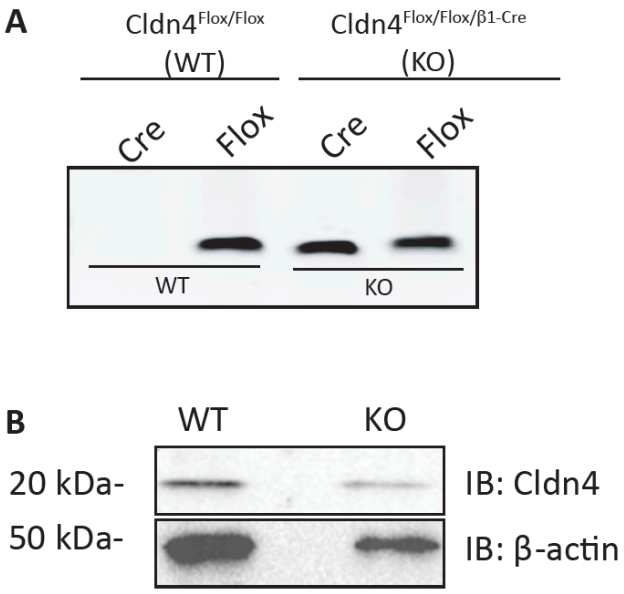

Figure 3. 1 Validation of IC cldn-4 KO mouse model

A, Representative result of a genotyping PCR experiment showing the presence of a flox but not a Cre allele in Cldn-4$^{Flox/Flox}$ mice, hereafter called WT, and both a flox allele and a Cre allele in Cldn-4$^{Flox/Flox/Cre}$ mice, hereafter called IC-Cldn4 KO mice. B, Representative Immunoblot from a minimum of 60 manually isolated CD from WT or IC-Cldn-4 KO mice. Note that the protein amount was not measured by BCA assay prior to the immunoblot experiment due to small quantity of lysates. The relative amount of cldn-4 protein in both WT and KO were normalized to ß-actin in 3 independent experiments.

Table 3. 1 Plasma electrolytes levels in WT and Cldn-4 KO mice at basal state on normal diet

Electrolyte	WT (n=16)	IC-Cldn4 KO (n=19)	P (T-Test)
Na^+ mmol/L	147.1 ± 1.2	147.6 ± 0.7	0.67
K^+ mmol/L	5.29 ± 0.30	5.05 ± 0.2	0.49
Cl^- mmol/L	117.1 ± 1.0	119.6 ± .9	0.09
TCO_2	23.13 ± .69	22.79 ±.65	0.70
BUN mg/dl	26.07 ± 2.26	25.25 ± 1.43	0.95
Glucose mg/dl	134.8 ± 6.32	126.7 ± 9.30	0.54
HCT mg/dl	40.56 ± 0.88	41.26 ± 1.27	0.19
pH	7.296 ± 0.03	7.3 ± 0.02	0.95
PCO_2 mmHg	45.87 ±3.31	44.69 ±2.557	0.94
HCO_3^- mmol/L	21.76 ±.62	21.51 ± .59	0.91
BEecf mmol/L	-4.15 ± 0.80	-4.54 ± 0.64	0.92
AnGap mmol/L	13.56 ± 0.86	12.0 ± 0.83	0.31
Hb gm/dl	13.8 ± 0.30	14.02 ± 0.43	0.18
MAP	73.97 ±3.76 (6)	85.08 ± 5.82 (6)	0.14
Urinary pH	6.374 ± 0.04	6.213 ± 0.05	0.08
$FE_{Na}^{+\%}$	0.087 ± 0.02	0.05 ± 0.01	0.15
$FE_{Cl}^{-\%}$	0.2 ± 0.09	0.08 ± 0.03	0.31
$FE_{Ca}^{2+\%}$	0.90 ± 0.4	0.31 ± 0.1	0.07
$FE_K^{+\%}$	4.56 ± 1.42	2.62 ± 0.79	0.40

HCT, hematocrit; BUN, Blood urea nitrogen; BEecf, Base Excess in the extracellular fluid;

AnGap, anion gap; Hb, Hemoglobin; MAP, Mean arterial pressure; FE: Fractional Excretion (%)

3.3.2 Tight junction mRNA and protein abundance is unchanged between cldn-4 KO and WT mice

Next we assessed tight junction protein and mRNA abundance from whole kidneys (Figure 3.2.). Although cldn-4 mRNA abundance was lower in KO animals, this did not reach statistical significance (Figure 3.2 C), cldn-4 protein abundance was similar in WT and KO animals (Figure 3.2 B). This lack of difference could be attributed to the use of whole kidney homogenates as opposed to isolated collecting ducts as in Figure 3.1. It could also originate from: (i) cldn-4 un-altered expression in PC in our mice, (ii) intact cldn-4 expression in the thin ascending limb of Henle's loop and connecting tubule[79], (iii) the low abundance of IC versus PC[258] and (iv) incomplete KO from the Cre promoter as previously described[252]. As cldn-8 is required for Cldn-4 to localize to the tight junction[259], cldn-8 mRNA and protein abundance was next assessed in WT and cldn-4 KO mice. No significant difference was observed compared to WT mice (Figure 3.2 A, B and C). We assessed the abundance of two other claudins expressed in the CD, cldn-7 and -3, and no difference was observed either. These results indicate that knocking cldn-4 out of IC does not dramatically alter tight junction composition.

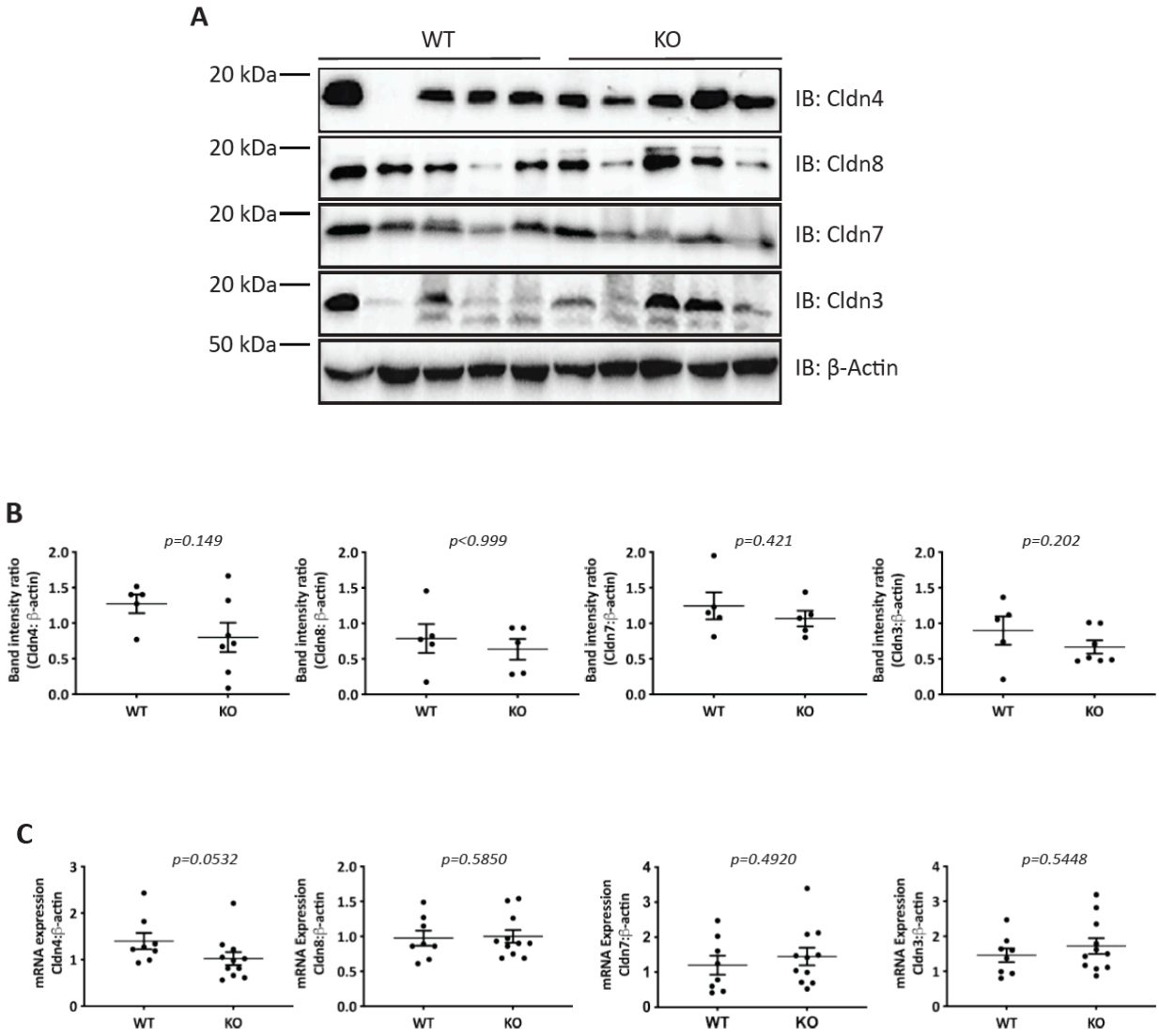

Figure 3. 2 Relative abundance of tight junction proteins and corresponding mRNA at basal state.

A, Representative immunoblots of WT and IC-cldn-4 KO mice kidney homogenates incubated with the indicated antibodies. B, Quantification of immunoblot bands normalized to housekeeping protein actin. C, mRNA quantification of the corresponding genes normalized to housekeeping gene. Statistical significance was determined by Student's t-test.

3.3.3 Abundance of IC-specific transcellular ion transporters is elevated in clnd-4 KO mice

Although plasma and urine composition were similar between WT and cldn-4 KO mice, we assessed CD transcellular transporters mRNA and protein abundance. As shown in Figure 3.3 A, B & C, although the abundance of the V-H^+-ATPase protein is unchanged in KO animals compared to WT, kAE1 and pendrin proteins are both significantly increased in the cldn-4 KO mice. Aligned with this result, type-B IC-specific protein NDCBE encoding mRNA increased significantly in the cldn-4 KO mice (an NDCBE antibody was not available to us) (Figure 3.3 D). The lack of change in V-H^+-ATPase abundance indicates that the up-regulation of these proteins is not reflective of an increase in type-A IC number in the KO mice compared to WT animals. PC marker AQP-2 protein and mRNA abundance and ENaC mRNA abundance were not significantly altered either despite a trend for an increased protein and mRNA abundance in KO mice, indicating that this increase is restricted to IC but not PC. The abundance of the thick ascending limb (TAL) marker sodium/potassium/chloride cotransporter (NKCC) was not significantly altered either between WT and KO mice (Figure 3.3 E). Together these results indicate a specific increase in abundance of IC proteins involved in transcellular sodium and chloride reabsorption, without a change in tight junction protein abundance.

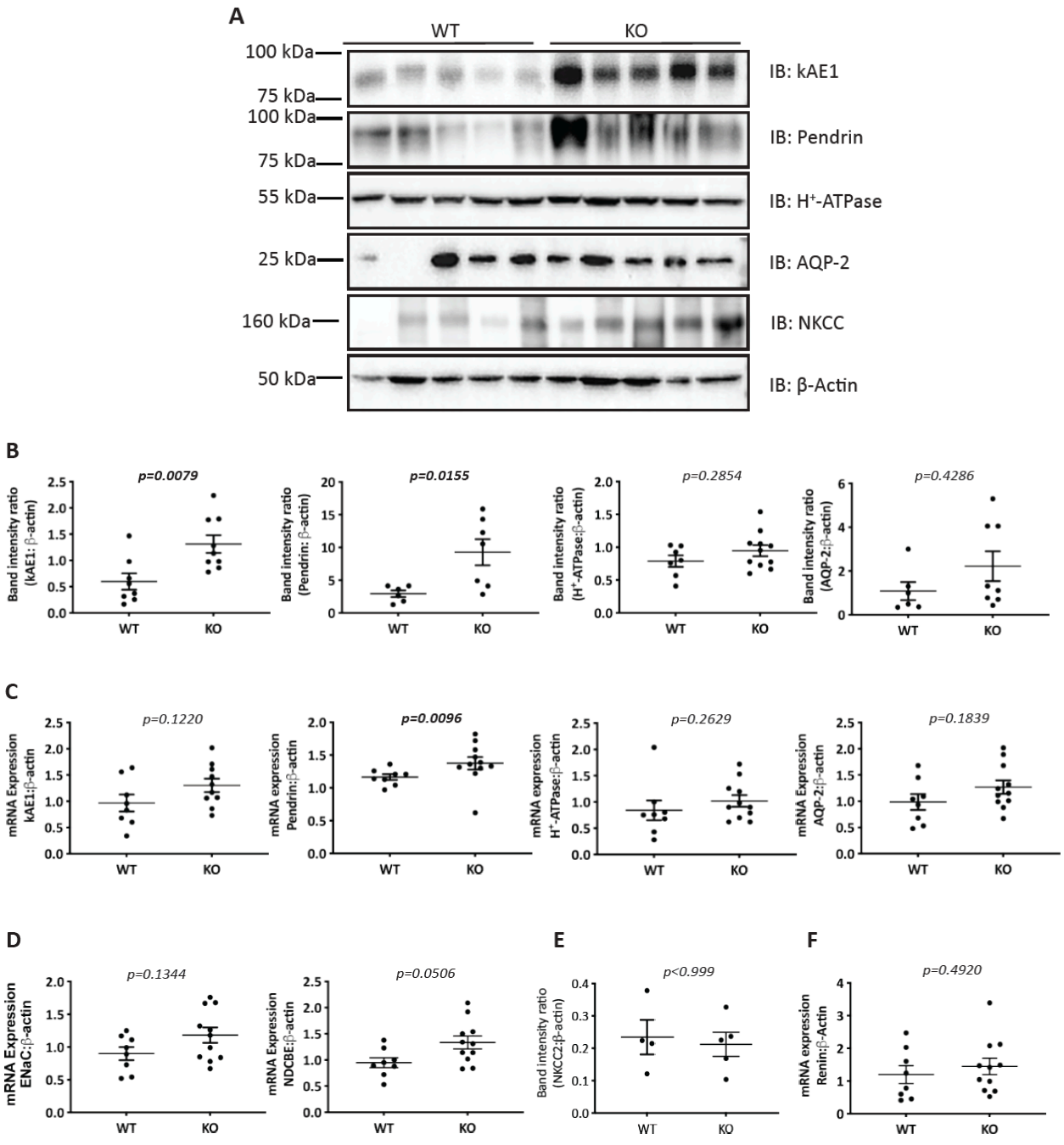

Figure 3. 3 Relative abundance of selected intercalated cell membrane proteins and corresponding mRNA at basal state.

A, Representative immunoblots of WT and IC-cldn4 KO mice kidney homogenates decorated with the indicated antibodies. B, Quantification of immunoblot bands normalized to housekeeping

protein actin. C, mRNA quantification of the corresponding genes normalized to housekeeping gene. D, mRNA quantification of ENaC, NDCBE, NKCC (E) and renin (F) gene expression normalized to housekeeping gene. Statistical significance was determined by Student's t-test.

3.3.4 Cldn-4 KO mice fed a low NaCl diet are wasting urinary sodium

The increased abundance of transcellular sodium and chloride IC transporters may reflect a compensatory mechanism to optimize reabsorption of these ions in the face of a defective paracellular pathway. To test this hypothesis, WT and cldn-4 KO mice were fed a low NaCl diet for 14 days and their plasma and urine composition analyzed (Table 3.2 & 3.3). We expected that if the KO mice have abnormal salt reabsorption, they may waste urinary sodium and chloride on a NaCl-depleted diet. Indeed, fractional excretion (FE%) of Na^+ was significantly higher (P=0.03) in the IC-cldn-4 KO mice compared to the WT mice. However, neither the FE% of Cl^- nor of Ca^{2+} and K^+ was different between groups. WT and KO mice did not differ in their blood pressure, plasma electrolyte composition or urine pH and osmolality either (Table 3.2). These results are consistent with cldn-4 KO mice being unable to maximize sodium reabsorption when fed a NaCl depleted diet.

Please refer to Table A5 and A6 for the gross anatomical and plasma electrolyte values for 6 month old mice and Table A13 and A14 for the 12 month old mice groups (appendices).

Table 3. 2 Plasma electrolytes levels in WT and Cldn4 KO mice on low NaCl diet

Electrolyte	WT (n=10)	IC-Cldn4 KO (n=12)	P (T -test)
Na^+ mmol/L	150 ± 1.13	146.8 ± 1.49	0.14
K^+ mmol/L	5.48 ± 0.22	6.51 ± 0.53	0.22
Cl^- mmol/L	118.9 ± 0.75	123 ± 2.01	0.23
TCO_2	25.4 ± 0.89	22 ±1.73	0.20
BUN mg/dl	24.3 ± 1.88	24.4 ± 2.18	0.98
Glucose mg/dl	146.1 ± 12.92	125.5 ± 10.79	0.26
HCT mg/dl	42.8 ± 0.96	40.17 ±1.38	0.16
pH	7.25 ± 0.03	7.24 ± 0.02	0.41
PCO_2 mmHg	55.85 ± 5.37	49.58 ± 5.23	0.63
HCO_3^- mmol/L	23.71 ± 0.79	20.43 ± 1.53	0.14
BEecf mmol/L	-3.4 ± 0.79	-7.08 ± 1.51	0.05
AnGap mmol/L	12.8 ± 1.04	12.3 ± 1.21	0.69
Hb gm/dl	14.55 ± 0.32	13.64 ± 0.47	0.16
MAP	77.58 ± 3.48. (6)	83.11 ± 2.98 (6)	0.25
Urinary pH	6.44 ± 0.05	6.40 ± 0.07	0.34

HCT, hematocrit; BUN, Blood urea nitrogen; BEecf, Base Excess in the extracellular fluid; AnGap, anion gap; Hb, Hemoglobin; MAP, Mean arterial pressure; FE: Fractional Excretion (%)

Table 3. 3 Fractional Excretion levels in WT and KO mice on low NaCl diet

Fractional Excretion (%)	WT (n=10)	IC-Cldn-4 KO (n=12)	P (T -test)
Na^+	0.001 ± 0.0002	0.01 ± 0.004	**0.03***
Cl^-	0.01 ± 0.001	0.01 ± 0.003	0.68
Ca^{2+}	0.23 ± 0.06	0.13 ± 0.03	0.44
K^+	4.92 ± 1.361	15.77 ± 6.21	0.51

3.3.5 Abundance of kAE1 and pendrin IC markers is elevated after a NaCl-depleted diet

To delineate the mechanism of the urinary sodium loss, we first compared cldn-4 and other claudins' abundance between the two strains after the NaCl-depleted diet. cdn-4 mRNA and protein abundance was significantly lower in the KO mice compared to the WT, while cldn-7, -8 and -3 protein and mRNA abundance was not significantly different (Figure 3.4 A, B & C). However, similar to a NaCl-replete diet, kAE1 and pendrin protein abundance was increased significantly in the cldn-4 KO mice compared to WT animals although the V-H^+-ATPase protein and mRNA abundance was not different (Figure 3.5). Neither pendrin nor kAE1 mRNA abundance was different in the KO despite increased protein abundance. In contrast to cldn-4 KO mice that had a significant increase in NDCBE mRNA abundance at the basal state (Figure 3.5 D), there was no significant difference between WT and cldn-4 KO mice after a NaCl-depleted diet. Neither the PC protein AQP-2 (protein and mRNA) and ENaC mRNA abundance nor NKCC mRNA abundance differed between WT and KO mice (Figure 3.5 D & E).

3.3.6 There is no difference in RAAS-triggering between cldn-4 KO and WT mice

Pendrin and kAE1 protein abundance are regulated by angiotensin II[216,260]. To assess whether the renin-angiotensin-aldosterone system (RAAS) contributes to elevated pendrin, kAE1 and NDCBE abundance, we measured renin gene expression in WT and cldn-4 KO animals on both NaCl replete and NaCl depleted diets. No difference was observed between the two genotypes in both diets (Figure 3.3 F and 3.5 F), indicating that a renin-independent process is likely responsible for the up-regulation of these transporters.

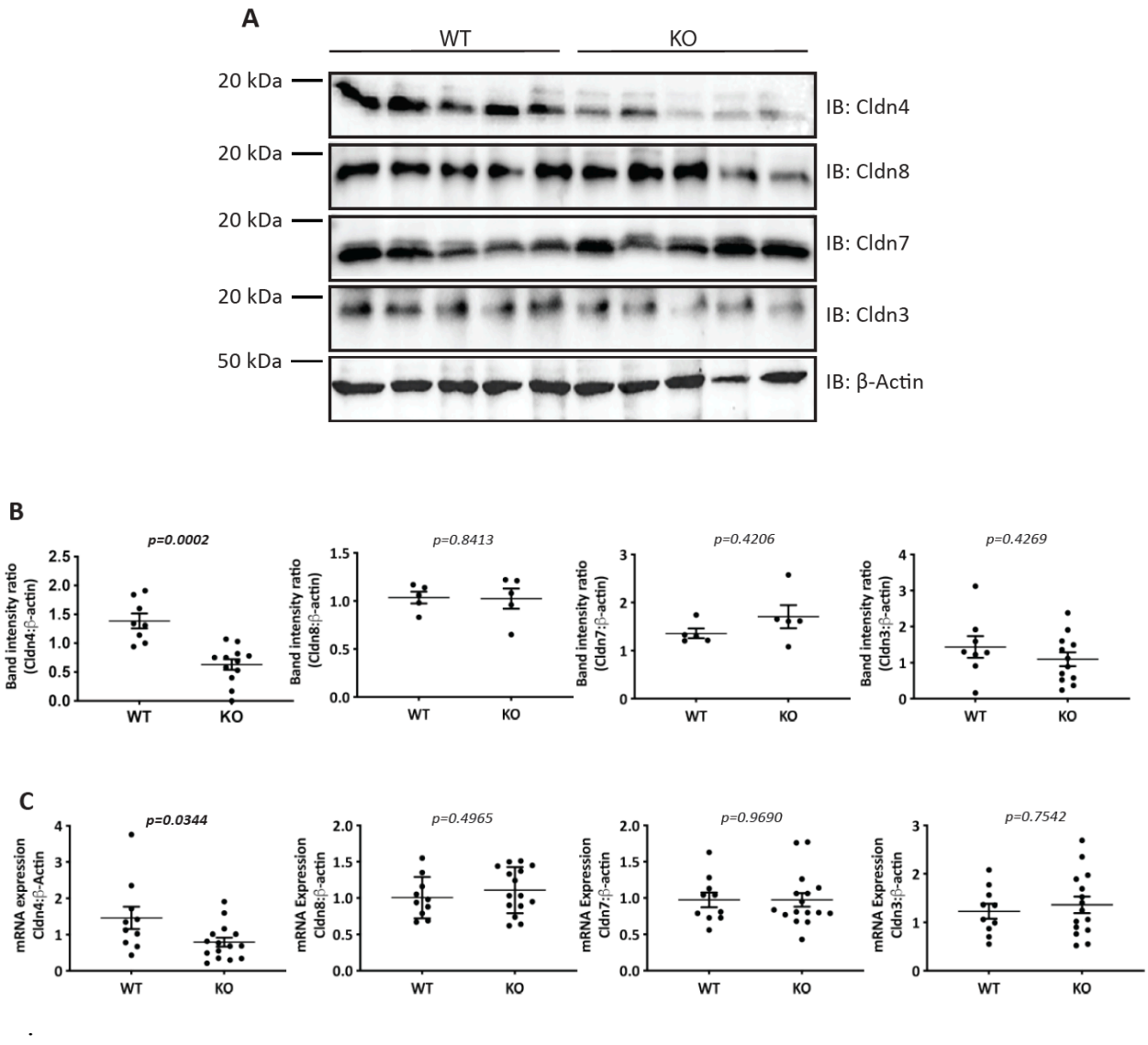

Figure 3. 4 Relative abundance of tight junction proteins and corresponding mRNA after a low NaCl diet.

A, Representative immunoblots of WT and IC-Cldn4 KO mice kidney homogenates decorated with indicated antibodies. B, Quantification of immunoblot bands normalized to housekeeping protein actin. C, mRNA quantification of the corresponding genes normalized to housekeeping gene. Statistical significance was determined by Student's t-test.

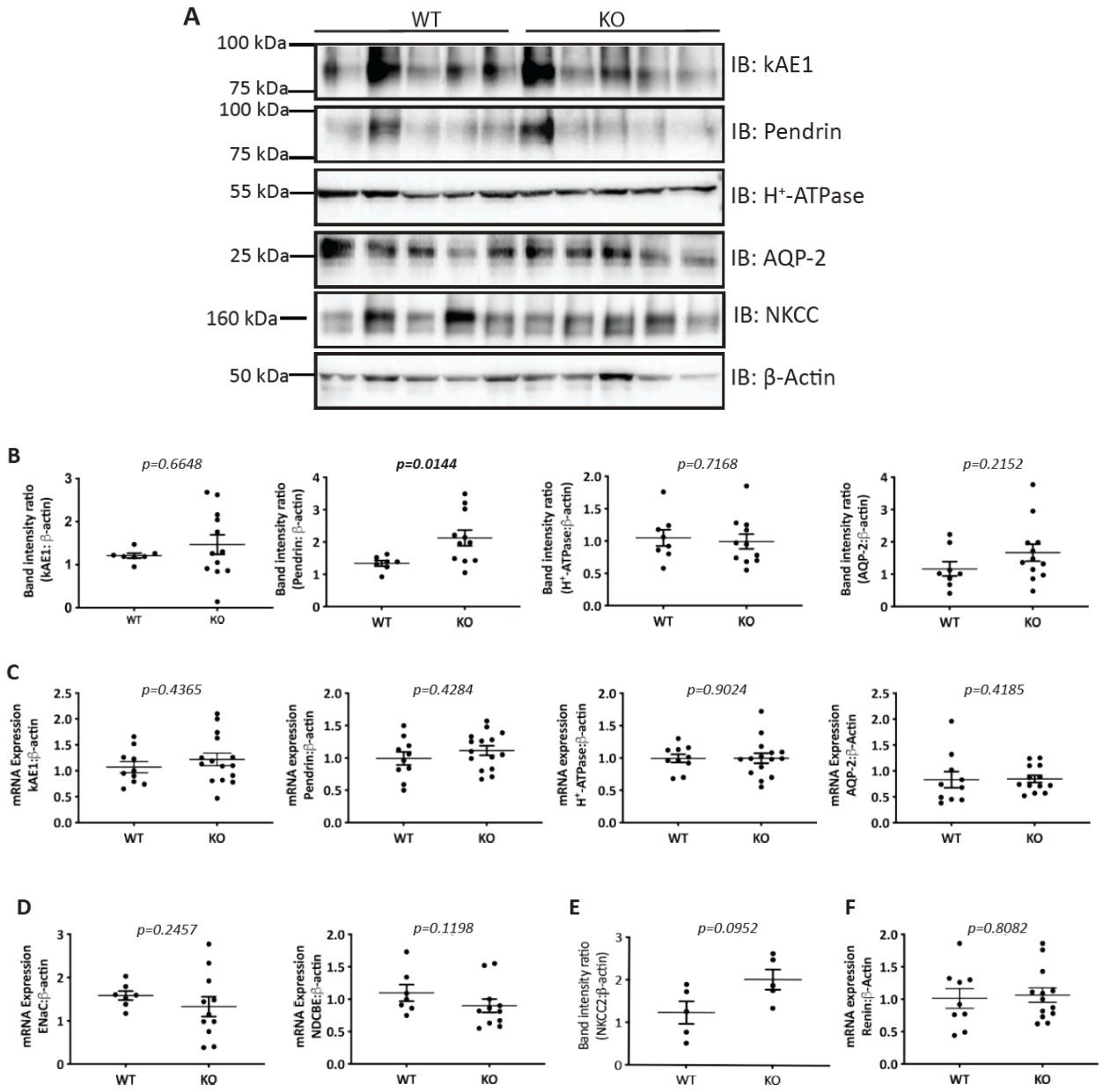

Figure 3. 5 Relative abundance of selected intercalated cell membrane proteins and corresponding mRNA after a low NaCl diet.

A, Representative immunoblots of WT and IC-Cldn4 KO mice kidney homogenates decorated with indicated antibodies. B, Quantification of immunoblot bands normalized to housekeeping protein actin. C, mRNA quantification of the corresponding genes normalized to housekeeping

gene. D, mRNA quantification of ENaC, NDCBE, NKCC (E) and renin (F) gene expression normalized to housekeeping gene. Statistical significance was determined by Student's t-test.

3.3.7 Cldn-4 KO mice maintain a normal acid-base balance

As cldn-4 was knocked out in both type-A IC that secrete acids and type-B IC that secrete bicarbonate, we asked whether cldn-4 KO impacts acid-base balance in these animals. WT or IC-ccldn-4 KO mice were fed an acidic diet for 24 hours and plasma composition and urine pH were examined. Table 3.4 shows that apart from plasma glucose that was significantly decreased in cldn-4 KO mice, no significant difference was found between WT and cldn-4 KO mice, indicating that cldn-4 KO mice are able to maintain a normal acid-base balance after an acid challenge and that IC-cldn-4 is therefore not required for preserving a neutral plasma pH.

Mice given similar acid load for a longer period time also did not show any significant differences between the WT and cldn-4 KO mice. We conducted long term acid load experiments on mice aged 3 month and 6 month. In both 3 month and 6 month age, both WT and KO mice showed a similar trend of urine acidification (Figures A2 and A4, appendices) without any significant difference between the WT and KO mice. There was also no significant difference in urine osmolarity in these 2 age group of mice (Figures A3 and A5, appendices). Please refer to Table A2 and A3 in the appendices for 3 month old mice's physical parameters and plasma electrolytes and Table A7 and A8 for 6 month old mice respectively.

Table 3. 4 Plasma electrolytes levels and fractional excretion in WT and Cldn4 KO mice after an acid challenge (0.28 M NH_4Cl H_2O)

Electrolyte	WT (n=10)	IC-Cldn4 KO (n=12)	P (T -test)
Na^+ mmol/L	146.5 ± 1.28	146.1 ± 2.52	0.98
K^+ mmol/L	5.5 ± 0.26	5.76 ± 0.41	0.73
Cl^- mmol/L	124.9 ± 2.25	128.7 ± 2.10	0.15
TCO_2	19.64 ± 0.92	18.17 ± 1.25	0.25
BUN mg/dl	22.91 ± 1.95	22.83 ± 1.01	0.75
Glucose mg/dl	108.8 ± 8.02	82.5 ± 5.04	**0.01***
HCT mg/dl	39 ± 2.19	35.08 ± 2.67	0.30
pH	7.255 ± 0.01	7.234 ± 0.02	0.47
PCO_2 mmHg	41.55 ± 1.68	40.38 ± 3.09	0.52
HCO_3^- mmol/L	18.47 ± 0.88	16.92 ± 1.19	0.20
BEecf mmol/L	-8.72 ± 1.09	-10.75 ± 1.51	0.05
AnGap mmol/L	12.93 ± 0.73	11.09 ± 1.87	0.08
Hb gm/dl	13.26 ± 0.74	12.83 ± 0.81	0.37
Urinary pH	5.72 ± 0.16	5.71 ± 0.1	0.49
FE_{Na^+}%	0.58 ± 0.2	0.62 ± 0.19	0.91
FE_{Cl^-}%	2.23 ± 1.03	1.86 ± 0.62	0.82
$FE_{Ca^{2+}}$%	1.15 ± 0.33	2.29 ± 0.74	0.63

HCT, hematocrit; BUN, Blood urea nitrogen; BEecf, Base Excess in the extracellular fluid; AnGap, anion gap; Hb, Hemoglobin; FE: Fractional Excretion (%)

3.3.8 Cldn-4 KO mice have a normal calcium homeostasis

As total cldn-4 KO mice displayed an increased fractional excretion of Ca^{2+} and hypocalcemia[110], we compared plasma and urine composition after a control or a low calcium diet in WT and cldn-4 KO mice. Table 3.5 shows that a calcium-depleted diet did not result in alterations in physical parameters, plasma electrolytes or fractional excretion of sodium, chloride or calcium. This finding supports that IC-specific cldn-4 KO mice are able to conserve calcium to the same extent as WT littermates, and that IC-cldn-4 is not involved in calcium homeostasis.

Six month old mice underwent the similar diet and experiments and there was no significant difference between the WT and KO mice in their physical parameters and plasma electrolytes (Tables A9 and A10 in the appendices).

Table 3. 5 Plasma electrolytes levels and fractional excretion in WT and Cldn4 KO mice after a low Calcium diet (0.01%)

Electrolyte	WT (n=10)	IC-Cldn4 KO (n=12)	P (T -test)
Na^+ mmol/L	146.5 ± 1.28	146.1 ± 2.52	0.98
K^+ mmol/L	5.78± 0.26	5.71 ± 0.41	0.52
Cl^- mmol/L	120.8 ± 0.31	119.2 ± 0.52	0.15
TCO_2	24.5 ± 0.65	24.89 ± 0.56	0.69
BUN mg/dl	15.75 ± 0.88	18.33 ± 1.58	0.38
Glucose mg/dl	131.1± 9.84	136.8 ± 7.83	0.79
HCT mg/dl	45.88 ± 0.78	44.78 ± 1.06	0.43
pH	7.271 ± 0.02	7.31 ± 0.02	0.30
$PCO_{2\ mmHg}$	41.55 ± 1.68	40.38 ± 3.09	0.52
HCO_3^- mmol/L	18.47 ± 0.88	16.92 ± 1.19	0.20
PCa^{2+} mmol/L	1.887± 0.19	1.87± 0.22	0.88
Urinary pH	5.69 ± 0.09	5.74 ± 0.03	0.83
$FE_{Na}{}^{+\%}$	0.1 ± 0.03	0.17 ± 0.04	0.20
$FE_{Cl}{}^{-\%}$	0.10 ± 0.02	0.20 ± 0.07	0.44
$FE_{Ca}{}^{2+\%}$	0.70 ± 0.27	0.5 ± 0.14	0.83

HCT, hematocrit; BUN, Blood urea nitrogen; BEecf, Base Excess in the extracellular fluid; AnGap, anion gap; Hb, Hemoglobin; FE: Fractional Excretion (%)

3.4 Discussion

In this work, we have assessed the contribution of IC cldn-4 to electrolyte and urinary composition at steady state, after an acid load or after a low NaCl or low calcium diet. Our results indicate that although plasma parameters were normal, a low NaCl diet unveils an inability to conserve sodium in cldn-4 KO mice. These results show that in IC, cldn-4 loss neither affects acid-base balance, calcium nor chloride homeostasis. However, cldn-4 is involved in sodium balance, in a mechanism that does not involve renin *Ren* gene up-regulation. This urinary sodium waste is synchronous with elevated protein and/or mRNA expression of IC-specific transcellular ion transporters such as kAE1, pendrin and NDCBE despite a similar RAAS status between WT and KO mice. No difference in PC-specific ion transporter ENaC or water channel AQP2 was detected. This work confirms the contribution of cldn-4 to the conservation of sodium via the paracellular reabsorption pathway in the CD and CNT. Indeed, although IC cldn-4 KO mice did not waste urinary sodium at the basal state, they did upon a NaCl depleted diet. Interestingly only sodium but not chloride urinary excretion was altered in IC cldn-4 KO mice. cldn-4 is a paracellular chloride pore and cation blocker[107,261]. Total cldn-4 KO animals displayed an increased fractional excretion of chloride with an insignificant trend for increased fractional excretion of sodium as well[110]. These animals showed an up-regulation of cldn-3 and a decrease in cldn-8 protein at the tight junction. PC-specific cldn-4 KO mice were hypotensive, hypochloremic and wasted both urinary sodium and chloride at steady state and upon a low NaCl diet[111]. The stronger phenotype of PC-specific cldn-4 KO mice versus IC-specific KO can be attributed to the combination of a higher abundance of PC versus IC in the CD with a potentially cleaner KO compared with the incomplete KO triggered by the B1-ATPase promoter used in our study[17,252]. This, however, does not explain the exclusive urinary waste of sodium but not of chloride. PC are involved in

electrogenic sodium reabsorption through apical ENaC and ROMK and basolateral Na^+/K^+-ATPase, while chloride is reabsorbed concomitantly via the transcellular and paracellular pathways. With the discovery that type-B intercalated cells are involved in electroneutral sodium and chloride reabsorption through pendrin and NDCBE on the apical side, and AE4 on the basolateral side[35,47,262], we propose that in IC-specific cldn-4 KO mice at steady state, the up-regulation of IC-specific transcellular transporters pendrin, NDCBE and kAE1 in cldn-4 KO mice reflects a successful mechanism to increase transcellular sodium and chloride reabsorption in compensation for defective paracellular transport. However, on a NaCl depleted diet, this compensatory mechanism becomes insufficient and urinary sodium is wasted. Specifically we speculate that when IC cldn-4 KO mice are exposed to a low NaCl diet, sodium leaks back into the lumen paracellularly through porous tight junctions that are lacking the sodium blocker cldn-4. However, the tight junction is impermeable to chloride ions due to the loss of chloride pore cldn-4, thereby preventing the leak of these anions paracellularly. However, there is an increase in the protein abundance of pendrin, which facilitates transcellular chloride reabsorption, hence, no increased chloride loss is observed in the urine. This process would translate into sodium but not chloride urinary wasting on a low NaCl diet.

Our work also confirms that knocking a tight junction protein out alters the transcellular ion reabsorption pathway. Our recent work showed that expression of kAE1 at the basolateral membrane of inner medullary collecting duct cells alters tight junction properties[113], illustrating the interplay between the two pathways. kAE1 expression in these polarized cells significantly lowered the transepithelial electrical resistance in a cldn-4-dependent mechanism. Such interplay has been demonstrated before, including between cldn-16 and TRPV5 in the mouse DCT[107]. TRPV5 apical localization is regulated by phosphorylation levels of cldn-16 in a parathyroid

hormone receptor-dependent pathway, a pathogenic process responsible for familial hypomagnesemia with hypercalciuria and nephrocalcinosis (FHHNC). Our work also confirms that knocking out another claudin in the CD affects IC-specific ion transporters.

Interestingly, no difference in renin gene expression was observed between WT and KO mice upon dietary NaCl restriction. Accordingly, no change in blood pressure was observed either between WT or IC-cldn-4 KO mice. Previous work showed that kAE1 protein is up regulated in the mouse kidney medulla by $NaHCO_3$ and DOCA, or $NaHCO_3$ alone[216]. We found that in IC-cldn-4 KO mice, both kAE1 mRNA and protein abundances were increased compared with WT animals at basal state but not after a low NaCl diet. This possibly suggests that at basal state, the already increased protein levels cannot be further augmented upon a low NaCl diet. Regulators of protein expression other than the renin-angiotensin-aldosterone (RAAS) system may be responsible for the up-regulation of kAE1 mRNA and proteins. Luminal secretion of prostaglandin 2 (PGE2) acts in a paracrine fashion to regulate neighbor cells in the CD[35,258,263]. In the CNT/CCD, PGE2 release is itself triggered by luminal ATP production, another paracrine molecule that originates from type-B IC locally and that regulates salt balance through PC ENaC and AQP2 in the medullary CD[35,263]. In addition, Cl^- reabsorption is regulated by both cAMP and nitric oxide (NO)[260,264,265]. The membrane abundance of pendrin is increased after an administration of NO synthase inhibitor without affecting subcellular assembly of the protein *in vivo*[262]. There are several ways NO could contribute to pendrin abundance, i.e., directly on protein translation and/or turnover[264] or indirectly by changes in the blood pressure and hormonal effects either in an endocrine or paracrine way[266,267].

Unlike kAE1 and pendrin, the V-H^+-ATPase protein and mRNA abundance remained unchanged in IC specific cldn-4 KO mice. As this ATPase is regulated by angiotensin II, this

finding aligns with a RAAS-independent regulatory process in play in these mice. This finding also indicates that there is no increase in the number of IC in cldn-4 KO mice as other IC proteins are up-regulated but not the ATPase. Our results however do not exclude a relocation of the ATPase from intracellular vesicles to the apical membrane, resulting in enhanced proton secretion. Our results also indicate a lack of contribution of IC-cldn-4 to acid-base balance. Type-A IC secrete urinary protons while reabsorbing bicarbonate to the interstitium, while type-B IC secrete bicarbonate and reabsorb protons to the interstitium. The combined activity of cytosolic carbonic anhydrase II, apical V-H^+-ATPase and basolateral kAE1 efficiently maintains acid and base secretion/reabsorption depending on the transporters' location within cells. Our results show that, despite the documented role of these cells in acid-base balance, tight junction cldn-4 therefore does not seem to be involved in acid-base balance. As PC-cldn-4 is expected to remain intact in IC cldn-4 KO mice, it is possible that it is abundant enough to prevent back flux of bicarbonate to the lumen.

Calcium balance was also unaffected in IC-cldn-4 KO mice, in contrast with global cldn-4 KO mice[110]. This finding either suggests that other cldn-4-expressing cells are involved in calcium balance in the global KO, or that the 49% reduction in cldn-4 observed in IC cldn-4 KO mice is not sufficient to unveil a calcium imbalance. Global cldn-4 KO mice displayed an upregulation of cldn-3 protein[110], which is likely a compensatory response to the lack of cldn-4. As cldn-3 acts as an ion blocker[268], it could contribute to the inhibition of Ca^{2+} reabsorption in the global cldn-4 KO. Our results neither indicated a change in cldn-3 protein abundance, nor at the mRNA level. This lack of change in Cldn-3 abundance may explain the normal calcium balance observed in IC-cldn-4 KO mice.

Overall, this work shows that IC-cldn-4 KO mice display an abnormal retention of urinary sodium after a NaCl depleted diet, despite a normal blood pressure, urinary chloride, urinary calcium, or pH. IC-cldn-4 KO mice display elevated IC-specific ion transporter mRNA and/or protein abundance.

CHAPTER FOUR

SUMMARY, LIMITATIONS AND FUTURE DIRECTIONS

4.1 Summary

This dissertation had two distinct objectives relative to the proteins SLC26A7 and cldn-4. We aimed to:

(*i*) characterize the SLC26A7 protein abundance and function at the basal state, in a medullary-mimicking hyperosmotic environment or in acidic pH growth medium mimicking acidosis, in the absence or presence of either kAE1 or kAE1 R901X dRTA mutant,

(ii) investigate whether IC specific cldn-4 KO mice are able to balance plasma and urine pH and electrolyte homeostasis as efficiently as the WT mice at the basal state, in low NaCl, acidic or low calcium diet conditions.

4.2 Characterization of SLC26A7: Summary, limitations and future directions

4.2.1 Summary

Four main findings were obtained from this study:

4.2.1.1 SLC26A7 is a Cl^-/HCO_3^- exchanger in MDCK cells

SLC26A7 acts either as a Cl^- channel in HEK293 cells[148] or a Cl^-/HCO_3^- exchanger in *Xenopus* oocytes[150] and our study confirmed that the protein is a Cl^-/HCO_3^- exchanger in MDCK cells which do not endogenously express this protein. Immunofluorescence experiments detected SLC26A7 intracellularly however, measuring a Cl^-/HCO_3^- exchange activity in these cells demonstrates SLC26A7 partial membrane localization. In contrast to SLC26A7, kAE1 showed a significantly higher ion exchange activity, suggesting a better membrane localization or a higher exchange efficiency in non-polarized MDCK cells.

4.2.1.2 Increased abundance of SLC26A7 in hyper-osmotic medium

We mimicked the hyper-osmotic medullary environment by increasing the cell culture medium osmolality and showed that the abundance of both SLC26A7 and kAE1 increases upon

growing them in the hyperosmotic medium compared to the normal growth medium (Figure 2 A & B). Cycloheximide chase experiments showed an increased SLC26A7 half-life in hyper-osmotic media, likely accounting for the increased overall protein abundance (Figure 2 A, B). However, when we examined the localization of the protein in hyper-osmotic growth medium in both polarized and non-polarized conditions, we did not observe a dramatic change . The abundance of the dRTA mutant kAE1 R901X abundance also did not change after incubating in hyperosmotic media.

4.2.1.3 Hyper-osmotic conditions do not increase SLC26A7 activity

Our next objective was to investigate if the Cl^-/HCO_3^- exchange activity is increased in hyperosmotic conditions in the cells expressing SLC26A7 or kAE1 proteins individually, or together. Functional assay experiments revealed that although the abundance of SLC26A7 increases in hyperosmotic condition, its activity does not. On the other hand, the activity of kAE1 protein increases only upon incubation in mannitol hyperosmotic media. kAE1 R901X dRTA mutant activity did not increase with osmolality as it remained inactive whatever osmolality of the growth medium.

4.2.1.4 SLC26A7 abundance decreases in cells grown at low extracellular pH

In MDCK cells expressing SLC26A7 or co-expressing SLC26A7 and kAE1 WT, and grown in acidic pH medium mimicking dRTA, the abundance of SLC26A7 decreased at a pH lower than 7.2 compared to physiological pH condition, whereas the abundance of kAE1 remained unchanged. This simple finding suggests that during uncorrected metabolic acidosis, SLC26A7 may be unable to compensate the loss of kAE1 function due to its decreased abundance . The underlying cause of this reduction is still unknown.

4.2.2 Limitations of the study

Our *in vitro* study had several shortcomings. First, the proteins of interest in this study were investigated in MDCK cells. These are epithelial cells derived from canine kidneys and have been used to characterize different proteins and their various mutant versions, such as kAE1[172], cldn-4[269], SLC26A7[223] and WNK4[270]. The MDCK cell line is an excellent expression system. Nevertheless, the use of this cell line has two constraints: *i)* the cell line was established from whole kidney and not specifically collecting duct[271], and *ii)* when expressed in MDCK cells vs mIMCD3 cells or animal models, kAE1 dRTA mutants have very distinct phenotypes[172,173]. For instance, in MDCK cells, the kAE1 R589H mutant was retained in the ER[172] but in mIMCD3 cells, the mutant was localized at the plasma/basolateral membrane as in kAE1 R607H knockin mouse model[173]. Another limitation is that MDCK cells do not express endogenous collecting duct proteins such as kAE1 or H^+ATPase and therefore do not fully mimic collecting duct cells.

A way to bypass these constraints is to use a different cell line such as mIMCD3 cells, derived from hyperosmotic inner medullary part of the kidney. Although this immortalized cell line is of collecting duct origin, it does not express endogenous kAE1 but carries the machinery for kAE1 membrane trafficking and function. Because most previous studies on SLC26A7 protein were conducted in MDCK cells, we were able to compare our findings to others and gain significant insight into the protein's function.

We used the constitutive expression system pCDNA3 for SLC26A7 and retroviral pQCXIH plasmid for kAE1 and R901X to express the SLC26A7, kAE1 and kAE1 R901X proteins. The drawbacks of this stable expression system are: *i)* the progressive loss of kAE1 and kAE1 R901X mutant expression in 14-21 days of reaching confluency, requiring regular new cell batch preparation; *ii)* variable transfection efficiency between experimental batches, and *iii)* the

time required to obtain a selected batch of cells (2-3 weeks). These flaws were reduced by normalizing proteins of interest against housekeeping protein (β-actin) as loading controls, optimizing experimental time to perform as many experiments per batch as possible, and planning regular infections to avoid wasting time and maintain continuity of experiments.

An alternative strategy would be to switch to a lentiviral inducible expression system that we have later developed for mIMCD3 cell lines expressing kAE1[113]. This strategy would allow us to overcome the main limitation of progressive loss of protein expression overtime and would have the following advantages: *i)* same batch of cells could be used from a single lentiviral infection, thereby eliminating the variability between experiments, and *ii)* maximizing the use of same batch of cells by inducing protein expression 24 to 48 hours prior to the experiment day.

An additional flaw to our expression study was the inability to adjust relative expression of kAE1 to SLC26A7 protein. The two expression systems (pCDNA3 and pQCXIH) had non-inducible promoters and resulted in different relative abundance between proteins. In particular, kAE1 R901X dRTA mutant had a low expression level, which complicated the interpretation of SLC26A7/kAE1 co-expression experiments.

4.2.3 Future Directions

Our results provided strong evidence that SLC26A7 is a Cl^-/HCO_3^- exchanger in MDCK cells and its abundance is variable based on growth media osmolarity. We also showed that SLC26A7 protein abundance is decreased when the cells are incubated in an acidic medium, possibly explaining why it is unable to correct an acidosis in dRTA. Our findings also showed that although the protein is primarily intracellular, it displays a Cl^-/HCO_3^- exchange activity, albeit at a lower level than kAE1. Overall, this research has improved our understanding of SLC26A7 protein's role in MDCK cells, alone and in combination with kAE1.

One weakness of our experiments was that they were performed *in vitro* and in a cell line that modestly reproduced intercalated cells. An *in vivo* validation would be highly beneficial, although the number of SLC26A7 animal studies is still quite low. There is only one mouse model that demonstrates that the deletion of SLC26A7 causes dRTA and perturbs gastric acid secretion[220]. However, its role relative to kAE1 was not investigated. An approach to answer our remaining questions, and validate our findings *in vivo*, would be to examine SLC26A7 protein abundance and localization in a kAE1 dRTA knockin (KI) mutant mouse model, such as the R607H Ae1 KI mice[173]. This model will give us a better insight into SLC26A7 characteristics and interaction with kAE1. Specifically, we could examine:

4.2.3.1 SLC26A7 protein expression and relative abundance

Our laboratory has recently acquired and is currently conducting experiments with R607H (murine equivalent of human R589H dRTA mutant) and L919X (murine equivalent of human R901X dRTA mutant) Ae1 KI mice (unpublished). Conducting immunoblot experiments from total kidney lysates would inform us about the relative abundance of the SLC26A7 protein in KI or WT mouse. Quantitative RT-PCR experiments from WT or KI mouse kidney mRNA would shed light on SLC26A7 gene expression of in WT or KI mice. Feeding the dRTA mutant or WT mice an acid diet would further validate whether SLC26A7 protein abundance decreases in acidosis.

4.2.3.2 SLC26A7 protein localization

Our immunofluorescence experiments in MDCK cells showed that SLC26A7 is mostly intracellular. However, the localization of the murine protein at basal state or in dRTA is unknown. To explore this, immunohistochemistry experiments could be conducted with kidney sections from kAE1 dRTA mutant KI mice to detect SLC26A7 and kAE1 localization .

4.2.3.3 Micro-perfusion study

The extent of intracellular pH change in cells expressing SLC26A7, kAE1, or kAE1 R901X was measured *in vitro* in our study. This informed us about the functional characteristics of SLC26A7 relative to kAE1 and kAE1 R901X . These findings could be validated *in vivo*. To assess the exchanger function of SLC26A7 relative to kAE1 or kAE1 L919X or R607H mutant, micro-perfusion studies on isolated collecting ducts from WT mice or kAE1 L919X or R607H KI mice could be conducted. Freshly dissected collecting ducts incubated with cell permeable, fluorescent pH-sensitive BCECF-AM dye could be exposed to a chloride-free bath solution to trigger chloride/bicarbonate exchange and intracellular alkalinisation. These experiments could also be conducted in the presence of pharmacological inhibitor DIDS; however, this approach would not definitely differentiate the individual contribution of SLC26A7 relative to kAE1[148].

4.3 Intercalated cell specific cldn-4 KO mouse model

4.3.1 Proposed mechanism

We propose the following mechanism for increased FE% in the NaCl depleted diet condition.

In the IC cldn-4 KO mice, since the TJ integrity is compromised because of the missing cldn-4 protein that normally acts as a chloride pore, less paracellular Cl- transport may occur. This would result in accumulation of Cl^- in the lumen making this side of the membrane electronegative. As a result, the cells may increase transcellular Cl^- reabsorption by upregulating proteins from the transcellular pathway such as pendrin and NDCBE. However, in the absence of the Na^+ blocker cldn-4, Na^+ ions that have accumulated in the interstitium may backflux to the luminal side to be excreted in the urine. This would result in increased FE of sodium but not chloride upon a low NaCl diet (Figure 4.1).

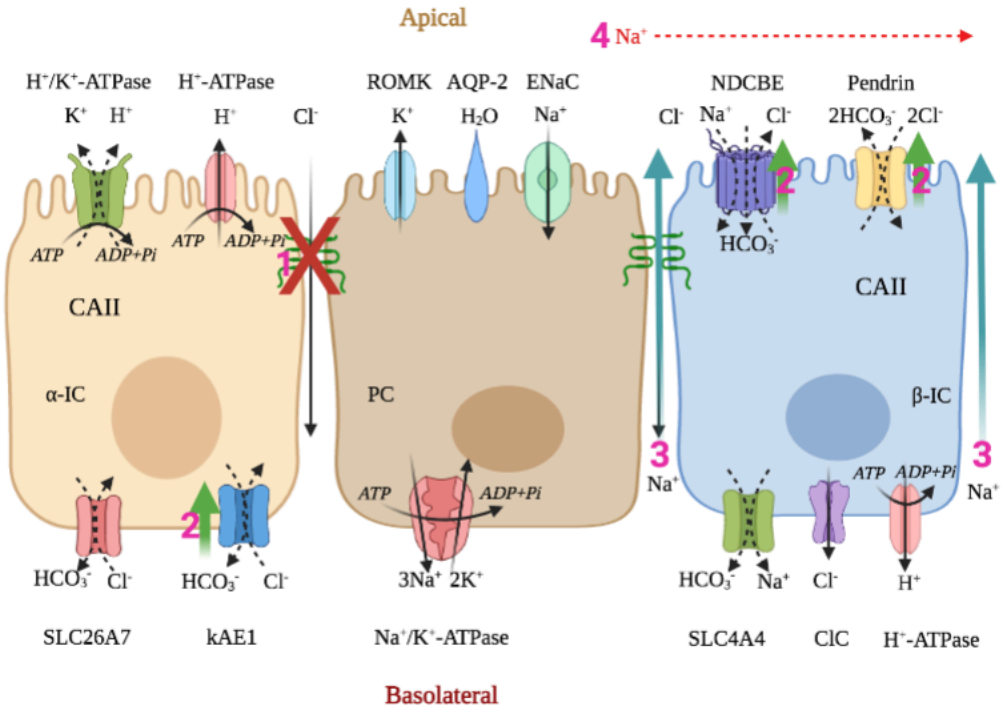

Figure 4. 1 Schematic proposed mechanism of normochloremia and hypernatriuria

Schematic diagram of the proposed mechanism of unchanged FE% of Cl^- and increased FE% of Na^+ in the NaCl depleted diet condition in the IC cldn-4 KO mice. The pink numbers depict the successive events taking place. 1) Absence of paracellular Cl^- facilitator cldn-4 increases luminal Cl^- concentration. The cells may compensate the loss of paracellular reabsorption by increasing the transcellular Cl^- reabsorption (2) via the upregulation of transcellular Cl^- reabsorption proteins pendrin, NDCBE and kAE1 to maintains a normochloremia. However, in the absence of the paracellular Na^+ barrier cldn-4, (3) Na^+ may back flux from the interstitium to the luminal side and (4) be excreted in the urine, resulting in an increased FE% of Na^+ and hypernatriuria.

4.3.2 Summary

4.3.2.1 TJ protein assembly is unchanged in Cldn-4 KO mice

After establishing the IC specific cldn-4 KO mice, we confirmed the cldn-4 KO by genotyping and assessing protein abundance from isolated collecting duct (Figure 3.1). We found that cldn-4 KO mice are viable and have no gross anatomical difference compared to the WT mice. Plasma and urine analysis revealed no difference in plasma electrolytes and urine composition at steady state between WT and KO mice, including urine pH and osmolality. We then measured the tight junction proteins and mRNA abundances from whole kidneys and did not observe a significant difference in tight junction proteins cldn-4, -8, -7 and -3 abundance between WT and cldn-4 KO mice. This finding suggests that the absence of IC cldn-4 caused no change in tight junction protein assembly.

4.3.2.2 IC transcellular proteins are increased in IC cldn-4 KO mice

Although there was no change in TJ protein abundance in the kidney of IC cldn-4 KO mice, we found that the type-A IC Cl^-/HCO_3^- exchanger kAE1 and type-B IC pendrin abundances were both significantly increased in the cldn-4 KO mice. We also found that type-B IC NDCBE mRNA is increased in the KO mice. However, PC markers AQP-2 (protein and mRNA) and ENaC (mRNA) were unchanged. The increase in IC proteins and mRNA suggests that they may be up regulated to allow sufficient sodium and chloride reabsorption in an epithelium where TJ are defective due to the lack of cldn-4.

4.3.2.3 Cldn-4 KO mice fed a NaCl-depleted diet waste urinary sodium

Given the up regulation of transcellular IC sodium and chloride transporters in the KO mice, we next fed them a NaCl depleted diet to assess their NaCl reabsorption ability. Our findings show that the cldn-4 KO mice have higher FE of Na^+ than WT animals, but no significant

difference in FE of Cl^-, Ca^{2+} or K^+. There was no difference found in plasma electrolytes, urine pH and osmolality between KO and WT mice.

Similar to their counterparts at basal state, KO mice fed a low NaCl diet did not demonstrate a significant change in TJ protein of mRNA abundance compared to WT animals , except for the expected reduction in cldn-4 abundance. These mice also displayed increased kAE1 and pendrin proteins abundance, but unchanged mRNA levels . Despite their Na^+ loosing phenotype, the KO mice kidneys did not display altered Na^+ channel ENaC's mRNA abundance . Assessment of renin mRNA abundance in the IC cldn-4 KO mice showed no difference with WT mice, suggesting that the increase in Cl^-/HCO_3^- exchangers' abundance is independent of RAAS activation.

4.3.2.4 Acid/base and calcium homeostasis are not altered in the cldn-4 KO mice

As type-A and -B IC are involved in acid and base secretion in the pre-urine, WT and cldn-4 mice were given 0.28M NH_4Cl H_2O for 24 hours. From this experiment, we showed that the cldn-4 KO mice can maintain a steady acid/base balance similar to WT mice and hence, that IC TJs are not involved in acid/base homeostasis.

Based on total cldn-4 KO mice which displayed increased FE of calcium and reduced plasma calcium, we fed the mice a low calcium diet to assess whether IC cldn-4 plays a role in calcium homeostasis. The plasma electrolytes and urine composition was not different between WT and KO mice after the low calcium diet and therefore, we concluded that IC cldn-4 is not involved in calcium homeostasis.

4.3.3 Limitations of the study

Generation of the IC cldn-4 KO mice was done using the Cre/LoxP strategy. Cre/LoxP technique is widely used to establish genetically engineered tissue/cell specific knock out animal

models[272]. Like all other systems, the Cre/LoxP systems has some drawbacks. For example, the tissue specificity of the KO is not always as precise as desired [273274]. The H^+ATPase displayed a 50% success rate in knocking out the protein of interest in CNT cells[252]. Two third of the CNT/CD cells are PCs while this ratio decreases in the medullary CD[258]. As a result we detected a 49% reduction in cldn-4 protein abundance in the KO mice CD (Figure 3.1). However, since PC Cldn-4 is intact in our mice, an immunohistochemistry experiment aimed at detecting a loss of IC cldn-4 proteins in cldn-4 KO mice remained inconclusive (data not shown). The alternative approach to assess the KO specificity would be to breed our mice with Rosa26-loxP-stop-loxP-yellow fluorescent protein reporter mice, , which would generate YFP fluorescent IC where Cre is active and hence where Cldn-4 is knocked out[275].

Availability of antibodies to detect proteins expressed in the CD was another limitation we experienced when conducting this research. In some cases, antibodies available to us failed to specifically detect the protein of interest (for example, ENaC or NDCBE). The alternative approach was to measure mRNA abundance by qRT PCR.

4.3.4 Future directions

4.3.4.1 Generation of CD specific KO mouse

Previous research characterized total KO cldn-4 mice[110] and PC specific cldn-4 KO mouse[111]. In our research we characterized the physiological role of IC cldn-4 . However, given the difference in PC and IC numbers, and the incomplete nature of IC cldn-4 KO, the overall physiological role of cldn-4 in the collecting duct remains unclear. To explore this, generating a cldn-4 KO mouse model targeted to both IC and PC could inform about the role of this protein and its contribution to sodium, chloride and pH homeostasis in the CD. Creating such a CD KO mouse model would be achieved by breeding cldn-4 Flox mice with Hoxb7-Cre transgenic mice since

this gene is expressed in both PC and IC[276]. Alternatively, this could be achieved by breeding PC specific (AQP-2 Cre mouse) cldn-4 KO mice with IC specific (B1-ATPase Cre mouse) cldn-4 KO mice. Conducting basal, low NaCl diet and acidic diet experiments as performed in this thesis would explore the role of CD cldn-4 protein.

4.3.4.2 Micro-perfusion studies on isolated CD from WT and cldn-4 KO mice

Our findings show a change in abundance of IC proteins involved in sodium, chloride and bicarbonate reabsorption. We hypothesized that the urinary sodium waste is caused by a paracellular back flux of sodium permitted by the loss of sodium blocker cldn-4. The loss of paracellular chloride pore cldn-4 is proposed to be compensated by the up regulation of pendrin, NDCBE and kAE1 at the basal state. However, this hypothesis would need to be further tested. Micro-perfusion of freshly dissected collecting ducts from WT or KO mice would allow measurements of transepithelial fluxes of sodium and chloride as well as of transepithelial voltage. By using this *ex vivo* technique we would be able to characterize the CD epithelial permeability to sodium and chloride and test our hypothesis.

4.3.4.3 Pharmacological inhibition of transport proteins

Despite the elevated FE of sodium in the cldn-4 KO mice, we did not measure a significant difference in abundance of the major sodium reabsorption protein, ENaC. Therefore, the role of ENaC in the IC specific cldn-4 KO mouse remains unclear, especially in the face of the sodium urinary waste upon a NaCl depleted diet. To further address ENaC's role, IC cldn-4 KO mice could be administered the ENaC inhibitor amiloride and the FE of sodium as well as NDCBE or ENaC protein abundance measured after a low NaCl diet. This experiment would shed light on the role of ENaC and other sodium transporters in the CD of IC cldn-4 KO mice.

Interestingly, upon a low NaCl diet, IC cldn-4 KO mice did not display an urinary chloride waste. this could be due to the increased abundance of pendrin protein in the cldn-4 KO mice. To assess whether pendrin is playing a critical role in chloride homeostasis , WT and IC cldn-4 KO mice could be administered with either furosemide (50% pendrin inhibition[277]) or NPPB (5-Nitro-2-[(3-phynylpropyl)amino]benzoic acid; 59% pendrin inhibition[277]) along with low NaCl diet. This experiment would inform about any interplay between pendrin and cldn-4 in chloride homeostasis in the CD.

Overall, this dissertation focused on two different proteins that are expressed in IC cells of the CD facilitating both transcellular and paracellular transport of ions. Our work with SLC26A7 (focuses the transcellular transport of anions) revealed a functional interplay between two chloride/bicarbonate exchangers with relevance to dRTA disease and its potential treatments. Our work with IC specific cldn-4 KO mice (the paracellular transport of anion) provided novel knowledge about the role of TJ proteins in the CD, and the interplay between the TJ versus basolateral proteins i.e. paracellular and transcellular transporters, thereby contributing to our growing knowledge of this complex transepithelial regulation.

BIBLIOGRAPHY

1. Widmaier EP, Raff H, Strang KT. *Vander's Human Physiology: The Mechanism of Body Function*. 14th ed. New York: McGraw-Hill; 2016.
2. Wolff GE, Crosby RD, Roberts JA, Wittrock DA. Differences in daily stress, mood, coping, and eating behavior in binge eating and nonbinge eating college women. *Addict Behav*. 2000;25(2):205-216. doi:10.1016/S0306-4603(99)00049-0
3. Treuting PM, Kowalewska J. *Urinary System*. First Edit. Elsevier Inc.; 2012. doi:10.1016/B978-0-12-381361-9.00016-0
4. Chertow G, Luyckx V, Marsden P, Skorecki K, Taal M, Yu A. *Brenner and Rector's The Kidney*. 11th ed. Philadelphia, PA: Elsevier; 2019. https://www.elsevier.com/books/brenner-and-rectors-the-kidney-2-volume-set/yu/978-0-323-53265-5.
5. Saxen L. *Organogenesis of the Kidney*. Cambridge: Cambridge University Press; 1987. doi:doi:10.1017/CBO9780511565083
6. Luyckx VA, Brenner BM. Low birth weight, nephron number, and kidney disease. *Kidney Int Suppl*. 2005;68(97):68-77. doi:10.1111/j.1523-1755.2005.09712.x
7. Kriz W, Kaissling B. *Structural Organization of the Mammalian Kidney*. Vol 1.; 2013. doi:10.1016/B978-0-12-381462-3.00020-3
8. Urity VB, Issaian T, Braun EJ, Dantzler WH, Pannabecker TL. Architecture of kangaroo rat inner medulla: Segmentation of descending thin limb of Henle's loop. *Am J Physiol - Regul Integr Comp Physiol*. 2012;302(6):720-726. doi:10.1152/ajpregu.00549.2011
9. Sherwood L, Kell R, Ward C. *Human Physiology: From Cells to Systems*. Second Can. Toronto, ON: Nelson Educaion Ltd.; 2013.
10. Lashhab R, Ullah AKMS, Cordat E. Renal collecting duct physiology and

pathophysiology. *Biochem Cell Biol*. 2019;97(3):234-242. doi:10.1139/bcb-2018-0192

11. Pearce D, Soundararajan R, Trimpert C, Kashlan OB, Deen PMT, Kohan DE. Collecting duct principal cell transport processes and their regulation. *Clin J Am Soc Nephrol*. 2015;10(1):135-146. doi:10.2215/CJN.05760513
12. Kloth S, Aigner J, Brandt E, Moll R, Minuth WW. Histochemical markers reveal an unexpected heterogeneous composition of the renal embryonic collecting duct epithelium. *Kidney Int*. 1993;44(3):527-536. doi:10.1038/ki.1993.277
13. Hansen GP, Tisher CC, Robinson RR. Response of the collecting duct to disturbances of acid-base and potassium balance. *Kidney Int*. 1980;17(3):326-337. doi:10.1038/ki.1980.38
14. Kim J, Kim YH, Cha JH, Tisher CC, Madsen KM. Intercalated cell subtypes in connecting tubule and cortical collecting duct of rat and mouse. *J Am Soc Nephrol*. 1999;10(1):1-12. doi:10.1681/asn.v1011
15. Teng-umnuay P, Verlander JW, Yuan W, Tisher CC, Madsen KM. Identification of distinct subpopulations of intercalated cells in the mouse collecting duct. *J Am Soc Nephrol*. 1996;7(2):260-274. doi:10.1681/asn.v72260
16. A L, CC T. Morphology of rabbit collecting duct. *Am J Anat*. 1979;155(1):111-124. doi:10.1002/aja.1001550108
17. Madsen KM, Tisher CC. Structural-functional relationships along the distal nephron. *Am J Physiol - Ren Fluid Electrolyte Physiol*. 1986;250(1 (19/1)). doi:10.1152/ajprenal.1986.250.1.f1
18. Duc C, Farman N, Canessa CM, Bonvalet JP, Rossier BC. Cell-specific expression of epithelial sodium channel α, β, and γ subunits in aldosterone-responsive epithelia from the rat: Localization by in situ hybridization and immunocytochemistry. *J Cell Biol*.

1994;127(6 II):1907-1921. doi:10.1083/jcb.127.6.1907

19. Hager H, Kwon TH, Vinnikova AK, et al. Immunocytochemical and immunoelectron microscopic localization of α-, β-, and γ-ENaC in rat kidney. *Am J Physiol - Ren Physiol*. 2001;280(6 49-6):1093-1106. doi:10.1152/ajprenal.2001.280.6.f1093

20. Loffing J, Pietri L, Aregger F, et al. Differential subcellular localization of ENaC subunits in mouse kidney in response to high- and low-Na diets. *Am J Physiol - Ren Physiol*. 2000;279(2 48-2):252-258. doi:10.1152/ajprenal.2000.279.2.f252

21. O'Neil RG, Helman SI. Transport characteristics of renal collecting tubules: influences of DOCA and diet. *Am J Physiol - Ren Fluid Electrolyte Physiol*. 1977;2(6). doi:10.1152/ajprenal.1977.233.6.f544

22. Schwartz GJ, Burg MB. Mineralocorticoid effects on cation transport by cortical collecting tubules in vitro. *Am J Physiol*. 1978;235(6). doi:10.1152/ajprenal.1978.235.6.f576

23. Mujais SK, Chekal MA, Jones WJ, John P. Hayslett, and Katz A 1. Regulation of Renal Na-K-ATPase in the Rat. 1984;73(January):13-19.

24. Garg LC, Knepper MA, Burg MB. MINERALOCORTICOID EFFECTS ON (Na + K)-ATPase IN RABBIT NEPHRON SEGMENTS. *Ann N Y Acad Sci*. 1981;372(1):79-80. doi:10.1111/j.1749-6632.1981.tb15459.x

25. Wade JB, Fang L, Coleman RA, et al. Differential regulation of ROMK (Kir1.1) in distal nephron segments by dietary potassium. *Am J Physiol - Ren Physiol*. 2011;300(6):1385-1393. doi:10.1152/ajprenal.00592.2010

26. Ishibashi K, Sasaki S, Fushimi K, Yamamoto T, Kuwahara M, Marumo F. Immunolocalization and effect of dehydration on AQP3, a basolateral water channel of

kidney collecting ducts. *Am J Physiol - Ren Physiol*. 1997;272(2 41-2). doi:10.1152/ajprenal.1997.272.2.f235

27. Kim S, Gresz V, Rojek A, et al. Decreased expression of AQP2 and AQP4 water channels and Na, K-ATPase in kidney collecting duct in AQP3 null mice. *Biol Cell*. 2005;97(10):765-778. doi:10.1042/bc20040148

28. Cells I, Schuster VL. Function and regulation of collecting duct intercalated cells. 1993;(87).

29. Roy A, Al-Bataineh MM, Pastor-Soler NM. Collecting duct intercalated cell function and regulation. *Clin J Am Soc Nephrol*. 2015;10(2):305-324. doi:10.2215/CJN.08880914

30. Trepiccione F, Prosperi F, de la Motte LR, et al. New Findings on the Pathogenesis of Distal Renal Tubular Acidosis. *Kidney Dis*. 2017;3(3):98-105. doi:10.1159/000478781

31. van Adelsberg J, Edwards JC, Takito J, Kiss B, Al-Awqati Q. An induced extracellular matrix protein reverses the polarity of band 3 in intercalated epithelial cells. *Cell*. 1994;76(6):1053-1061. doi:10.1016/0092-8674(94)90382-4

32. Gao XB, Eladari D, Leviel F, et al. Deletion of hensin/DMBT1 blocks conversion of β- To α-intercalated cells and induces distal renal tubular acidosis. *Proc Natl Acad Sci U S A*. 2010;107(50):21872-21877. doi:10.1073/pnas.1010364107

33. Park J, Shrestha R, Qiu C, et al. Single-cell transcriptomics of the mouse kidney reveals potential cellular targets of kidney disease. *Science (80-)*. 2018;360(6390):758-763. doi:10.1126/science.aar2131

34. Sebastian A, McSherry E, Morris RC. Impaired renal conservation of sodium and chloride during sustained correction of systemic acidosis in patients with type 1, classic renal tubular acidosis. *J Clin Invest*. 1976;58(2):454-469. doi:10.1172/JCI108490

35. Gueutin V, Vallet M, Jayat M, et al. Renal β-intercalated cells maintain body fuid and electrolyte balance. *J Clin Invest*. 2013;123(10):4219-4231. doi:10.1172/JCI63492

36. Reeves W., Andreoli T. *Sodium Chloride Transport in the Loop of Henle, Distal Convoluted Tubule, and Collecting Duct*. Vol 1. Fourth Edi. Elsevier Inc.; 2013. doi:10.1016/B978-0-12-381462-3.00034-3

37. Pao AC. There and back again: Insulin, ENaC, and the cortical collecting duct. *Physiol Rep*. 2016;4(10):4-6. doi:10.14814/phy2.12809

38. Wall SM. Renal intercalated cells and blood pressure regulation. *Kidney Res Clin Pract*. 2017;36(4):305-317. doi:10.23876/j.krcp.2017.36.4.305

39. Kabra R, Knight KK, Zhou R, Snyder PM. Nedd4-2 Induces Endocytosis and Degradation of Proteolytically Cleaved Epithelial Na+ Channels. *J Biol Chem*. 2008;283(10):6033-6039. doi:10.1074/jbc.M708555200

40. Soundararajan R, Pearce D, Hughey RP, Kleyman TR. Role of Epithelial Sodium Channels and Their Regulators in Hypertension. *J Biol Chem*. 2010;285(40):30363-30369. doi:10.1074/jbc.R110.155341

41. Bhalla V, Soundararajan R, Pao AC, Li H, Pearce D. Disinhibitory pathways for control of sodium transport: regulation of ENaC by SGK1 and GILZ. *Am J Physiol Physiol*. 2006;291(4):F714-F721. doi:10.1152/ajprenal.00061.2006

42. Lang F, Huang DY, Vallon V. SGK, renal function and hypertension. *J Nephrol*. 2012;23 Suppl 1(6):S124-9. http://www.ncbi.nlm.nih.gov/pubmed/21170869.

43. Verrey F, Schaerer E, Zoerkler P, et al. Regulation by aldosterone of Na+,K+-ATPase mRNAs, protein synthesis, and sodium transport in cultured kidney cells. *J Cell Biol*. 1987;104(5):1231-1237. doi:10.1083/jcb.104.5.1231

44. Hou J. Paracellular transport in the collecting duct. *Curr Opin Nephrol Hypertens*. 2016;25(5):424-428. doi:10.1097/MNH.0000000000000253

45. Hou J. Claudins and mineral metabolism. *Curr Opin Nephrol Hypertens*. 2016;25(4):308-313. doi:10.1097/MNH.0000000000000239

46. Gong Y, Wang J, Yang J, Gonzales E, Perez R, Hou J. KLHL3 regulates paracellular chloride transport in the kidney by ubiquitination of claudin-8. *Proc Natl Acad Sci U S A*. 2015;112(14):4340-4345. doi:10.1073/pnas.1421441112

47. Leviel F, Hübner CA, Houillier P, et al. Erratum: The Na+-dependent chloride-bicarbonate exchanger SLC4A8 mediates an electroneutral Na+ reabsorption process in the renal cortical collecting ducts of mice (The Journal of Clinical Investigation (2011), 121, 4, (1668) DOI: 10.1172/JCI57722). *J Clin Invest*. 2011;121(4):1668. doi:10.1172/JCI57722

48. Nanami M, Pham TD, Kim YH, et al. The role of intercalated cell Nedd4–2 in BP regulation, ion transport, and transporter expression. *J Am Soc Nephrol*. 2018;29(6):1706-1719. doi:10.1681/ASN.2017080826

49. Olesen ETB, Fenton RA. Aquaporin-2 membrane targeting: Still a conundrum. *Am J Physiol - Ren Physiol*. 2017;312(4):F744-F747. doi:10.1152/ajprenal.00010.2017

50. Andersen OS, Silveira JE, Steinmetz PR. Intrinsic characteristics of the proton pump in the luminal membrane of a tight urinary epithelium. The relation between transport rate and delta mu H. *J Gen Physiol*. 1985;86(2):215-234. doi:10.1085/jgp.86.2.215

51. Wagner CA. Effect of Mineralocorticoids on Acid-Base Balance. *Nephron Physiol*. 2014;128(1-2):26-34. doi:10.1159/000368266

52. Quade BN, Parker MD, Occhipinti R. The therapeutic importance of acid-base balance.

Biochem Pharmacol. 2020;183(January). doi:https://doi.org/10.1016/j.bcp.2020.114278

53. Poupin N, Calvez J, Lassale C, Chesneau C, Tomé D. Impact of the diet on net endogenous acid production and acid-base balance. *Clin Nutr*. 2012;31(3):313-321. doi:10.1016/j.clnu.2012.01.006

54. Goel N, Calvert J. Understanding blood gases/acid-base balance. *Paediatr Child Health (Oxford)*. 2012;22(4):142-148. doi:10.1016/j.paed.2011.09.005

55. Mark PB, Stevens KK, Jardine AG. Electrolytes: Acid-Base Balance. *Encycl Hum Nutr*. 2012;2-4:139-145. doi:10.1016/B978-0-12-375083-9.00087-8

56. Pereira P, Miranda D, Oliveira E, Simoes e Silva A. Molecular Pathophysiology of Renal Tubular Acidosis. *Curr Genomics*. 2009;10(1):51-59. doi:10.2174/138920209787581262

57. Unwin RJ, Shirley DG, Capasso G. Urinary acidification and distal renal tubular acidosis. *J Nephrol*. 2002;15(5):S142-50.

58. Eladari D, Kumai Y. Renal acid-base regulation: new insights from animal models. *Pflugers Arch Eur J Physiol*. 2015;467(8):1623-1641. doi:10.1007/s00424-014-1669-x

59. Gong F, Alzamora R, Smolak C, et al. Vacuolar H + -ATPase apical accumulation in kidney intercalated cells is regulated by PKA and AMP-activated protein kinase. *Am J Physiol Physiol*. 2010;298(5):F1162-F1169. doi:10.1152/ajprenal.00645.2009

60. Sun X, Stephens L, DuBose TD, Petrovic S. Adaptation by the collecting duct to an exogenous acid load is blunted by deletion of the proton-sensing receptor GPR4. *Am J Physiol Physiol*. 2015;309(2):F120-F136. doi:10.1152/ajprenal.00507.2014

61. Brown D, Wagner CA. Molecular Mechanisms of Acid-Base Sensing by the Kidney: Figure 1. *J Am Soc Nephrol*. 2012;23(5):774-780. doi:10.1681/ASN.2012010029

62. Farquhar MG, Palade GE. Junctional complexes in various epithelia. *J Cell Biol*.

1963;17:375-412. doi:10.1083/jcb.17.2.375

63. Acharya P, Beckel J, Ruiz WG, et al. Distribution of the tight junction proteins ZO-1, occludin, and claudin-4, -8, and -12 in bladder epithelium. *Am J Physiol - Ren Physiol*. 2004;287(2 56-2). doi:10.1152/ajprenal.00341.2003

64. Martìn-Padura I, Lostaglio S, Schneemann M, et al. Junctional adhesion molecule, a novel member of the immunoglobulin superfamily that distributes at intercellular junctions and modulates monocyte transmigration. *J Cell Biol*. 1998;142(1):117-127. doi:10.1083/jcb.142.1.117

65. Itoh M, Sasaki H, Furuse M, Ozaki H, Kita T, Tsukita S. Junctional adhesion molecule (JAM) binds to PAR-3: A possible mechanism for the recruitment of PAR-3 to tight junctions. *J Cell Biol*. 2001;154(3):491-497. doi:10.1083/jcb.200103047

66. Steed E, Rodrigues NTL, Balda MS, Matter K. Identification of MarvelD3 as a tight junction-associated transmembrane protein of the occludin family. *BMC Cell Biol*. 2009;10:1-14. doi:10.1186/1471-2121-10-95

67. Ikenouchi J, Furuse M, Furuse K, Sasaki H, Tsukita S, Tsukita S. Tricellulin constitutes a novel barrier at tricellular contacts of epithelial cells. *J Cell Biol*. 2005;171(6):939-945. doi:10.1083/jcb.200510043

68. Furuse M, Hirase T, Itoh M, et al. Occludin: A novel integral membrane protein localizing at tight junctions. *J Cell Biol*. 1993;123(6 II):1777-1788. doi:10.1083/jcb.123.6.1777

69. Cording J, Berg J, Käding N, et al. In tight junctions, claudins regulate the interactions between occludin, tricellulin and marvelD3, which, inversely, modulate claudin oligomerization. *J Cell Sci*. 2013;126(2):554-564. doi:10.1242/jcs.114306

70. Saitou M, Furuse M, Sasaki H, et al. Complex phenotype of mice lacking occludin, a

component of tight junction strands. *Mol Biol Cell*. 2000;11(12):4131-4142. doi:10.1091/mbc.11.12.4131

71. Furuse M, Hata M, Furuse K, et al. Claudin-based tight junctions are crucial for the mammalian epidermal barrier: A lesson from claudin-1-deficient mice. *J Cell Biol*. 2002;156(6):1099-1111. doi:10.1083/jcb.200110122

72. Furuse M, Fujita K, Hiiragi T, Fujimoto K, Tsukita S. Claudin-1 and -2: Novel Integral Membrane Proteins Localizing at Tight Junctions with No Sequence Similarity to Occludin. 1998;141(7):1539-1550.

73. Günzel D, Yu ASL. CLAUDINS AND THE MODULATION OF TIGHT JUNCTION PERMEABILITY TIGHT JUNCTIONS AND THEIR ROLE IN ... 2013;93:525-569. doi:10.1152/physrev.00019.2012

74. Tsukita S, Tanaka H, Tamura A, Em F. The Claudins : From Tight Junctions to Biological Systems. *Trends Biochem Sci*. 2019;44(2):141-152. doi:10.1016/j.tibs.2018.09.008

75. Loh YH, Christoffels A, Brenner S, Hunziker W, Venkatesh B. Extensive Expansion of the Claudin Gene Family in the Teleost Fish , Fugu rubripes. 2004:1248-1257. doi:10.1101/gr.2400004.

76. Krause G, Winkler L, Mueller SL, Haseloff RF, Piontek J, Blasig IE. Structure and function of claudins. *Biochim Biophys Acta - Biomembr*. 2008;1778(3):631-645. doi:10.1016/j.bbamem.2007.10.018

77. Blasig IE, Winkler L, Lassowski B, et al. On the self-association potential of transmembrane tight junction proteins. *Cell Mol Life Sci*. 2006;63(4):505-514. doi:10.1007/s00018-005-5472-x

78. Piorntek J, Winkler L, Wolburg H, et al. Formation of tight junction: determinants of

homophilic interaction between classic claudins. *FASEB J*. 2008;22(1):146-158. doi:10.1096/fj.07-8319com

79. Yu ASL. Claudins and the Kidney. *Yu, Alan S L*. 2015;26:11-19. doi:10.1681/ASN.2014030284

80. Van Itallie CM, Anderson JM. Claudins and epithelial paracellular transport. *Annu Rev Physiol*. 2006;68:403-429. doi:10.1146/annurev.physiol.68.040104.131404

81. Contacts C, Cukierman L, Meertens L, Bertaux C, Kajumo F, Dragic T. Residues in a Highly Conserved Claudin-1 Motif Are Required for Hepatitis C Virus Entry and Mediate the Formation of. *J Virol*. 2009;83(11):5477-5484. doi:10.1128/JVI.02262-08

82. Colegio OR, Itallie CMVAN, Crea HJMC, et al. Claudins create charge-selective channels in the paracellular pathway between epithelial cells. 2002;283:142-147. doi:10.1152/ajpcell.00038.2002.

83. Katahira J, Inoue N, Horiguchi Y, Matsuda M, Sugimoto N. Molecular Cloning and Functional Characterization of the Receptor for. *J Cell Biol*. 1997;136(6):1239-1247.

84. Katahira J, Sugiyama H, Inoue N, et al. Clostridium perfringens Enterotoxin Utilizes Two Structurally Related Membrane Proteins as Functional Receptors in Vivo *. *J Biol Chem*. 1997;272(42):26652-26658. doi:10.1074/jbc.272.42.26652

85. Itoh M, Furuse M, Morita K, Kubota K, Saitou M, Tsukita S. Direct Binding of Three Tight Junction-associated MAGUKs, ZO-1, ZO-2, and ZO-3, with the COOH Termini of Claudins. *Cell*. 1999;147(6):1351-1363. https://www.ncbi.nlm.nih.gov/pmc/articles/PMC2168087/pdf/9906071.pdf.

86. Rüffer C, Gerke V. The C-terminal cytoplasmic tail of claudins 1 and 5 but not its PDZ-binding motif is required for apical localization at epithelial and endothelial tight

junctions. *Eur J Cell Biol*. 2004;83(4):135-144. doi:10.1078/0171-9335-00366

87. Arabzadeh A, Troy T, Turksen K. Role of the Cldn6 Cytoplasmic Tail Domain in Membrane Targeting and Epidermal Differentiation In Vivo. *Mol Cell Biol*. 2006;26(15):5876-5887. doi:10.1128/mcb.02342-05

88. Müller D, Kausalya PJ, Meij IC, Hunziker W. Familial hypomagnesemia with hypercalciuria and nephrocalcinosis: Blocking endocytosis restores surface expression of a novel Claudin-16 mutant that lacks the entire C-terminal cytosolic tail. *Hum Mol Genet*. 2006;15(7):1049-1058. doi:10.1093/hmg/ddl020

89. Van Itallie CM, Colegio OR, Anderson JM. The cytoplasmic tails of claudins can influence tight junction barrier properties through effects on protein stability. *J Membr Biol*. 2004;199(1):29-38. doi:10.1007/s00232-004-0673-z

90. Shigetomi K, Ikenouchi J. Regulation of the epithelial barrier by post-translational modifications of tight junction membrane proteins. *J Biochem*. 2018;163(4):265-272. doi:10.1093/jb/mvx077

91. González-Mariscal L, Garay E, Quirós M. *Regulation of Claudins by Posttranslational Modifications and Cell-Signaling Cascades*. Vol 65.; 2010. doi:10.1016/S1063-5823(10)65006-5

92. Ikari A, Matsumoto S, Harada H, et al. Phosphorylation of paracellin-1 at Ser217 by protein kinase A is essential for localization in tight junctions. *J Cell Sci*. 2006;119(9):1781-1789. doi:10.1242/jcs.02901

93. Souza TD, Agarwal R, Morin PJ. Phosphorylation of Claudin-3 at Threonine 192 by cAMP-dependent Protein Kinase Regulates Tight Junction Barrier Function in Ovarian Cancer Cells *. *J Biol Chem*. 2008;280(28):26233-26240. doi:10.1074/jbc.M502003200

94. Yamauchi K, Rai T, Kobayashi K, et al. Disease-causing mutant WNK4 increases paracellular chloride permeability and phosphorylates claudins. *Proc Natl Acad Sci U S A*. 2004;101(13):4690-4694. doi:10.1073/pnas.0306924101

95. Tatum R, Zhang Y, Salleng K, et al. Renal salt wasting and chronic dehydration in claudin-7-deficient mice. *Am J Physiol - Ren Physiol*. 2010;298(1):24-34. doi:10.1152/ajprenal.00450.2009

96. Suzuki H, Tani K, Fujiyoshi Y. Crystal structures of claudins: Insights into their intermolecular interactions. *Ann N Y Acad Sci*. 2017;1397(1):25-34. doi:10.1111/nyas.13371

97. Nitta T, Hata M, Gotoh S, et al. Size-selective loosening of the blood-brain barrier in claudin-5-deficient mice. *J Cell Biol*. 2003;161(3):653-660. doi:10.1083/jcb.200302070

98. Wilcox ER, Burton QL, Naz S, et al. Mutations in the gene encoding tight junction claudin-14 cause autosomal recessive deafness DFNB29. *Cell*. 2001;104(1):165-172. doi:10.1016/S0092-8674(01)00200-8

99. Ben-Yosef T, Belyantseva IA, Saunders TL, et al. Claudin 14 knockout mice, a model for autosomal recessive deafness DFNB29, are deaf due to cochlear hair cell degeneration. *Hum Mol Genet*. 2003;12(16):2049-2061. doi:10.1093/hmg/ddg210

100. Gow A, Southwood CM, Li JS, et al. CNS Myelin and Sertoli Cell Tight Junction Strands Are Absent in Osp/Claudin-11 Null Mice Early in vitro evidence indicates that occludin is cen-tral to the biogenesis of tight junctions and mediates Mount Sinai School of Medicine One Gustave L. Levy Plac. *Mol Biol † Dep Ophthalmol*. 1999;99:649-659. https://www.cell.com/action/showPdf?pii=S0092-8674%2800%2981553-6.

101. Hayashi D, Tamura A, Tanaka H, et al. Deficiency of claudin-18 causes paracellular H+

leakage, up-regulation of interleukin-1β, and atrophic gastritis in mice. *Gastroenterology*. 2012;142(2):292-304. doi:10.1053/j.gastro.2011.10.040

102. Tamura A, Kitano Y, Hata M, et al. Megaintestine in Claudin-15-Deficient Mice. *Gastroenterology*. 2008;134(2):523-534. doi:10.1053/j.gastro.2007.11.040

103. Muto S, Hata M, Taniguchi J, et al. Claudin-2-deficient mice are defective in the leaky and cation-selective paracellular permeability properties of renal proximal tubules. *Proc Natl Acad Sci U S A*. 2010;107(17):8011-8016. doi:10.1073/pnas.0912901107

104. Buchert M, Papin M, Bonnans C, et al. Symplekin promotes tumorigenicity by up-regulating claudin-2 expression. *Proc Natl Acad Sci U S A*. 2010;107(6):2628-2633. doi:10.1073/pnas.0903747107

105. Kawai Y, Hamazaki Y, Fujita H, et al. Claudin-4 induction by E-protein activity in later stages of CD4/8 double-positive thymocytes to increase positive selection efficiency. *Proc Natl Acad Sci U S A*. 2011;108(10):4075-4080. doi:10.1073/pnas.1014178108

106. Kiuchi-Saishin Y, Gotoh S, Furuse M, Takasuga A, Tano Y, Tsukita S. Differential expression patterns of claudins, tight junction membrane proteins, in mouse nephron segments. *J Am Soc Nephrol*. 2002;13(4):875-886.

107. Hou J, Renigunta A, Yang J, Waldegger S. Claudin-4 forms paracellular chloride channel in the kidney and requires claudin-8 for tight junction localization. *Proc Natl Acad Sci U S A*. 2010;107(42):18010-18015. doi:10.1073/pnas.1009399107

108. Angelow S, Ahlstrom R, Yu ASL. Biology of claudins. *Am J Physiol - Ren Physiol*. 2008;295(4). doi:10.1152/ajprenal.90264.2008

109. Itallie CM Van, Mitic LL, Anderson JM, Carolina N, Hill C, Carolina N. Claudin-2 Forms Homodimers and Is a Component of a High Molecular Weight Protein Complex * □.

2011;286(5):3442-3450. doi:10.1074/jbc.M110.195578

110. Fujita H, Hamazaki Y, Noda Y, Oshima M, Minato N. Claudin-4 Deficiency Results in Urothelial Hyperplasia and Lethal Hydronephrosis. *PLoS One*. 2012;7(12):1-9. doi:10.1371/journal.pone.0052272

111. Gong Y, Yu M, Yang J, et al. The Cap1-claudin-4 regulatory pathway is important for renal chloride reabsorption and blood pressure regulation. *Proc Natl Acad Sci U S A*. 2014;111(36):E3766-E3774. doi:10.1073/pnas.1406741111

112. Toye AM, Banting G, Tanner MJA. Regions of human kidney anion exchanger 1 (kAE1) required for basolateral targeting of kAE1 in polarized kidney cells: Mis-targeting explains dominant renal tubular acidosis (dRTA). *J Cell Sci*. 2004;117(8):1399-1410. doi:10.1242/jcs.00974

113. Lashhab R, Rumley AC, Arutyunov D, et al. The kidney anion exchanger 1 affects tight junction properties via claudin-4. *Sci Rep*. 2019;9(1):1-16. doi:10.1038/s41598-019-39430-9

114. Fairbanks G, Theodore LS, Wallach DF. Electrophoretic analysis of the major polypeptides of the human erythrocyte membrane. *Biochemistry*. 1971;10(13):2606-2617. doi:https://doi.org/10.1021/bi00789a030

115. Kopito RR, Lodish HF. Primary structure and transmembrane orientation of the murine anion exchange protein. *Nature*. 1985;316(6025):234-238. doi:10.1038/316234a0

116. Chang SH, Low PS. Identification of a critical ankyrin-binding loop on the cytoplasmic domain of erythrocyte membrane band 3 by crystal structure analysis and site-directed mutagenesis. *J Biol Chem*. 2003;278(9):6879-6884. doi:10.1074/jbc.M211137200

117. Pasternack GR, Anderson RA, Leto TL, Marchesi VT. Interactions between protein 4.1

and band 3. An alternative binding site for an element of the membrane skeleton. *J Biol Chem*. 1985;260(6):3676-3683. doi:10.1016/s0021-9258(19)83676-1

118. Low PS. Structure and function of the cytoplasmic domain of band 3: center of erythrocyte membrane-peripheral protein interactions. *BBA - Rev Biomembr*. 1986;864(2):145-167. doi:10.1016/0304-4157(86)90009-2

119. Rogalski AA, Steck TL, Waseem A. Association of glyceraldehyde-3-phosphate dehydrogenase with the plasma membrane of the intact human red blood cell. *J Biol Chem*. 1989;264(11):6438-6446. doi:10.1016/s0021-9258(18)83368-3

120. Sahr KE, Taylor WM, Daniels BP, Rubin HL, Jarolim P. The structure and organization of the human erythroid anion exchanger (AE1) gene. *Genomics*. 1994;24(3):491-501. doi:10.1006/geno.1994.1658

121. Arakawa T, Kobayashi-Yurugi T, Alguel Y, et al. Crystal structure of the anion exchanger domain of human erythrocyte band 3. *Science (80-)*. 2015;350(6261):680-684. doi:10.1126/science.aaa4335

122. Sterling D, Reithmeier RAF, Casey JR. A transport metabolon: Functional interaction of carbonic anhydrase II and chloride/bicarbonate exchangers. *J Biol Chem*. 2001;276(51):47886-47894. doi:10.1074/jbc.M105959200

123. Wu F, Saleem MA, Kampik NB, et al. Anion exchanger 1 interacts with nephrin in podocytes. *J Am Soc Nephrol*. 2010;21(9):1456-1467. doi:10.1681/ASN.2009090921

124. Keskanokwong T, Shandro HJ, Johnson DE, et al. Interaction of integrin-linked kinase with the kidney chloride/bicarbonate exchanger, kAE1. *J Biol Chem*. 2007;282(32):23205-23218. doi:10.1074/jbc.M702139200

125. Wu C, Dedhar S. Integrin-linked kinase (ILK) and its interactors: A new paradigm for the

coupling of extracellular matrix to actin cytoskeleton and signaling complexes. *J Cell Biol*. 2001;155(3):505-510. doi:10.1083/jcb.200108077

126. Legate KR, Montañez E, Kudlacek O, Fässler R. ILK, PINCH and parvin: The tIPP of integrin signalling. *Nat Rev Mol Cell Biol*. 2006;7(1):20-31. doi:10.1038/nrm1789

127. Williamson RC, Brown ACN, Mawby WJ, Toye AM. Human kidney anion exchanger 1 localisation in MDCK cells is controlled by the phosphorylation status of two critical tyrosines. *J Cell Sci*. 2008;121(20):3422-3432. doi:10.1242/jcs.035584

128. Dai C, Stolz DB, Bastacky SI, et al. Essential role of integrin-linked kinase in podocyte biology: Bridging the integrin and slit diaphragm signaling. *J Am Soc Nephrol*. 2006;17(8):2164-2175. doi:10.1681/ASN.2006010033

129. Kanasaki K, Kanda Y, Palmsten K, et al. Integrin β1 Mediated Matrix Assembly and Signaling is Critical for the Normal Development and Function of the Kidney Glomerulus. *Dev Biol*. 2008;313(2):584-593. doi:10.1016/j.ydbio.2007.10.047.Integrin

130. Genetet S, Ripoche P, Le Van Kim C, Colin Y, Lopez C. Evidence of a structural and functional ammonium transporter RhBG·anion exchanger 1·ankyrin-G complex in kidney epithelial cells. *J Biol Chem*. 2015;290(11):6925-6936. doi:10.1074/jbc.M114.610048

131. Piermarini PM, Kim EY, Boron WF. Evidence against a direct interaction between intracellular carbonic anhydrase II and pure C-terminal domains of SLC4 bicarbonate transporters. *J Biol Chem*. 2007;282(2):1409-1421. doi:10.1074/jbc.M608261200

132. Sorrell SL, Golder ZJ, Johnstone DB, Karet Frankl FE. Renal peroxiredoxin 6 interacts with anion exchanger 1 and plays a novel role in pH homeostasis. *Kidney Int*. 2016;89(1):105-112. doi:10.1038/ki.2015.277

133. Su Y, Blake-Palmer KG, Fry AC, et al. Glyceraldehyde 3-phosphate dehydrogenase is

required for band 3 (anion exchanger 1) membrane residency in the mammalian kidney. *Am J Physiol - Ren Physiol*. 2011;300(1). doi:10.1152/ajprenal.00228.2010

134. Su Y, Al-Lamki RS, Blake-Palmer KG, et al. Physical and functional links between anion exchanger-1 and sodium pump. *J Am Soc Nephrol*. 2015;26(2):400-409. doi:10.1681/ASN.2013101063

135. Sawasdee N, Junking M, Ngaojanlar P, et al. Human kidney anion exchanger 1 interacts with adaptor-related protein complex 1 μ1A (AP-1 mu1A). *Biochem Biophys Res Commun*. 2010;401(1):85-91. doi:10.1016/j.bbrc.2010.09.015

136. Almomani EY, King JC, Netsawang J, et al. Adaptor protein 1 complexes regulate intracellular trafficking of the kidney anion exchanger 1 in epithelial cells. *Am J Physiol - Cell Physiol*. 2012;303(5):554-566. doi:10.1152/ajpcell.00124.2012

137. Junking M, Sawasdee N, Duangtum N, Cheunsuchon B, Limjindaporn T, Yenchitsomanus P thai. Role of Adaptor Proteins and Clathrin in the Trafficking of Human Kidney Anion Exchanger 1 (kAE1) to the Cell Surface. *Traffic*. 2014;15(7):788-802. doi:10.1111/tra.12172

138. Almomani EY, Touret N, Cordat E. Adaptor protein 1 B mu subunit does not contribute to the recycling of kAE1 protein in polarized renal epithelial cells. *Mol Membr Biol*. 2017;34(1-2):50-64. doi:10.1080/09687688.2018.1451662

139. Deborde S, Perret E, Gravotta D, et al. Clathrin is a key regulator of basolateral polarity. 2008;452(April). doi:10.1038/nature06828

140. Su Y, Hiemstra TF, Yan Y, et al. PDLIM5 links kidney anion exchanger 1 (kAE1) to ILK and is required for membrane targeting of kAE1. *Sci Rep*. 2017;7(August 2016):1-11. doi:10.1038/srep39701

141. Sun X, Soleimani M, Petrovic S. Decreased expression of Slc26a4 (Pendrin) and Slc26a7 in the kidneys of carbonic anhydrase II-deficient mice. *Cell Physiol Biochem*. 2008;21(1-3):95-108. doi:10.1159/000113751

142. Cordat E, Reithmeier RAF. Structure, function, and trafficking of SLC4 and SLC26 anion transporters. In: *Current Topics in Membranes*. Vol 73. 1st ed. Elsevier Inc.; 2014:1-67. doi:10.1016/B978-0-12-800223-0.00001-3

143. Alper SL, Sharma AK. The SLC26 Gene Family of Anion Transporters and Channels. *Mol Aspects Med*. 2013;34(2-3):494-515. doi:10.1016/j.mam.2012.07.009

144. Plain A, Pan W, O'neill D, et al. Claudin-12 knockout mice demonstrate reduced proximal tubule calcium permeability. *Int J Mol Sci*. 2020;21(6):1-18. doi:10.3390/ijms21062074

145. Moseley RH, Höglund P, Wu GD, et al. Downregulated in adenoma gene encodes a chloride transporter defective in congenital chloride diarrhea. *Am J Physiol - Gastrointest Liver Physiol*. 1999;276(1 39-1):185-192. doi:10.1152/ajpgi.1999.276.1.g185

146. Ohana E, Shcheynikov N, Yang D, So I, Muallem S. Determinants of coupled transport and uncoupled current by the electrogenic SLC26 transporters. *J Gen Physiol*. 2011;137(2):239-251. doi:10.1085/jgp.201010531

147. Ohana E, Yang D, Shcheynikov N, Muallem S. Diverse transport modes by the solute carrier 26 family of anion transporters. In: *Journal of Physiology*. Vol 587. ; 2009:2179-2185. doi:10.1113/jphysiol.2008.164863

148. Kim KH, Shcheynikov N, Wang Y, Muallem S. SLC26A7 is a Cl- channel regulated by intracellular pH. *J Biol Chem*. 2005;280(8):6463-6470. doi:10.1074/jbc.M409162200

149. Petrovic S, Ma L, Wang Z, Soleimani M. Identification of an apical Cl-/HCO3- exchanger in rat kidney proximal tubule. *Am J Physiol - Cell Physiol*. 2003;285(3 54-3):608-617.

doi:10.1152/ajpcell.00084.2003

150. Petrovic S, Barone S, Xu J, et al. SLC26A7: A basolateral Cl-/HCO3- exchanger specific to intercalated cells of the outer medullary collecting duct. *Am J Physiol - Ren Physiol*. 2004;286(1 55-1):161-169. doi:10.1152/ajprenal.00219.2003

151. Petrovic S, Ju X, Barone S, et al. Identification of a basolateral Cl-/HCO3- exchanger specific to gastric parietal cells. *Am J Physiol - Gastrointest Liver Physiol*. 2003;284(6 47-6):1093-1103. doi:10.1152/ajpgi.00454.2002

152. Kim KX, Sanneman JD, Kim HM, et al. Slc26a7 chloride channel activity and localization in mouse reissner's membrane epithelium. *PLoS One*. 2014;9(5):1-10. doi:10.1371/journal.pone.0097191

153. Dudas PL, Mentone S, Greineder CF, et al. Immunolocalization of anion transporter Slc26a7 in mouse kidney. 2022;8029:937-945. doi:10.1152/ajprenal.00197.2004.

154. Sun X. Increased Acid Load and Deletion of AE1 Increase Slc26a7 Expression. 2008:29-35. doi:10.1159/000145465

155. Petrovic S, Amlal H, Sun X, Karet F, Barone S, Soleimani M. Vasopressin induces expression of the Cl-/HCO3- exchanger SLC26A7 in kidney medullary collecting ducts of Brattleboro rats. *Am J Physiol - Ren Physiol*. 2006;290(5):1194-1201. doi:10.1152/ajprenal.00247.2005

156. Kujala M, Tienari J, Lohi H, et al. SLC26A6 and SLC26A7 anion exchangers have a distinct distribution in human kidney. *Nephron - Exp Nephrol*. 2005;101(2):50-58. doi:10.1159/000086345

157. Li J, Xia F, Reithmeier RAF. N-glycosylation and topology of the human SLC26 family of anion transport membrane proteins. *Am J Physiol - Cell Physiol*. 2014;306(10).

doi:10.1152/ajpcell.00030.2014

158. Cangul H, Liao XH, Schoenmakers E, et al. Homozygous loss-of-function mutations in SLC26A7 cause goitrous congenital hypothyroidism. *JCI insight*. 2018;3(20):1-10. doi:10.1172/jci.insight.99631

159. Cordat E, Reithmeier RAF. *Structure, Function, and Trafficking of SLC4 and SLC26 Anion Transporters*. Vol 73. 1st ed. Elsevier Inc.; 2014. doi:10.1016/B978-0-12-800223-0.00001-3

160. Mohebbi N, Wagner CA. Pathophysiology, diagnosis and treatment of inherited distal renal tubular acidosis. *J Nephrol*. 2018;31(4):511-522. doi:10.1007/s40620-017-0447-1

161. Cordat E, Casey JR. Bicarbonate transport in cell physiology and disease. *Biochem J*. 2009;417(2):423-439. doi:10.1042/BJ20081634

162. Bruce LJ, Cope DL, Jones GK, et al. Familial distal renal tubular acidosis is associated with mutations in the red cell anion exchanger (Band 3, AE1) gene. *J Clin Invest*. 1997;100(7):1693-1707. doi:10.1172/JCI119694

163. Jarolim P, Shayakul C, Prabakaran D, et al. Autosomal Dominant Distal Renal Tubular Acidosis Is Associated in Three Families with Heterozygosity for the R589H Mutation in the AE1 (Band 3) Cl−/HCO3−Exchanger. *J Biol Chem*. 1998;273(11):6380-6388. doi:10.1074/jbc.273.11.6380

164. Karet FE, Gainza FJ, Györy AZ, et al. Mutations in the chloride-bicarbonate exchanger gene AE1 cause autosomal dominant but not autosomal recessive distal renal tubular acidosis. *Proc Natl Acad Sci U S A*. 1998;95(11):6337-6342. doi:10.1073/pnas.95.11.6337

165. Karet FE, Finberg KE, Nelson RD, et al. Mutations in the gene encoding B1 subunit of H+-ATPase cause renal tubular acidosis with sensorineural deafness. *Nat Genet*.

1999;21(1):84-90. doi:10.1038/5022

166. Lewis SE, Erickson RP, Barnett LB, Venta PJ, Tashian RE. N-ethyl-N-nitrosourea-induced null mutation at the mouse Car-2 locus: an animal model for human carbonic anhydrase II deficiency syndrome. *Proc Natl Acad Sci*. 1988;85(6):1962-1966. doi:10.1073/pnas.85.6.1962

167. Zhang Z, Liu KX, He JW, et al. Identification of Two Novel Mutations in the SLC4A1 Gene in Two Unrelated Chinese Families with Distal Renal Tubular Acidosis. *Arch Med Res*. 2012;43(4):298-304. doi:10.1016/j.arcmed.2012.05.001

168. Fry AC, Su Y, Yiu V, Cuthbert AW, Trachtman H, Karet Frankl FE. Mutation conferring apical-targeting motif on AE1 exchanger causes autosomal dominant distal RTA. *J Am Soc Nephrol*. 2012;23(7):1238-1249. doi:10.1681/ASN.2012020112

169. Park E, Cho MH, Hyun HS, et al. Genotype–Phenotype Analysis in Pediatric Patients with Distal Renal Tubular Acidosis. *Kidney Blood Press Res*. 2018;43(2):513-521. doi:10.1159/000488698

170. Devonald MAJ, Smith AN, Poon JP, Ihrke G, Karet FE. Non-polarized targeting of AE1 causes autosomal dominant distal renal tubular acidosis. *Nat Genet*. 2003;33(2):125-127. doi:10.1038/ng1082

171. Cordat E, Reithmeier RAF. Expression and interaction of two compound heterozygous distal renal tubular acidosis mutants of kidney anion exchanger 1 in epithelial cells. *Am J Physiol - Ren Physiol*. 2006;291(6):1354-1361. doi:10.1152/ajprenal.00015.2006

172. Cordat E, Kittanakom S, Yenchitsomanus PT, et al. Dominant and recessive distal renal tubular acidosis mutations of kidney anion exchanger induce distinct trafficking defects in MDCK cells. *Traffic*. 2006;7(2):117-128. doi:10.1111/j.1600-0854.2005.00366.x

173. Mumtaz R, Trepiccione F, Hennings JC, et al. Intercalated Cell Depletion and Vacuolar H+-ATPase Mistargeting in an Ae1 R607H Knockin Model. *J Am Soc Nephrol*. 2017;28(5):1507-1520. doi:10.1681/ASN.2016020169

174. Merkulova M, Paunescu TG, Azroyan A, Marshansky V, Breton S, Brown D. Mapping the H+ (V)-ATPase interactome: Identification of proteins involved in trafficking, folding, assembly and phosphorylation. *Sci Rep*. 2015;5(October):1-15. doi:10.1038/srep14827

175. Merkulova M, Păunescu TG, Nair A V., et al. Targeted deletion of the Ncoa7 gene results in incomplete distal renal tubular acidosis in mice. *Am J Physiol Physiol*. 2018;315(1):F173-F185. doi:10.1152/ajprenal.00407.2017

176. Laing CM, Toye AM, Capasso G, Unwin RJ. Renal tubular acidosis: developments in our understanding of the molecular basis. *Int J Biochem Cell Biol*. 2005;37(6):1151-1161. doi:10.1016/j.biocel.2005.01.002

177. Ring T, Frische S, Nielsen S. Clinical review: Renal tubular acidosis - A physicochemical approach. *Crit Care*. 2005;9(6):573-580. doi:10.1186/cc3802

178. Krishnan D, Pan W, Beggs MR, et al. Deficiency of Carbonic Anhydrase II Results in a Urinary Concentrating Defect. *Front Physiol*. 2018;8. doi:10.3389/fphys.2017.01108

179. Zhou Y, Greka A. Calcium-permeable ion channels in the kidney. *Am J Physiol Physiol*. 2016;310(11):F1157-F1167. doi:10.1152/ajprenal.00117.2016

180. Clapham DE. Calcium Signaling. *Cell*. 2007;131(6):1047-1058. doi:10.1016/j.cell.2007.11.028

181. Adamczak M, Więcek A. *Endocrine Disorders in Chronic Kidney Disease*.; 2014. doi:10.1007/978-3-642-54637-2_19

182. Kumar R. Calcium Metabolism. In: Jacobson H, Striker G, Klahr S, eds. *The Principles*

and Practices of Nephrology. St. Louis: Mosby-Year Book; 1995:964-971.

183. Blaine J, Chonchol M, Levi M. Renal Control of Calcium , Phosphate , and Magnesium. 2015. doi:10.2215/CJN.09750913

184. Alexander RT, Rievaj J, Dimke H. Paracellular calcium transport across renal and intestinal. 2014;480(April):467-480.

185. Moor MB, Bonny O. Ways of calcium reabsorption in the kidney. *Am J Physiol Ren Physiol*. 2016;310:1337-1350. doi:10.1152/ajprenal.00273.2015.-The

186. Rao R, Bhalla V, Pastor-Soler NM. Intercalated Cells of the Kidney Collecting Duct in Kidney Physiology. *Semin Nephrol*. 2019;39(4):353-367. doi:10.1016/j.semnephrol.2019.04.005

187. Negri AL. Brief review Role of claudins in renal calcium handling ☆. *Nefrol (English Ed*. 2015;35(4):347-352. doi:10.1016/j.nefroe.2015.09.006

188. White KE, Gesek FA, Friedman PA. Structural and functional analysis of Na+/Ca2+ exchange in distal convoluted tubule cells. *Am J Physiol*. 1996;271(3 PART 2). doi:10.1152/ajprenal.1996.271.3.f560

189. Beggs MR, Young K, Pan W, et al. Claudin-2 and claudin-12 form independent, complementary pores required to maintain calcium homeostasis. *Proc Natl Acad Sci*. 2021;118(48):e2111247118. doi:10.1073/pnas.2111247118

190. Gong Y, Renigunta V, Himmerkus N, et al. Claudin-14 regulates renal Ca ++ transport in response to CaSR signalling via a novel microRNA pathway. *EMBO J*. 2012;31(8):1999-2012. doi:10.1038/emboj.2012.49

191. Dimke H, Desai P, Borovac J, Lau A, Pan W, Alexander RT. Activation of the Ca2+-sensing receptor increases renal claudin-14 expression and urinary Ca2+ excretion. *Am J*

Physiol - Ren Physiol. 2013;304(6). doi:10.1152/ajprenal.00263.2012

192. Yu ASL, Cheng MH, Angelow S, et al. Molecular basis for cation selectivity in claudin-2-based paracellular pores: Identifi cation of an electrostatic interaction site. *J Gen Physiol*. 2009;133(1):111-127. doi:10.1085/jgp.200810154

193. Figueres L, Hourmant M, Lemoine S. Understanding and managing hypercalciuria in adults with nephrolithiasis : keys for nephrologists. 2020;(June 2019):573-575. doi:10.1093/ndt/gfz099

194. Kojetin DJ, Venters RA, Kordys DR, Thompson RJ, Kumar R, Cavanagh J. Structure, binding interface and hydrophobic transitions of Ca 2+-loaded calbindin-D28K. *Nat Struct Mol Biol*. 2006;13(7):641-647. doi:10.1038/nsmb1112

195. Laytton J, Lee S, Lee W, et al. The Kidney Sodium-Calcium Exchanger. *Annnal New York Acad Sci*. 1996;779(1):58-72. doi:https://doi.org/10.1111/j.1749-6632.1996.tb44770.x

196. Nigwekar S. Vitamin-D and Parathyroid Hormone in Kidney Disease. In: Rhee CM, et al, eds. *Endocrine Disorders in Kidney Disease*. Switzerland: Springer, Nature; :223-229.

197. Bronner F. Calcium absorption - A paradigm for mineral absorption. *J Nutr*. 1998;128(5):917-920. doi:10.1093/jn/128.5.917

198. Bronner F, Pansu D. Nutritional aspects of calcium absorption. *J Nutr*. 1999;129(1):9-12. doi:10.1093/jn/129.1.9

199. Duflos C, Bellaton C, Pansu D, Bronner F. Calcium solubility, intestinal sojourn time and paracellular permeability codetermine passive calcium absorption in rats. *J Nutr*. 1995;125(9):2348-2355. doi:10.1093/jn/125.9.2348

200. Bronner F. Mechanisms of intestinal calcium absorption. In: *Journal of Cellular*

Biochemistry. Vol 88. ; 2003:387-393. doi:10.1002/jcb.10330

201. Fujita H, Sugimoto K, Inatomi S, et al. Tight Junction Proteins Claudin-2 and -12 Are Critical for Vitamin D-dependent Ca 2+ Absorption between Enterocytes. Nusrat A, ed. *Mol Biol Cell*. 2008;19(5):1912-1921. doi:10.1091/mbc.e07-09-0973
202. Wasserman RH. Vitamin D and the Dual Processes of Intestinal Calcium Absorption. *J Nutr*. 2004;134(11):3137-3139. doi:10.1093/jn/134.11.3137
203. Peacock M. Calcium metabolism in health and disease. *Clin J Am Soc Nephrol*. 2010;5(SUPPL. 1). doi:10.2215/CJN.05910809
204. Ohyama Y, Shinki T. Calcitriol. In: *Handbook of Hormones*. 2nd ed. Cambride, Massachusetts: Academic Press; 2021:971-973. doi:10.1016/B978-0-12-820649-2.00268-0
205. Morel F. Mode of action of hormones on the kidney. *Intensive Care Med*. 1977;3(4):231-232. doi:10.1007/BF01641111
206. WESSON LG. Hormonal influences on renal function. *Annu Rev Med*. 1961;12:77-92. doi:10.1146/annurev.me.12.020161.000453
207. Salomon MI, Poon TP, Goldblatt M, Tchertkoff V. Renal lesions in heroin addicts. A study based on kidney biopsies. *Nephron*. 1972;9(6):356-363. doi:10.1159/000180169
208. Souma T, Suzuki N, Yamamoto M. Renal erythropoietin-producing cells in health and disease. *Front Physiol*. 2015;6(JUN):1-10. doi:10.3389/fphys.2015.00167
209. Alpern RJ, Caplan MJ, Moe OW, eds. *Seldin and Geibisch's The Kidney: Physiology and Pathophysiology*. Cambride, Massachusetts: Academic Press; 2012.
210. Karim Z, Szutkowska M, Vernimmen C, Bichara M. Renal handling of NH3/NH4+: Recent concepts. *Nephron - Physiol*. 2005;101(4):77-81. doi:10.1159/000087575

211. Sebastian A, Sutton JM, Hulter HN, Schambelan M, Poler SM. Effect of mineralocorticoid replacement therapy on renal acid-base homeostasis in adrenalectomized patients. *Kidney Int*. 1980;18(6):762-773. doi:10.1038/ki.1980.195

212. Palmer LG, Frindt G. Na+ and K+ transport by the renal connecting tubule. *Curr Opin Nephrol Hypertens*. 2007;16(5):477-483. doi:10.1097/MNH.0b013e32820ac850

213. Frindt G, Palmer LG. Low-conductance K channels in apical membrane of rat cortical collecting tubule. *Am J Physiol - Ren Fluid Electrolyte Physiol*. 1989;256(1 (25/1)). doi:10.1152/ajprenal.1989.256.1.f143

214. Najjar F, Zhou H, Morimoto T, et al. Dietary K+ regulates apical membrane expression of maxi-K channels in rabbit cortical collecting duct. *Am J Physiol - Ren Physiol*. 2005;289(4 58-4):922-932. doi:10.1152/ajprenal.00057.2005

215. Rothenberger F, Velic A, Stehberger PA, Kovacikova J, Wagner CA. Angiotensin II stimulates vacuolar H+-ATPase activity in renal acid-secretory intercalated cells from the outer medullary collecting duct. *J Am Soc Nephrol*. 2007;18(7):2085-2093. doi:10.1681/ASN.2006070753

216. Mohebbi N, Perna A, van der Wijst J, Becker HM, Capasso G, Wagner CA. Regulation of Two Renal Chloride Transporters, AE1 and Pendrin, by Electrolytes and Aldosterone. *PLoS One*. 2013;8(1). doi:10.1371/journal.pone.0055286

217. Wagner CA, Finberg KE, Breton S, Marshansky V, Brown D, Geibel JP. Renal vacuolar H+-ATPase. *Physiol Rev*. 2004;84(4):1263-1314. doi:10.1152/physrev.00045.2003

218. Sakairi Y, Jacobson HR, Noland TD, Breyer MD. Luminal prostaglandin E receptors regulate salt and water transport in rabbit cortical collecting duct. *Am J Physiol Physiol*. 1995;269(2):F257-F265. doi:10.1152/ajprenal.1995.269.2.F257

219. Fountain J, Lappin S. *Physiology, Renin Angiotensin System*. Treasure Island, FL: StatPearls (Internet); 2021. https://pubmed.ncbi.nlm.nih.gov/29261862/.

220. Xu J, Song P, Nakamura S, et al. Deletion of the chloride transporter Slc26a7 causes distal renal tubular acidosis and impairs gastric acid secretion. *J Biol Chem*. 2009;284(43):29470-29479. doi:10.1074/jbc.M109.044396

221. Yin K, Paine ML. Bicarbonate Transport During Enamel Maturation. *Calcif Tissue Int*. 2017;101(5):457-464. doi:10.1007/s00223-017-0311-2

222. Zou M, Alzahrani AS, Al-Odaib A, et al. Molecular Analysis of Congenital Hypothyroidism in Saudi Arabia: SLC26A7 Mutation Is a Novel Defect in Thyroid Dyshormonogenesis. *J Clin Endocrinol Metab*. 2018;103(5):1889-1898. doi:10.1210/jc.2017-02202

223. Xu J, Worrell RT, Li HC, et al. Chloride/bicarbonate exchanger SLC26A7 is localized in endosomes in medullary collecting duct cells and is targeted to the basolateral membrane in hypertonicity and potassium depletion. *J Am Soc Nephrol*. 2006;17(4):956-967. doi:10.1681/ASN.2005111174

224. Vince JW, Reithmeier RAF. Carbonic anhydrase II binds to the carboxyl terminus of human band 3, the erythrocyte Cl-/HCO3/- exchanger. *J Biol Chem*. 1998;273(43):28430-28437. doi:10.1074/jbc.273.43.28430

225. Yenchitsomanus P, Kittanakom S, Rungroj N. Molecular mechanisms of autosomal dominant and recessive distal renal tubular acidosis caused by SLC4A1 (AE1) mutations. *J Mol Genet Med*. 2005;01(02):49-62. doi:10.4172/1747-0862.1000013

226. Beckmann R, Toye AM, Smythe JS, Anstee DJ, Tanner MJA. An N-terminal GFP tag does not alter the functional expression to the plasma membrane of red cell and kidney

anion exchanger (AE1) in mammalian cells. *Mol Membr Biol*. 2002;19(3):187-200. doi:10.1080/09687680210141043

227. Cheidde L, Vieira TC, Lima PRM, Saad STO, Heilberg IP. A Novel Mutation in the Anion Exchanger 1 Gene Is Associated With Familial Distal Renal Tubular Acidosis and Nephrocalcinosis. *Pediatrics*. 2003;112(6):1361-1367. doi:10.1542/peds.112.6.1361

228. Quilty JA, Cordat E, Reithmeier RAF. Impaired trafficking of human kidney anion exchanger (kAE1) caused by hetero-oligomer formation with a truncated mutant associated with distal renal tubular acidosis. *Biochem J*. 2002;368(3):895-903. doi:10.1042/BJ20020574

229. Shao L, Xu Y, Dong Q, Lang Y, Yue S, Miao Z. A novel SLC4A1 variant in an autosomal dominant distal renal tubular acidosis family with a severe phenotype. *Endocrine*. 2010;37(3):473-478. doi:10.1007/s12020-010-9340-6

230. Cordat E, Li J, Reithmeier RAF. Carboxyl-terminal truncations of human anion exchanger impair its trafficking to the plasma membrane. *Traffic*. 2003;4(9):642-651. doi:10.1034/j.1600-0854.2003.00123.x

231. Alper SL. Familial renal tubular acidosis. *J Nephrol*. 23 Suppl 1:S57-76. http://www.ncbi.nlm.nih.gov/pubmed/21170890.

232. Stehberger PA, Shmukler BE, Stuart-Tilley AK, Peters LL, Alper SL, Wagner CA. Distal renal tubular acidosis in mice lacking the AE1 (Band3) Cl -/HCO3- exchanger (slc4a1). *J Am Soc Nephrol*. 2007;18(5):1408-1418. doi:10.1681/ASN.2006101072

233. Vichot AA, Zsengellér ZK, Shmukler BE, Adams ND, Dahl NK, Alper SL. Loss of kAE1 expression in collecting ducts of end-stage kidneys from a family with SLC4A1 G609R-associated distal renal tubular acidosis. *Clin Kidney J*. 2017;10(1):135-140.

doi:10.1093/ckj/sfw074

234. Chu C, Woods N, Sawasdee N, et al. Band 3 Edmonton I, a novel mutant of the anion exchanger 1 causing spherocytosis and distal renal tubular acidosis. *Biochem J*. 2010;426(3):379-388. doi:10.1042/BJ20091525

235. Chu CYS, King JC, Berrini M, Alexander RT, Cordat E. Functional Rescue of a Kidney Anion Exchanger 1 Trafficking Mutant in Renal Epithelial Cells. *PLoS One*. 2013;8(2). doi:10.1371/journal.pone.0057062

236. Sterling D, Casey JR. Transport activity of AE3 chloride/bicarbonate anion-exchange proteins and their regulation by intracellular pH. *Biochem J*. 1999;344(1):221-229. doi:10.1042/0264-6021:3440221

237. Toye AM, Bruce LJ, Unwin RJ, Wrong O, Tanner MJA. Band 3 Walton, a C-terminal deletion associated with distal renal tubular acidosis, is expressed in the red cell membrane but retained internally in kidney cells. *Blood*. 2002;99(1):342-347. doi:10.1182/blood.V99.1.342

238. Devuyst O, Beauwens R, Denef JF, Crabbé J, Abramow M. Subtypes of Madin-Darby canine kidney (MDCK) cells defined by immunocytochemistry: Further evidence for properties of renal collecting duct cells. *Cell Tissue Res*. 1994;277(2):231-237. doi:10.1007/BF00327770

239. Fernández R, Malnic G. H + ATPase and Cl − Interaction in Regulation of MDCK Cell pH. *J Membr Biol*. 1998;163(2):137-145. doi:10.1007/s002329900378

240. Chu CY, King J, Berrini M, et al. Degradation mechanism of a Golgi-retained distal renal tubular acidosis mutant of the kidney anion exchanger 1 in renal cells. *Am J Physiol - Cell Physiol*. 2014;307(3):296-307. doi:10.1152/ajpcell.00310.2013

241. Almomani E, Lashhab R, Alexander RT, Cordat E. The carboxyl-terminally truncated kidney anion exchanger 1 R901X dRTA mutant is unstable at the plasma membrane. *Am J Physiol - Cell Physiol*. 2016;310(9):C764-C772. doi:10.1152/ajpcell.00305.2015

242. Lee JW, Chou CL, Knepper MA. Deep sequencing in microdissected renal tubules identifies nephron segment-specific transcriptomes. *J Am Soc Nephrol*. 2015;26(11):2669-2677. doi:10.1681/ASN.2014111067

243. Chen L, Lee JW, Chou CL, et al. Transcriptomes of major renal collecting duct cell types in mouse identified by single-cell RNA-seq. *Proc Natl Acad Sci U S A*. 2017;114(46):E9989-E9998. doi:10.1073/pnas.1710964114

244. Ohtaka A, Muto S, Nemoto J, Kawakami K, Nagano K, Asano Y. Hyperosmolality stimulates Na-K-ATPase gene expression in inner medullary collecting duct cells. *Am J Physiol*. 1996;270(5 PART 2):728-738. doi:10.1152/ajprenal.1996.270.5.f728

245. Ko SBH, Shcheynikov N, Choi JY, et al. A molecular mechanism for aberrant CFTR-dependent HCO3- transport in cystic fibrosis. *EMBO J*. 2002;21(21):5662-5672. doi:10.1093/emboj/cdf580

246. Saxena V, Gao H, Arregui S, et al. Kidney intercalated cells are phagocytic and acidify internalized uropathogenic Escherichia coli. *Nat Commun*. 2021;12(1):1-15. doi:10.1038/s41467-021-22672-5

247. Anderson JM, Itallie VM. Physiology and Function of the Tight Juncton. *Cold Spring Harb Perspect Biol*. 2009;1:a002584.

248. Tsukita S, Furuse M, Itoh M. Multifunctional strands in tight junctions. *Nat Rev Mol Cell Biol*. 2001;2(4):285-293. doi:10.1038/35067088

249. Van Itallie CM, Anderson JM. Claudins and epithelial paracellular transport. *Annu Rev*

Physiol. 2006;68(Table 4):403-429. doi:10.1146/annurev.physiol.68.040104.131404

250. Furuse M. Molecular basis of the core structure of tight junctions. *Cold Spring Harb Perspect Biol*. 2010;2(1):1-14. doi:10.1101/cshperspect.a002907

251. Kage H, Flodby P, Gao D, et al. Claudin 4 knockout mice: Normal physiological phenotype with increased susceptibility to lung injury. *Am J Physiol - Lung Cell Mol Physiol*. 2014;307(7):L524-L536. doi:10.1152/ajplung.00077.2014

252. Miller RL, Lucero OM, Riemondy KA, et al. The V-ATPase B1-subunit promoter drives expression of Cre recombinase in intercalated cells of the kidney. *Kidney Int*. 2009;75(4):435-439. doi:10.1038/ki.2008.569

253. De Seigneux S, Malte H, Dimke H, Frøkiær J, Nielsen S, Frische S. Renal compensation to chronic hypoxic hypercapnia: Downregulation of pendrin and adaptation of the proximal tubule. *Am J Physiol - Ren Physiol*. 2007;292(4):1256-1266. doi:10.1152/ajprenal.00220.2006

254. Frische S, Chambrey R, Trepiccione F, et al. H+-ATPase B1 subunit localizes to thick ascending limb and distal convoluted tubule of rodent and human kidney. *Am J Physiol - Ren Physiol*. 2018;315(3):F429-F444. doi:10.1152/ajprenal.00539.2017

255. Kim YH, Kwon TH, Frische S, et al. Immunocytochemical localization of pendrin in intercalated cell subtypes in rat and mouse kidney. *Am J Physiol - Ren Physiol*. 2002;283(4 52-4):744-754. doi:10.1152/ajprenal.00037.2002

256. Grinstein M, Dingwall HL, Shah RR, Capellini TD, Galloway JL. A robust method for RNA extraction and purification from a single adult mouse tendon. *PeerJ*. 2018;2018(4):1-17. doi:10.7717/peerj.4664

257. Macedo NJ, Ferreira TL. Maximizing Total RNA Yield from TRIzol ® Reagent Protocol :

A Feasibility Study. *Macedo, Nicholas J Ferreira, Tracie L*. 2014:1-8. http://www.asee.org/documents/zones/zone1/2014/Student/PDFs/89.pdf%0Ahttp://asee-ne.org/proceedings/2014/Student Papers/89.pdf.

258. Hao CM, Breyer MD. Physiological regulation of prostaglandins in the kidney. *Annu Rev Physiol*. 2008;70:357-377. doi:10.1146/annurev.physiol.70.113006.100614

259. Hou J, Renigunta A, Yang J, Waldegger S. Claudin-4 forms paracellular chloride channel in the kidney and requires claudin-8 for tight junction localization. *Proc Natl Acad Sci*. 2010;107(42):18010-18015. doi:10.1073/pnas.1009399107

260. Pech V, Thumova M, Dikalov SI, et al. Nitric oxide reduces Cl- absorption in the mouse cortical collecting duct through an ENaC-dependent mechanism. *Am J Physiol - Ren Physiol*. 2013;304(11):1390-1397. doi:10.1152/ajprenal.00292.2012

261. Van Itallie C, Rahner C, Anderson JM. Regulated expression of claudin-4 decreases paracellular conductance through a selective decrease in sodium permeability. *J Clin Invest*. 2001;107(10):1319-1327. doi:10.1172/JCI12464

262. Verlander JW, Hong S, Pech V, et al. Angiotensin II acts through the angiotensin 1a receptor to upregulate pendrin. *Am J Physiol - Ren Physiol*. 2011;301(6):1314-1325. doi:10.1152/ajprenal.00114.2011

263. Eladari D, Chambrey R, Peti-Peterdi J. A new look at electrolyte transport in the distal tubule. *Annu Rev Physiol*. 2012;74:325-349. doi:10.1146/annurev-physiol-020911-153225

264. Thumova M, Pech V, Froehlich O, et al. Pendrin protein abundance in the kidney is regulated by nitric oxide and cAMP. *Am J Physiol - Ren Physiol*. 2012;303(6):812-820. doi:10.1152/ajprenal.00577.2011

265. Victor S, Stokes JB. Chloride transport by the cortical and outer medullary collecting duct.

Am J Physiol - Ren Fluid Electrolyte Physiol. 1987;253(2):203-212. doi:10.1152/ajprenal.1987.253.2.f203

266. Mattson DL, Meister CJ. Sodium sensitivity of arterial blood pressure in L-NAME hypertensive but not eNOS knockout mice. *Am J Hypertens*. 2006;19(3):327-329. doi:10.1016/j.amjhyper.2005.09.012

267. Navarro J, Sanchez A, Saiz J, et al. Hormonal, renal, and metabolic alterations during hypertension induced by chronic inhibition of NO in rats. *Am J Physiol - Regul Integr Comp Physiol*. 1994;267(6 36-6). doi:10.1152/ajpregu.1994.267.6.r1516

268. Milatz S, Krug SM, Rosenthal R, et al. Claudin-3 acts as a sealing component of the tight junction for ions of either charge and uncharged solutes. *Biochim Biophys Acta - Biomembr*. 2010;1798(11):2048-2057. doi:10.1016/j.bbamem.2010.07.014

269. Tanos BE, Bay AEP, Salvarezza S, et al. IQGAP1 controls tight junction formation through differential regulation of claudin recruitment. *J Cell Sci*. 2015;128(5):853-862. doi:10.1242/jcs.118703

270. Kahle KT, MacGregor GG, Wilson FH, et al. Paracellular Cl- permeability is regulated by WNK4 kinase: Insight into normal physiology and hypertension. *Proc Natl Acad Sci U S A*. 2004;101(41):14877-14882. doi:10.1073/pnas.0406172101

271. Gaush CR, Hard WL, Smith TF. Characterization of an Established Line of Canine Kidney Cells (MDCK). *Exp Biol Med*. 1966;122(3):931-935. doi:10.3181/00379727-122-31293

272. Kim H, Kim M, Im S-K, Fang S. Mouse Cre-LoxP system: general principles to determine tissue-specific roles of target genes. *Lab Anim Res*. 2018;34(4):147. doi:10.5625/lar.2018.34.4.147

273. Sauer B. Inducible gene targeting in mice using the Cre/lox system. *Methods A Companion to Methods Enzymol*. 1998;14(4):381-392. doi:10.1006/meth.1998.0593

274. PECHISKER A. TARGETING YOUR DNA WITH THE CRE/LOX SYSTEM. *Sci Creat Q*. August 2004. https://www.scq.ubc.ca/targeting-your-dna-with-the-crelox-system/#:~:text=The two primary disadvantages of,sometimes cause unintended gene expression.

275. Miller RL, Zhang P, Smith M, et al. V-ATPase B1-subunit promoter drives expression of EGFP in intercalated cells of kidney, clear cells of epididymis and airway cells of lung in transgenic mice. *Am J Physiol - Cell Physiol*. 2005;288(5 57-5):1134-1144. doi:10.1152/ajpcell.00084.2004

276. Stegbauer J, Gurley SB, Sparks MA, et al. AT1 receptors in the collecting duct directly modulate the concentration of urine. *J Am Soc Nephrol*. 2011;22(12):2237-2246. doi:10.1681/ASN.2010101095

277. Bernardinelli E, Costa R, Nofziger C, Paulmichl M, Dossena S. Effect of known inhibitors of ion transport on pendrin (SLC26A4) activity in a human kidney cell line. *Cell Physiol Biochem*. 2016;38(5):1984-1998. doi:10.1159/000445559

APPENDICES

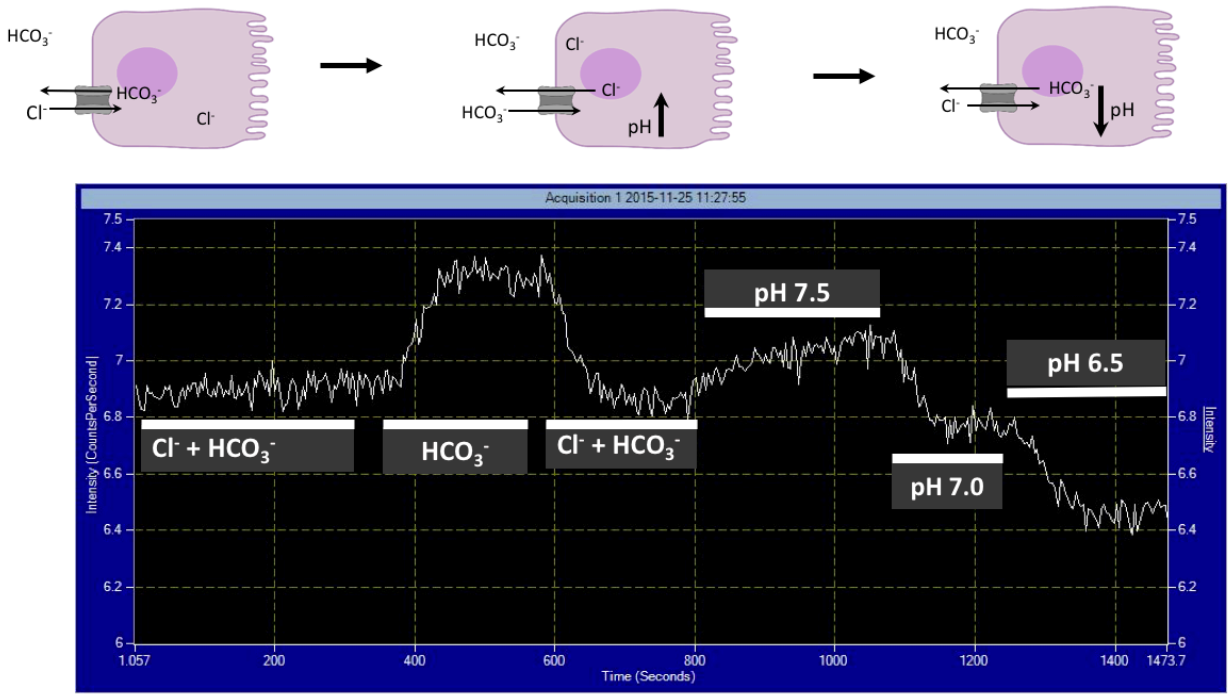

Figure A 1 BCECF-AM based functional assay principle

The cells expressing desired proteins are grown in a specially cut coverslip at about 70% confluency in Ringer's buffer. The cells are perfused in Ringer's buffer that is complemented with a pH sensitive fluorescent dye, BCECF-AM. Cells are first perfused with a Ringer's solution which contains both chloride and bicarbonate, and the ratio of fluorescence emitted at wavelengths 490 and 470 nm is measured. The cells are next perfused with Ringer's buffer devoid of chloride (substituted by gluconate). In the presence of a functional chloride/bicarbonate exchanger, removal of extracellular chloride will trigger the exchanger function and result in chloride efflux in exchange for bicarbonate influx, resulting in alkalization in the cell and increase in cytosolic pH. After returning to initial cytosolic pH by reperfusing the cells with the original Ringer's buffer, solutions of known pH (pH 7.5, 7.0 and 6.5) supplemented with the H^+/K^+ ionophore nigericin are used to calibrate BCECF fluorescence to cytosolic pH. From the function of these calibration solutions, the rate of intracellular pH change is calculated by measuring the slope of the first 60 seconds upon incubation with chloride-free Ringer's solution.

Table A 1 List of primer and probe sequences used for qRTPCR in chapter 3

Gene	Primer and Probe sequences
Actin	5′-GACTCATCGTACTCCTGCTTG-3′ 5′-GATTACTGCTCTGGCTCCTAG-3′ 5′-/56-FAM/CTGGCCTCA/ZEN/CTGTCCACCTTCC/3IABkFQ/-3′
Cldn 4	5′-AACACTTTCTCAGCCCTCTG-3′ 5′-CAGGACTGCCAAGGAGATTC-3′ 5′-/56-FAM/CATAGACGC/ZEN/CATCGCTCAGCCTC/3IABkFQ/-3′
Cldn 8	5′-AGCTGGATACAATTTGGGAGG-3′ 5′-CCACTGAGGCATGATAGTCAC-3′ 5′-/56-FAM/TGCAGCCAT/ZEN/TTGAAGAGCGTAGGT/3IABkFQ/-3′
Cldn 3	5′-CACCAAGATCCTCTATTCTGCG-3′ 5′-GGTTCATCGACTGCTGGTAG-3′ 5′-′/56-FAM/CCCCTCAGA/ZEN/CGTAGTCCTTGCG/3IABkFQ/-3
Cldn 7	5′-GTTTTCCCAGTCACGAC-3′ 5′-TGGCGACAAACATGGCTA-3′ 5′-′/56-FAM/CCTTAATGG/ZEN/TGGTGTCCCTGGTGT/3IABkFQ/-3
kAE1	5′-GTACAGGAAGATGCCGAAGAG-3′ 5′-AAGAGGTCAAGGAACAGCG-3′ 5′-/56-FAM/CCCACAAGC/ZEN/ACAGAGACCAGGAG/3IABkFQ/-3′
Pendrin	5′-CAGAAAACACTTGCAGAGACTG-3′ 5′-TGATGGAGGCAGAGATGAATG-3′ 5′-/56-FAM/ATGTTCAGG/ZEN/ATGAGGCCATGCGTAG/3IABkFQ/-3′
NDCBE	5′-ACGTGCTCTTTTGGTCCTG-3′ 5′-ATGGTGAAGATGGTGAGGAAC-3′ 5′-/56-FAM/AAGGTGCTG/ZEN/GAGACGATGAAGGTG/3IABkFQ/-3′
H^+-ATPase	5′-AGTCAGATTTCGAGCAGAATGG-3′ 5′-CTTCTCACACTGGTAGGCAAG-3′ 5′-/56-FAM/CCGCTCAAT/ZEN/CGTAGGGTCATTGGC/3IABkFQ/-3′
AQP-2	5′-GAAGAGCTCCACAGTCACC-3′ 5′-GCCATCCTCCATGAGATTACC-3′ 5′-/56-FAM/CTCTCCACA/ZEN/ACAATGCAACAGCCG/3IABkFQ/-3′

Table A 2 Physical parameters of WT and Cldn-4 KO mice with long term acid load 3 month age

Parameter	**cldn-4$^{Flox/Flox}$ (n=10)**	**cldn-4$^{Flox/Flox/\beta 1Cre}$ (n=12)**	**Significance (P)**
Body weight, g	23.08 ± 0.51	24.47 ± 0.77	0.25
Food consumption	14.45 ± 0.36	13.80 ± 0.72	0.54
Water consumption	14.73 ± 0.65	14.17 ± 0.77	0.62
Urine volume	42.39 ± 3.29	51.89 ± 4.57	0.14
Feces mass	36.79 ± 2.63	29.97 ± 1.96	0.06

Table A 3 Plasma electrolytes levels in WT and Cldn-4 KO mice with long term acid load 3 month age

Electrolyte	**cldn-4$^{Flox/Flox}$ (10) Mean±SEM**	**cldn-4$^{Flox/Flox/\beta 1Cre}$ (12) Mean±SEM**	**Significance (P)**
Na mmol/L	145.5 ± 0.86	147.7 ± 0.89	0.06
K mmol/L	5.31 ± 0.26	5.77 ± 0.29	0.23
Cl mmol/L	121.1 ± 1.59	118.7 ± 1.53	0.87
TCO_2	22.4 ± 1.11	24.92 ± 1.00	0.09
BUN mg/dl	17.00 ± 2.02	24.42 ± 2.76	0.07
Glucose mg/dl	118.4 ± 8.69	97.83 ± 9.009	0.16
HCT mg/dl	37.4 ± 1.86	41.08 ± 1.93	0.13
pH	7.307 ± 0.01	7.324 ± 0.01	0.30
PCO_2 mmHg	42.15 ± 2.35	45.68 ± 2.34	0.16
HCO_3^- mmol/L	21.03 ± 1.05	23.58 ± 0.92	0.09
BEecf mmol/L	-5.2 ± 1.17	-2.58 ± 0.95	0.09
AnGap mmol/L	8.7 ± 1.23	11.33 ± 1.60	0.11
Hb gm/dl	12.71 ± 0.59	13.98 ± 0.66	0.13

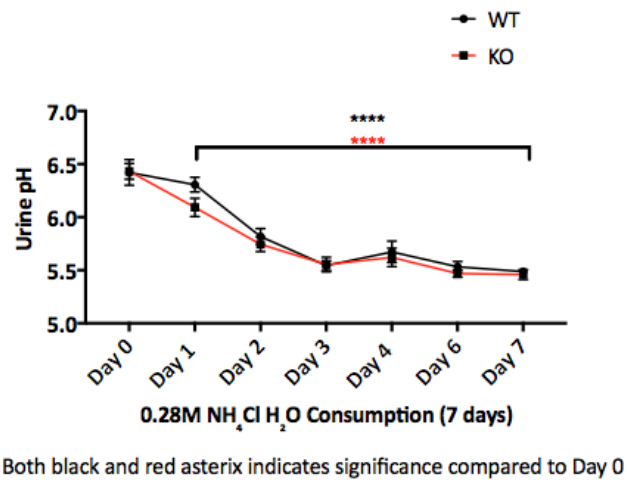

Figure A 2 Urine pH in WT and KO mice at 3 month age

Urine pH of WT (black line) and IC cldn-4 KO (red line) mice at 3 month age after 0.28M NH_4Cl H_2O load for 7 consecutive days. Day 0 represents urine pH before acid load and from day 1 to day 7 after acid load. Urine pH was significantly lower from day 1 to day 7 compared to day 0 in both WT (black asterisk) and cldn-4 KO (red asterisk) mice. However, there was no significant difference between the WT and the KO mice on any given day. *, $P<0.05$, **,$P<0.001$.

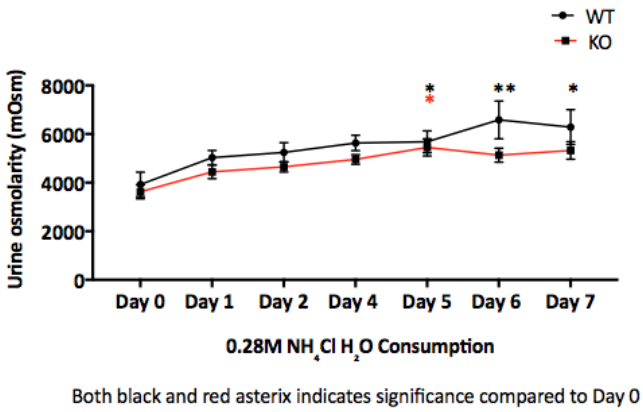

Figure A 3 Urine osmolarity in WT and IC cldn-4 KO mice after acid load at 3 month age

Urine osmolarity in WT (black line) and IC cldn-4 KO mice (red line) after 7 consecutive days of 0.28M NH_4Cl H_2O load. Day 0 represents the initial day with normal drinking water, and from day 1 to day 7 represent the days with acid load. There is no statistical significance in both WT (black asterisk) and IC cldn-4 (red asterisk) until day 5 of acid load. However, there is no significant difference between the WT and IC cldn-4 KO mice in any day.

Table A 3 Physical parameters of WT and Cldn-4 KO mice at steady state on normal diet at 6 months

Parameter	**cldn-4$^{Flox/Flox}$ (n=9)**	**cldn-4$^{Flox/Flox/\beta 1Cre}$ (n=9)**	**Significance (P)**
Body weight, g	28.07 ± 1.55	25.71 ± 1.04	0.19
Food consumption	8.69 ± 1.65	12.78 ± 1.50	0.11
Water consumption	17.28 ± 2.73	20.03 ± 4.81	0.99
Urine volume	22.29 ± 4.23	32.0 ± 3.29	0.09
Feces mass	19.37 ± 3.07	27.01 ± 2.69	0.11
Urine pH	5.9 ± 0.11	5.89 ± 0.05	0.84

Table A 4 Plasma electrolytes levels in WT and Cldn-4 KO mice at steady state on normal diet at 6 month age

Electrolyte	**cldn-4$^{Flox/Flox}$** (9) **Mean**±SEM	**cldn-4$^{Flox/Flox/\beta 1Cre}$** (9) **Mean**±SEM	***P (T-Test)***
Na mmol/L	148.6 ± 0.60	147.8 ± 0.6	0.36
K mmol/L	5.28 ± 0.25	5.33 ± 0.19	0.68
Cl mmol/L	118.4 ± 1.1	117.2 ± 1.39	0.45
TCO_2	22.78 ± 0.77	23.67 ±1.82	0.50
BUN mg/dl	19.00 ± 2.38	21.56 ± 4.27	0.94
Glucose mg/dl	159.6 ±11.51	128.8 ± 10.08	0.06
HCT mg/dl	42.00 ±1.06	41.44 ±0.83	0.92
pH	7.248 ± 0.03	7.28 ±0.02	0.19
PCO_2 mmHg	49.39 ± 4.18	47.24 ± 3.18	0.99
HCO_3^- mmol/L	21.230 ± 0.69	22.37 ± 1.7	0.44
BEecf mmol/L	-5.88 ± 0.69	-4.22 ± 1.92	0.24
AnGap mmol/L	14.11 ± 0.78	13.44 ± 0.83	0.74
Hb gm/dl	14.27 ± 0.36	14.11 ± 0.28	0.28

Table A 5 Physical parameters of WT and Cldn-4 KO mice on low NaCl diet at 6 month age

Parameter	**cldn-4$^{Flox/Flox}$ (n=8)**	**cldn-4$^{Flox/Flox/\beta 1Cre}$ (n=9)**	**Significance (P)**
Body weight, g	27.42 ± 1.31	30.27 ± 1.38	0.71
Food consumption	9.34 ± 1.7	13.29 ± 2.05	0.09
Water consumption	12.64 ± 2.5	17.84 ± 4.82	0.47
Urine volume	16.99 ± 3.01	33.69 ± 6.93	0.06
Feces mass	17.7 ± 3.58	25.8 ± 3.87	0.19
Urine pH	6.04 ± 0.10	6.22 ± 0.12	0.14

Table A 6 Plasma electrolytes levels in WT and Cldn-4 KO mice on low NaCl diet at 6 month age

Electrolyte	**cldn-4$^{Flox/Flox}$ (n=8) Mean±SEM**	**cldn-4$^{Flox/Flox/\beta 1Cre}$ (n=9) Mean±SEM**	***P (T-Test)***
Na mmol/L	147.9 ± 0.67	148.8 ± 1.17	0.81
K mmol/L	5.91 ± 0.35	5.33 ± 0.19	0.68
Cl mmol/L	118.4 ± 0.95	117.4 ± 0.94	0.53
TCO_2	24.89 ± 1.1	24.78 ± 0.66	0.74
BUN mg/dl	23.22 ± 1.89	21.67 ± 1.7	0.65
Glucose mg/dl	148.0 ± 13.4	144.9 ± 8.79	0.38
HCT mg/dl	42.56 ± 1.00	43.00 ± 0.95	0.71
pH	7.253 ± 0.01	7.26 ± 0.01	0.56
PCO_2 mmHg	53.04 ± 2.95	51.56 ± 2.24	0.79
HCO_3^- mmol/L	23.32 ± 1.11	23.34 ± 0.65	0.68
BEecf mmol/L	-3.778 ± 1.10	-3.66 ± 0.72	0.74
AnGap mmol/L	11.78 ± 0.57	12.67 ± 0.74	0.34
Hb gm/dl	14.47 ± 0.33	14.61 ± 0.31	0.71

Table A 7 Physical parameters of WT and Cldn-4 KO mice with long term acid load 6 month age

Parameter	**cldn-4$^{Flox/Flox}$ (n=10)**	**cldn-4$^{Flox/Flox/\beta 1Cre}$ (n=11)**	**Significance (P)**
Body weight, g	25.51 ± 1.71	25.93 ± 1.06	0.79
Food consumption	13.36 ± 0.69	13.42 ± 1.05	0.70
Water consumption	18.32 ± 1.6	18.23 ± 1.76	0.73
Urine volume	51.88 ± 4.85	45.37 ± 5.39	0.38
Feces mass	29.15 ± 1.76	32.27 ± 3.98	0.70

Table A 8 Plasma electrolytes levels in WT and Cldn-4 KO mice with long term acid load 6 month age

Electrolyte	**cldn-4$^{Flox/Flox}$ (n=10) Mean**±SEM	**cldn-4$^{Flox/Flox/\beta 1Cre}$ (n=11) Mean**±SEM	***P (T-Test)***
Na mmol/L	145.3 ± 1.49	145.0 ± 1.58	0.89
K mmol/L	5.25 ± 0.39	4.9 ± 0.21	0.69
Cl mmol/L	122.1 ± 1.7	121.8 ± 1.79	0.87
TCO_2	24.1 ± 1.12	23.64 ± 1.47	0.56
BUN mg/dl	20.8 ± 2.615	16.36 ± 2.76	0.34
Glucose mg/dl	124.1 ± 13.91	120.2 ± 11.67	0.90
HCT mg/dl	37.4 ± 2.40	36.64 ± 2.53	0.82
pH	7.269 ± 0.01	7.28 ±0.01	0.65
PCO_2 mmHg	49.46 ± 2.83	47.18 ± 2.65	0.52
HCO_3^- mmol/L	22.55 ± 1.08	22.27 ± 1.38	0.71
BEecf mmol/L	-4.5 ± 1.17	-4.45 ± 1.53	0.99
AnGap mmol/L	6.3 ± 2.23	5.818 ± 1.74	0.63
Hb gm/dl	12.71 ± 0.81	13.16 ± 0.49	0.95

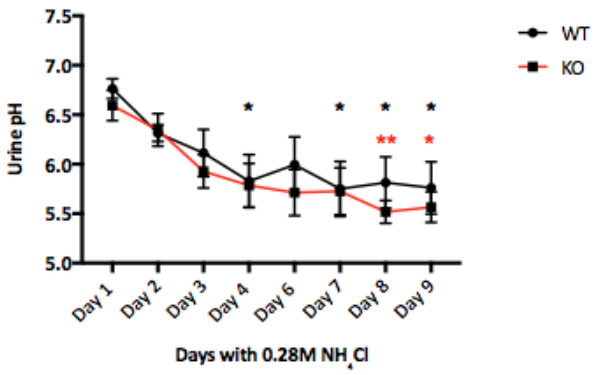

Figure A 4 Urine pH in WT and KO mice at 6 month age

Urine pH of WT (black line) and IC cldn-4 KO (red line) mice at 6 month age after 0.28M NH_4Cl H_2O load for 9 consecutive days. Day 1 represents urine pH before acid load and from day 2 to day 9 after acid load. Urine pH was significantly lower on day 4 in the WT (black asterisk) and on day 8 in the IC cldn-4 KO mice (red asterisk) compared to day 1. However, there was no significant difference between the WT and the KO mice on any given day. *, $P<0.05$, **,$P<0.001$.

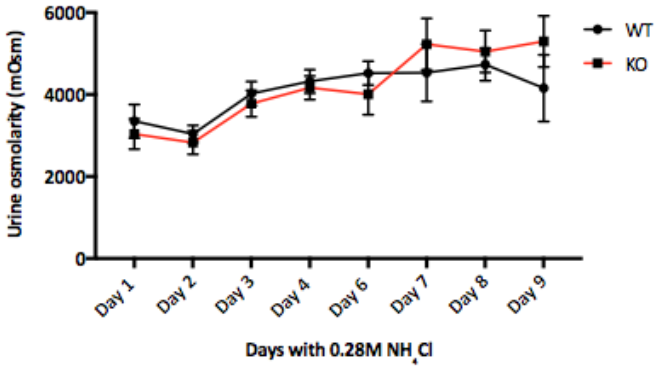

Figure A 5 Urine osmolarity in WT and IC cldn-4 KO mice after acid load at 6 month age

Urine osmolarity in WT (black line) and IC cldn-4 KO mice (red line) after 7 consecutive days of 0.28M NH_4Cl H_2O load. Day 0 represents the initial day with normal drinking water, and from day 1 to day 7 represent the days with acid load. There is no statistical significance in both WT (black asterisk) and IC cldn-4 (red asterisk) until day 5 of acid load. However, there is no significant difference between the WT and IC cldn-4 KO mice in any day.

Table A 9 Physical parameters of WT and Cldn-4 KO mice with 0.01% Ca^{2+} diet at 6 month age

Parameter	**cldn-4$^{Flox/Flox}$ (n=7)**	**cldn-4$^{Flox/Flox/\beta 1Cre}$ (n=9)**	**Significance (P)**
Body weight, g	30.82 ± 1.55	27.42 ± 0.93	0.05
Food consumption	7.06 ± 0.82	8.19 ± 0.90	0.46
Water consumption	10.02 ± 1.27	11.41 ± 0.89	0.53
Urine volume	43.63 ± 9.37	46.96 ± 13.27	0.77
Feces mass	4.71 ± 0.46	5.13 ± 0.65	0.60
Urine pH	5.81 ± 0.04	5.80 ± 0.04	0.99
U $_{Ca/Creatinine}$	0.0012 ± 0.00	0.0013 ± 0.00	0.42

Table A 10 Plasma electrolytes levels in WT and Cldn-4 KO mice with 0.01% Ca^{2+} diet at 6 month age

Electrolyte	**cldn-4$^{Flox/Flox}$ (n=7) Mean±SEM**	**cldn-4$^{Flox/Flox/\beta 1Cre}$ (n=9) Mean±SEM**	***P (T-Test)***
Na mmol/L	147.4 ± 0.36	146.4 ± 0.50	0.25
K mmol/L	5.28 ± 0.23	5.4 ± 0.31	0.97
Cl mmol/L	120.3 ± 0.6	119.6 ± 0.83	0.48
TCO_2	24.14 ± 0.79	24.11 ± 0.42	0.99
BUN mg/dl	21.86 ± 2.005	20.00 ± 1.95	0.45
Glucose mg/dl	96.29 ± 22.35	110.3 ± 14.08	0.58
HCT mg/dl	42.71 ± 1.64	41.67 ± 0.86	0.35
pH	7.293 ± 0.01	7.326 ± 0.01	0.26
PCO_2 mmHg	47.09 ± 1.66	43.5 ± 1.04	0.89
HCO_3^- mmol/L	22.83 ± 0.81	22.69 ± 0.39	0.71
BEecf mmol/L	-3.71 ± 0.94	-3.33 ± 0.44	0.64
AnGap mmol/L	9.7 ± 1.19	9.333 ± 1.18	0.54
Hb gm/dl	14.96 ± 27	14.18 ± 0.29	0.10

Table A 11 Physical parameters of WT and Cldn-4 KO mice at steady state on normal diet at 12 months

Parameter	**cldn-4$^{Flox/Flox}$ (n=7)**	**cldn-4$^{Flox/Flox/\beta 1Cre}$ (n=8)**	**Significance (P)**
Body weight, g	34.17 ± 2.00	35.1 ± 2.3	0.86
Food consumption	5.26 ± 1.11	5.41 ± 1.02	0.95
Water consumption	7.12 ± 1.08	6.94 ± 1.21	0.99
Urine volume	21.8 ± 5.47	18.33 ± 2.76	0.77
Feces mass	12.89 ± 2.63	11.29 ± 1.96	0.77
Urine pH	6.16 ± 0.14	6.07 ± 0.09	0.78

Table A 12 Plasma electrolytes levels in WT and Cldn-4 KO mice at steady state on normal diet at 12 month age

Electrolyte	**cldn-4$^{Flox/Flox}$ (7) Mean±SEM**	**cldn-4$^{Flox/Flox/\beta 1Cre}$ (8) Mean±SEM**	***P (T-Test)***
Na mmol/L	147.3 ± 1.27	147.8 ± 0.6	0.59
K mmol/L	5.6 ± 0.40	5.76 ± 0.27	0.55
Cl mmol/L	120.0 ± 2.24	118.5 ± 1.19	0.84
TCO_2	20.83 ± 2.21	24.13 ± 1.00	0.20
BUN mg/dl	20.6 ± 3.72	21.00 ± 3.12	0.99
Glucose mg/dl	154.0 ± 16.66	142.5 ± 8.94	0.69
HCT mg/dl	40.00 ± 1.265	37.5 ± 1.025	0.22
pH	7.307 ± 0.02	7.29 ± 0.01	0.45
PCO_2 mmHg	37.18 ± 7.36	45.97 ± 2.88	0.35
HCO_3^- mmol/L	19.72 ± 2.03	22.75 ± 0.94	0.19
BEecf mmol/L	-8.5 ± 2.327	-4.00 ± 1.43	0.10
AnGap mmol/L	12.5 ± 2.59	11.67 ± 1.33	0.99
Hb gm/dl	13.6 ± 0.42	12.77 ± 0.35	0.22

Table A 13 Physical parameters of WT and Cldn-4 KO mice on low NaCl diet at 12 month age

Parameter	**cldn-4$^{Flox/Flox}$ (n=8)**	**cldn-4$^{Flox/Flox/\beta 1Cre}$ (n=9)**	**Significance (P)**
Body weight, g	29.44 ± 1.47	32.04 ± 2.27	0.67
Food consumption	8.01 ± 0.52	5.84 ± 0.93	0.04*
Water consumption	13.86 ± 3.27	10.34 ± 1.82	0.84
Urine volume	22.34 ± 3.30	21.71 ± 4.63	0.74
Feces mass	17.59 ± 1.08	11.37 ± 1.55	0.008*
Urine pH	6.31 ± 0.13	6.25 ± 0.06	0.55

Table A 14 Plasma electrolytes levels in WT and Cldn-4 KO mice on low NaCl diet at 12 month age

Electrolyte	**cldn-4$^{Flox/Flox}$** (8) **Mean**±SEM	**cldn-4$^{Flox/Flox/\beta 1Cre}$** (9) **Mean**±SEM	***P (T-Test)***
Na mmol/L	148.3 ± 0.77	145.9 ± 1.38	0.68
K mmol/L	5.15 ± 0.32	5.63 ± 0.47	0.46
Cl mmol/L	120.3 ± 1.04	123.8 ± 1.52	0.16
TCO_2	23.25 ± 0.75	22.33 ± 1.24	0.65
BUN mg/dl	15.67 ± 2.39	19.1 ± 2.78	0.79
Glucose mg/dl	110.8 ± 9.36	120.8 ± 9.44	0.28
HCT mg/dl	39.25 ± 1.278	37.22 ± 1.45	0.33
pH	7.34 ± 0.008	7.324 ± 0.02	0.49
PCO_2 mmHg	40.4 ± 1.91	40.47 ± 2.59	0.67
HCO_3^- mmol/L	19.72 ± 2.03	22.75 ± 0.94	0.76
BEecf mmol/L	-3.87 ± 2.327	-5.00 ± 1.41	0.96
AnGap mmol/L	11.0 ± 1.15	7.5 ± 1.72	0.15
Hb gm/dl	13.34 ± 0.43	12.66 ± 0.49	0.33